University of Massachusetts Amherst

A Lower Limb Prosthesis with Active Alignment for Reduced Limb Loading

Item Type	dissertation
Authors	LaPre, Andrew
DOI	10.7275/9053494.0
Download date	2025-01-04 05:47:42
Link to Item	https://hdl.handle.net/20.500.14394/19995

A LOWER LIMB PROSTHESIS WITH ACTIVE ALIGNMENT FOR REDUCED LIMB LOADING

A Dissertation Presented

By

ANDREW K. LAPRE

Submitted to the Graduate School of the
University of Massachusetts Amherst in partial fulfillment
of the requirements for the degree of

DOCTOR OF PHILOSOPHY

September 2016

Mechanical Engineering

© Copyright by Andrew K. LaPrè 2016

All Rights Reserved

A LOWER LIMB PROSTHESIS WITH ACTIVE ALIGNMENT FOR REDUCED LIMB LOADING

A Dissertation Presented

by

ANDREW K. LAPRE

Approved as to style and content by:

_____
Frank C Sup, Chair

_____
Yossi Chait, Member

_____
Brian Umberger, Member

_____
Ian Grosse, Member

_____
Sundar Krishnamurty, Department Chair
Mechanical Engineering

DEDICATION

To my parents Maribeth and Robert LaPre, for their unconditional love and support.

ACKNOWLEDGMENTS

I would like to express my genuine appreciation to my advisor, Professor Frank Sup, for his endless guidance and support throughout my graduate studies. He has been an invaluable source of expertise in the field of robotics, and his patience has been unyielding. I truly owe the direction of my motivation, focus and career to him. I would also like to show immense gratitude to members of my committee, Professors Ian Grosse, Yossi Chait, and Brian Umberger. They have always kept an open door for discussions and guidance, each playing an integral role in driving my inspiration.

I would like to thank friends and mentors whom I've had the pleasure of acquiring at the University of Massachusetts, particularly Professor David Schmidt, whom I owe the experience of my graduate studies to. This achievement would not have been possible without the enormous amount of academic and emotional support I've received from everyone.

I would like to thank all subjects who have participated in experimentation throughout my studies. Your time has helped to progress this research, which will someday positively impact the lives of many individuals.

Last but not least, I am immensely grateful for the countless friends and family members who have at one time or another offered a helping hand, a shoulder to lean on, or money for rent, making all of this a possibility. Words alone cannot express my gratitude.

This work was supported by NSF National Robotics Initiative grant, IIS-1526986, and by a pilot grant given by the NCSRR OpenSim team at Stanford University.

ABSTRACT

A LOWER LIMB PROSTHESIS WITH ACTIVE ALIGNMENT FOR REDUCED LIMB LOADING

SEPTEMBER 2016

ANDREW KENNEDY LAPRE

B.Sc., UNIVERSITY OF MASSACHUSETTS AMHERST

M.Sc., UNIVERSITY OF MASSACHUSETTS AMHERST

Ph.D., UNIVERSITY OF MASSACHUSETTS AMHERST

Directed by: Professor Frank Sup

Over the past decade, the growing field of robotics has created new possibilities in lower limb prostheses. The focus of these new prostheses has been replicating the dynamics of the lost limb in order to restore gait of individuals with lower limb amputations to healthy norms. This places demanding loads on the residual limb. Compensation by the rest of body is high, causes overloading of intact joints and can lead to deterioration of mobility and overall health. Abnormalities remain present in the person's gait, stemming from the loading of soft tissue and the altered anatomy of the affected limb. In this dissertation, an experimental prosthesis is developed with systematic, simulation based techniques. Kinematics and kinetics of the prosthesis design are altered in order to actively realign the limb in relation to the center of pressure during stance, allowing positive power to be generated by the prosthesis while actively reducing the magnitude of the sagittal moment transferred to the residual limb. Initial findings show that during walking with the experimental device compared to a daily use prosthesis, peak pressures on the residual limb are lowered by over 10% while maintaining walking speed.

TABLE OF CONTENTS

Page

ACKNOWLEDGMENTS v
ABSTRACT vi
LIST OF TABLES x
LIST OF FIGURES xi
CHAPTER
1. INTRODUCTION 1
1.1 Current Lower Limb Prosthesis Technology 1
1.2 Problems Faced by Persons with Lower-limb Amputations 4
1.3 Research Objectives 6
1.4 Dissertation Overview 7
2. REDEFINING PROSTHETIC ANKLE MECHANICS 10
2.1 Introduction 11
2.2 An Altered Biomechanics Study 14
2.3 Non-Anthropomorphic Prosthesis Design 16
2.3.1 Mechanical Design 16
2.3.2 Actuation 19
2.3.3 Sensing 20
2.4 Conclusion 20
2.5 Acknowledgement 21
3. SIMULATION OF A POWERED ANKLE PROSTHESIS WITH ACTIVE ALIGNMENT 22
3.1 Introduction 23
3.2 Modeling and Simulation 25
3.3 Results 28
3.4 Discussion 29
3.5 Acknowledgements 30
4. A ROBOTIC ANKLE-FOOT PROSTHESIS WITH ACTIVE ALIGNMENT 31
4.1 Introduction 32
4.2 Methods 36
4.2.1 Design of Robotic Ankle Prosthesis with Active Alignment 36
4.2.2 Sensing and Control 41

4.2.3 Device Characterization 42
4.2.4 Active Alignment Evaluation 46
4.3 Results 49
4.4 Discussion 52
4.5 Conclusion 56
4.6 Acknowledgement 57
5. A CONTROL STRATEGY FOR AN ACTIVE ALIGNMENT TRANSTIBIAL PROSTHESIS 58
5.1 Introduction 58
5.2 Methods 61
5.3 Controller 63
5.4 Results 66
5.5 Discussion and Conclusion 68
5.6 Acknowledgement 69
6. AN APPROACH FOR WHOLE BODY INVERSE KINEMATICS AND INVERSE DYNAMICS INCLUDING THE RESIDUUM-SOCKET INTERFACE UING MARKER-BASED MOTION CAPTURE 70
6.1 Introduction 70
6.2 Methods 74
6.2.1 A Generic Musculoskeletal Model with Unilateral Transtibial Amputation 74
6.2.2 Experimental Procedures 75
6.2.3 Model Scaling 77
6.2.4 Data Post Processing 78
6.3 Results 80
6.4 Discussion 83
6.5 Conclusion 89
6.6 Acknowledgement 89
7. EVALUATION OF A ROBOTIC ANKLE PROSTHESIS PROTOTYPE WITH ACTIVE ALIGNMENT 90
7.1 Introduction 90
7.2 Methods 91
7.2.1 Prosthesis Hardware and Controller Updates 91
7.2.2 Experimental Procedures 95
7.2.3 Data Processing 99
7.3 Results and Discussion 101
7.4 Conclusion 111

8. SUMMARY, CONCLUSIONS AND FUTURE WORK 113
8.1 Summary 113
8.2 Conclusions 114
8.3 Future Work 115
8.3.1 Potential Improvements for the First Generation Prototype 115
8.3.2 Design of a Second Generation Prosthesis Prototype 117
BIBLIOGRAPHY 118

LIST OF TABLES

Table Page

2.1 Design parameter values found to obtain desired axis translation for a 1.67 m tall subject. 18

6.1 The test subject information is presented, highlighting key attributes. 76

6.2 Socket-limb joint configurations, showing free coordinates for the accompanying configuration and description. 79

7.1 Test subject data. 95

7.2 Peak power generation, absorption, net work and net positive work are shown for all biological joints when using the active prosthesis and the daily use passive prosthesis. 110

LIST OF FIGURES

Figure Page

1.1 Examples of commercially available ankle-foot prostheses designed for walking are shown. 3

1.2 Large moments are generated in the sagittal plane during stance and is transferred from the prosthesis socket to the residual limb. 5

2.1 Transtibial socket loading during gait with highlighted regions of high pressure. 13

2.2 Socket interface moment reduction by aligning the shank with the CoP. Peak moments were reduced from 1.25 to 0.64 Nm/kg (a 50% reduction) at 60% of the gait stance phase. 15

2.3 Illustration of concept showing shank angle modified during late stance to reduce moment transfer at the socket residual limb interface. 16

2.4 Four bar mechanism shown with link lengths l1, l2, l3, l4 fixed joint angles θ1, θ3, used to attain desired rotation and translation of the foot, and dynamic angle θ2 which dictates the motion of the device. 17

2.5 The test apparatus mechanical assembly concept is shown with the main mechanical components, demonstrating the altered kinematics. 19

3.1 Comparison alignment of the GRF vector with the socket for conventional and Active Alignment prostheses. 23

3.2 Active Alignment prosthesis uses a four-bar linkage with unequal link lengths that both rotate and translate the joint when actuated. 25

3.3 Simulation models used for comparison of biomechanics and resultant residuum-socket moments. 26

3.4 Knee angle, knee moment, pelvis height, and socket moment during stance. 28

4.1 The gastrocnemius and soleus muscles in a person with amputation generate a majority of the sagittal moment about the ankle, but also counter the moment transfer through bone tissue, keeping the tibia mostly in compression (a). 33

4.2 Active Alignment Prosthesis tethered prototype shown with protective covers and foot shell. 35

4.3 A solid model of the Active Alignment Prosthesis is shown. 36

4.4 A drawing of the four-bar linkage is shown with design parameters with optimal values. 38

4.5 The single axis moment sensor is shown with strain gages on the underside (a) and the custom sensor PCB (b) which amplifies the moment sensor signal and measures inertial dynamics. 41

4.6 Experimental setups used for characterization and initial testing. 44

4.7 Experimental prosthesis able-bodied adapters allow a person without amputation to walk on the prosthesis for preliminary testing. 46

4.8 The flow diagram of the control methodology used is presented. 47

4.9 Moment sensor accuracy showing the known applied moment in comparison to the moment recorded by the moment sensor, and the RMS deviation as a shaded region. 50

4.10 Moment generated at the moment sensor of the prosthesis when fixed extended 66% in a bench top jig and commanded a maximum current to the motor. 51

4.11 Closed loop force control frequency response of the prosthesis extended 66%. 52

4.12 Comparison of moments recorded by the prosthesis moment sensor while walking on a treadmill at a constant speed of 1.0 m/s while the prosthesis is regulating at a neutral alignment (red), and actively aligning (blue). 53

5.1 Experimental tethered robotic prosthesis with active alignment, shown with covers installed (top) and removed revealing mechatronic internals (bottom). 59

5.2 During gait, large sagittal moments from ground reaction forces acting on the prosthetic foot must be transferred through the socket interface, resulting in high pressure concentrations on the residual limb (a). 60

5.3 Experimental prosthesis able-bodied adapters allow a non-amputee to walk on the prosthesis for preliminary testing, controller development and tuning without the need for test subjects. 62

5.4 A flow diagram of the control methodology is shown. 64

5.5 Able-body adapter implementation during treadmill walking showing active alignment different phases of gait. 65

5.6 Comparison of moments recorded by the prosthesis moment sensor while walking on a treadmill for 10 steps at a constant rate of 1.0 m/s while the prosthesis is regulating at a neutral alignment (red), and actively aligning (blue). 67

5.7 Shown is treadmill walking while reducing from a fast pace of 1.3 m/s to a medium pace of 0.9 m/s. 68

6.1 A generic model with transtibial amputation was created by modifying the gait2354 model provided by OpenSim. 72

6.2 Test subject standing for the standing calibration pose. 77

6.3 Inverse kinematics model marker error RMS, averaged across preferred speed walking trials for each model variation tested, is presented normalized to the Rigid model marker error RMS with the SR-0 frame, which exhibited the largest error value of all models. 80

6.4 The resultant average kinematic (top) and kinetic (bottom) data are shown for the ankle/prosthetic foot (left), knees (middle) and hips (right). 81

6.5 Average vertical (top) and horizontal (bottom) ground reaction forces (GRFs) are shown for the affected amputated left side with ESR (energy storage and return) foot/ankle prosthesis, and the right intact foot. 82

6.6 The inverse kinematics for preferred speed walking are shown for the 4-DOF socket-limb model, and compared across the different reference frames defined. 84

6.7 The inverse dynamics are shown for the 4-DOF socket-limb model for preferred speed walking trials, for comparison across different reference frame variations. 85

7.1 The modified prosthesis is shown with redesigned neutral position hard-stops, new hardware and redesigned load cell. 92

7.2 The maximum force output of the prosthesis is presented, used to determine how to modify the prosthesis. 93

7.3 The subject's residual limb is shown with pressure sensors being mounted on the tibial tubercle and limb posterior. 96

7.4 The novel pressure system used to record intra-socket pressures is shown with two 3x4 grid capacitive sensors and the custom RF data synchronization trigger. 97

7.5 The subject is shown posing for a static standing calibration trial, where marker positions are recorded to be used for model scaling during data post processing. 98

7.6 The workflow of the model matching algorithm is presented. 100

7.7 Average sagittal plane biomechanics data are presented for the ankle, knee and hip joints. 102

7.8 Average normalized ground reaction forces are shown for trials where the test subject used the passive energy storage and return (ESR) foot prosthesis and the active alignment prosthesis (AAP). 103

7.9 Socket mechanics plots with average normalized sagittal plane generalized socket movements, forces and power are shown for trials where the test subject used the passive energy storage and return (ESR) foot prosthesis and the active alignment prosthesis (AAP). 104

7.10 The COM trajectory during gait is shown zeroed to the second peak, seen during contralateral stance. 105

7.11 Prosthesis, average extension, actuator force and power data are shown for the active alignment prosthesis. 106

7.12 Average moment sensor data from 5 steps are shown while the experimental prosthesis regulates a neutral position, and employs active alignment..... 107

7.13 Combined intact joint power is presented showing the natural power flow (left) and phase synced (right). 108

7.14 Average and peak pressures are shown for the tibial tubercle region, and mid posterior region of the residual limb throughout the gait cycle. 109

CHAPTER 1

INTRODUCTION

Persons with lower limb amputations face many physical challenges that compromise their health and mobility [1]. Contemporary prosthesis design aims to restore a natural and efficient gait by means of passive and active components that are optimized to replicate characteristics of an intact limb [2]. Current solutions improve prosthetic gait, but have limitations as well. A person with transtibial (below knee) amputation using a commercially available prosthesis will experience unnatural loading on their residual limb at the socket interface [3,4]. During walking, the load must be transmitted between the skeletal structure and prosthesis through soft tissue, with loading patterns that are a result of both gait dynamics and prosthesis design [5–7]. Tissue of the residual limb is not evolved to transmit such compressive and shear loads repetitively, and can become damaged as a result. This is often a source of discomfort to the prosthesis wearer, and has been found to cause a number of related health problems in both the residuum and rest of body as time progresses [8–12]. Further loss of functionality stems from the altered anatomy of the affected limb, such as the severed gastrocnemius which normally transmits energy from the healthy ankle to the knee [13].

1.1 Current Lower Limb Prosthesis Technology

A prosthesis socket is the interface connecting a prosthetic limb to a wearer's residual limb. A socket for a below knee amputation must transfer high forces generated during walking, and must be comfortable to the wearer in order to sustain utility. Ideally, the socket connection should be a rigid interface allowing highly efficient load transfer with no movement of the prosthesis in relation to the residual limb [14,15]. This would require a very tight socket resulting in discomfort to the individual as well as further possible damage to the residual limb from high pressures and restricted

blood flow. Conversely, a socket that is too loose would compromise the person's stability and also be uncomfortable due to high peak pressure regions caused by poor fit [16–18]. To address both performance and comfort, sockets are made from rigid composite materials and are formed to distribute forces in areas of the limb that are more tolerant to pressure [19]. The two most common transtibial socket types that do this are the patellar tendon bearing socket, and total surface bearing socket [19–21]. Gel liners are also used to disperse pressure further, however this reduces user sensitivity and efficient energy transfer [22,23]. The best result of current socket technology is a semi-rigid connection that compromises some efficiency for comfort and health.

Lower limb prostheses designed for walking are highly influenced by the physiology of the missing limb [24]. Experimental and commercial passive feet have been designed with optimized stiffness, rollover shape and effective foot length ratio to provide maximum energy return, and reduce loading on healthy joints [25–29]. Examples of modern passive energy storage and return (ESR) feet designed for walking can be seen in Figure 1.1 (top). These feet store energy during early stance to be released during push-off. Generally, the larger the prosthesis spring, the better it is at this task. However, a foot that is too stiff won't conform to the ground under the user's weight and may be unstable to walk on. A wide variety of passive feet are available to accommodate the many activity and amputation levels seen in the diverse population of persons with lower limb amputation. Modulated quasi-passive systems have been designed to actively modify passive properties of prosthetic ankles and feet. Figure 1.1 (mid-left) shows the commercially available Ossur Proprio, which modulates the ankle equilibrium angle in the sagittal plane in order to facilitate walking on slopes. The Endolite Elon is also shown (mid-right), which modulates the sagittal plane rotational damping stiffness of the pin-joint ankle. These quasi-passive ankle-foot prostheses make use of microprocessors, various feedback sensors, small motors and battery packs to sense the environment, and adjust appropriate passive parameters. Many fully active robotic ankle-foot prostheses have been developed in an effort to absorb and inject power into gait during

Figure 1.1: Examples of commercially available ankle-foot prostheses designed for walking are shown. Passive energy storage and return (ESR) ankle-feet (top) are optimized for stiffness and length ratios for a wide range of activity levels, user weight and residuum length. Modulated passive ankle-feet (mid) use micro-controllers and low power active components to modulate passive characteristics of the prosthesis such as damping stiffness and equilibrium angle. Fully powered ankle-feet (bottom) aim to fully restore healthy joint performance using high power components.

early and late stance respectively, in an effort to reduce shock loading and metabolic cost [30–36]. Figure 1.1 (bottom) shows the commercialized version of the SpringActive Odyssey, and the iWalk Biom. Both are heavy in comparison to other prosthetic ankles and require larger battery packs due to higher energy requirements, but are capable of producing near healthy joint dynamics through a single degree of freedom pin joint. An examination of gait dynamics indicates that with healthy power introduced locally with a powered prosthesis, there is an improvement in whole body angular momentum [37]. However even with additional joint torque supplied, there isn't a statistically significant increase in ground reaction force during late stance in comparison with a purely passive spring ankle-foot [37].

The devices described are designed to restore natural and efficient gait by mimicking the morphology of a sound limb. None directly address the effects of unnatural loading at the socket interface in combination with the altered physiology of the amputee. The current standard approach to address excessive loading is focused on the improvement of socket technology [38,39].

Significant effects on amputee gait mechanics are still observed, and added stress is introduced to the entire body.

1.2 Problems Faced by Persons with Lower-limb Amputations

Over 600,000 people in the U.S. are afflicted by major lower limb amputation [40]. Amputation can be a result of traumatic injuries and ailments such as cancer, however between 1988 and 1996 dysvascular disease accounted for 82% of all limb loss of which 97% was lower limb [41,42]. With the prevalence of these diseases, the population size of persons with lower limb amputation is expected to double by 2050 [43]. Post amputation, many new problems arise. Asymmetric gait patterns emerge with compensation from the rest of the person's body, leading to a higher metabolic cost and increased intact joint loading [37,44–46]. Most people with lower limb amputation have reported increased back pain post amputation [47]. High pressures on the residual limb increase discomfort, can result in pressure ulcers or deep tissue injury, and overload other parts of the user's body as the they adapt to the device [8–12]. Probability of pain in the intact contralateral knee doubles, and risk of osteoarthritis increases by a factor of 17 [48–50]. A decline in mobility leads to a more sedentary lifestyle due to discomfort and a fear of falling [51,52]. This further compromises ones health through muscle atrophy, weight gain, dysvascular disease and further secondary complications [53]. With reduced mobility, overall health can worsen in a circular fashion, diminishing the person's quality of life quickly. In an attempt to understand the onset of so many new problems, the unique physiology of a transtibial amputated limb is considered.

The physiology of the residual limb consists of remaining bone surrounded by muscle, tendons and other soft tissue that must heal after surgery [54]. A loss of functionality is a result of the discontinuity in the structural support (residual bone and prosthesis) and loss of coupled forces across joints. Post amputation, ground reaction forces are transmitted through the soft tissue on the residual limb. This causes inefficiency in load transfer, added whole body motion from socket movement, and discomfort from pressures on the residual limb primarily from large sagittal

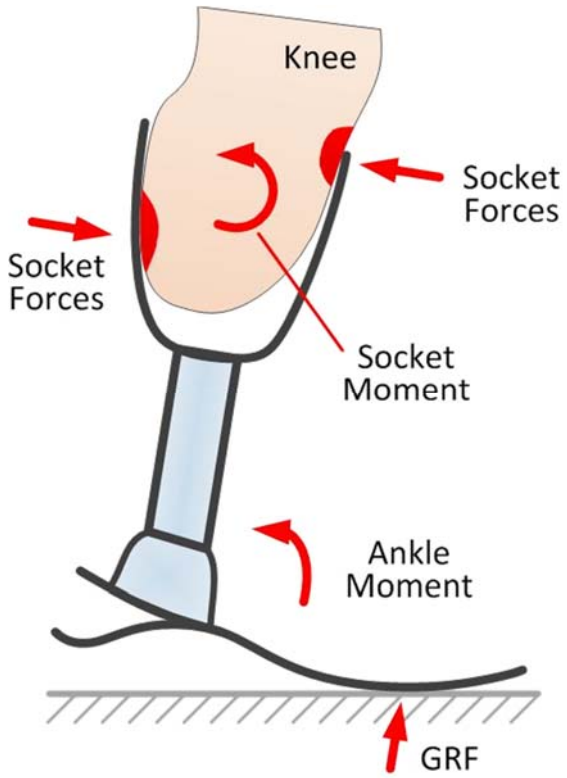

Figure 1.2: Large moments are generated in the sagittal plane during stance and is transferred from the prosthesis socket to the residual limb. 100% of this load must be borne by soft tissue, resulting in high peak pressures in concentrated areas.

moments generated during late stance (Figure 1.2). Coupled forces are lost when the gastrocnemius muscle is severed during amputation. The gastrocnemius muscle is normally biarticular, acting across both knee and ankle joints; healthy coupling of joint forces enables effective energy transfer [55,56] and contributes to whole body angular momentum [57]. Post amputation, effective energy transfer between the intact knee and prosthesis is limited, and additional muscles are likely needed to compensate [13]. This combined loss of functionality renders the subject unable to produce and transmit forces as a person with intact limbs can, resulting in an inefficient gait.

It is clear that there is a loss of efficient energy transfer between the person with amputation and prosthesis during walking. Even with the emergence of robotic prostheses having the capability to produce healthy mechanics, and good fitting sockets having little relative movement, amputee

gait still appears to have limits that stem from an altered physiology and the connection of the prosthesis to the residual limb.

1.3 Research Objectives

This dissertation is aimed to understand the fundamentals driving gait abnormalities of persons with lower limb amputation, and to demonstrate how prosthetic devices can be designed to be synergistic with the altered limb anatomy. Our prosthesis design process is focused on optimizing device mechanics to work with the fundamental loading limitations of the residual limb. Through computational biomechanics simulation, design of complimentary robotic prosthetic devices and evaluation of resulting gait mechanics, our predictions and analyses intend to expose underlying limitations of prosthetic gait and to highlight how alternative devices can be designed to circumvent these limitations for a more efficient and comfortable gait.

Specifically, the objective of this dissertation is to demonstrate that with a synergistic design approach focusing on the physical interaction between the wearer and device, peak pressures on the residual limb during gait can be reduced while increasing power contribution to locomotion from the prosthetic device, and reduce compensation from the rest of the body. This is accomplished through a systematic design and evaluation process, developing an alternative solution to restoring efficient gait by redirecting forces. A concept prosthesis prototype is presented, designed to introduce positive power during stance while lowering peak loading and peak pressures at the residuum-socket interface. The effectiveness of the prosthesis is evaluated at a system level, which includes the wearer and interaction. Success of this work is identified by calculated generalized force transfer within the socket, calculated whole body joint torque/power/work, and measured intra-socket pressures.

The developments of this dissertation deliver an important insight into the physiological limitations of prosthetic gait reported in the literature, and demonstrate how residual limb and

prosthesis kinetics can be altered for reduced loading demand on the residual limb while increasing prosthetic power contribution during stance. The conclusions reported in this dissertation are expected to be of central importance in the design of prosthetic devices for reduced limb loading and rest-of-body compensation of persons with lower limb amputation.

1.4 Dissertation Overview

The remainder of this dissertation is focused on accomplishing the abovementioned research objective. All human subject studies were performed with protocol approved by the University of Massachusetts Amherst Institutional Review Board. In view of that, the rest of this thesis is organized as follows.

Chapter 2 is adapted from a paper presented at the 2013 International Conference on Rehabilitative Robotics in Seattle Washington [58]. Here, the idea of altered biomechanics is developed. Traditional design specifications of lower limb prosthetic devices that aim to restore the local morphology and capability of the lost limb are examined, and a more systematic design approach is used to develop new design specifications which take into account the loading of the residual limb. It is assumed that moment transfer at the residuum-socket interface is directly correlated with peak pressures on the limb, and analysis results are presented to show how altered kinematics can reduce moment transfer. A novel alternative prosthesis design concept is introduced, aimed to satisfy the analysis results.

Chapter 3 is adapted from a paper presented at the 2014 Engineering in Medicine and Biology Conference [59]. Simulations are presented of whole-body prosthetic locomotion with passive, active and concept prostheses with the assumption of an ideal rigid socket interface, in comparison to a simulation of able-bodied gait. It is acknowledged that the assumption of an ideal rigid interface may be a gross overestimation of socket performance, however this is consistent with the design processes for ankle-foot prostheses which are optimized for performance characteristics of an intact

limb. An ankle prosthesis design based on the kinematics of the simulation with concept prosthesis is presented. Results of this chapter establish that with the assumption of an ideal rigid residuum-socket interface, near normal gait mechanics are achievable with considerably less peak generalized loads transferred to the amputated limb.

Chapter 4 presents a complete design and characterization of a robotic ankle-foot prosthesis with active alignment. The fabricated device is characterized on a custom benchtop dynamometer. We demonstrate reduction of generalized force transfer to the limb during gait via able-bodied adapters, which enable a person with intact limbs to walk on the prosthesis. The results clearly establish the potential of the novel device, validating earlier simulations with experimental data. This chapter is published in the June 2016ASME Journal of Medical Devices [60].

Chapter 5 consists of a paper presented at the 2015 Dynamic Systems and Controls Conference (DSCC) [61]. Here, a control approach for active alignment is developed, and controller adaptation to user walking speed is demonstrated.

In Chapter 6, modeling the residuum-socket interface for whole body biomechanics analyses is addressed for evaluation of a prototype prosthesis. A novel approach to estimating socket mechanics is developed using marker based motion capture technology. Current approaches to inverse kinematics analyses with marker based motion capture involve globally minimizing the error between experimentally recorded marker trajectories and model markers attached to all segments of a kinematically constrained, scaled musculoskeletal model of the subject. The inability to track relative motion between the socket and residual limb is addressed by using a 4-DOF residuum-socket model, leveraging kinematic joint constraints used by this type of analysis. Our findings clearly establish that with our approach, whole body motions of persons with lower limb amputation can be reconstructed with an accuracy that is observed when performing the same analysis on individuals with intact limbs, while gaining insight into residuum-socket mechanics.

Additionally, our approach enables the separation of prosthesis socket and mechanism performance evaluation. This chapter is in preparation for submission to the Journal of Computer Methods in Biomechanics and Biomedical Engineering.

Chapter 7 presents a case study of the robotic prototype developed in the chapters 2-4, evaluating the effects of Active Alignment during prosthetic locomotion in comparison with gait mechanics of the same individual using their daily-use prosthesis. Motion capture techniques and our approach to modeling residuum-socket mechanics developed in chapter 5 are used to calculate subject kinematics, in-ground load cells are used to collect ground reaction forces for dynamics calculations, and pressure sensors are used to capture the peak pressures. This chapter connects the findings of previous chapters and research objective, and presents new findings based on the device evaluation. Results confirm that power can be introduced into prosthetic locomotion while decreasing loading demand. With minimal training, more symmetric gait patterns emerged. Further, the test subject reported that it was easier to walk with the experimental device compared to their daily use prosthesis despite it weighing twice as much. The findings are significant in regards to future prosthesis design methodology, with implications on how restoration of gait can be addressed for an efficient solution.

The final chapter of this dissertation provides a summary of the key findings presented in this manuscript, and conclusions of these findings are documented. Suggestions for the future direction of this work are presented and discussed.

CHAPTER 2

REDEFINING PROSTHETIC ANKLE MECHANICS

This chapter is adapted from a conference paper titled *Redefining Prosthetic Ankle Mechanics* written with second author Professor Frank Sup of UMass Amherst. The paper was presented at the 2013 International Conference on Rehabilitative Robotics (ICORR) and published in the proceedings [58]. In this paper, we considered how the residuum-socket interface is loaded during gait, and questioned whether designing a prosthesis to mimic the lost physiological form and function of a missing limb was the best solution for restoring locomotion to an individual with a transtibial amputation. With the assumption that moment is related to peak pressures on the residual limb, altered gait kinematics of the residual limb were explored with the intent of reducing moment transfer to the residual limb. Design specifications for reducing generalized forces on the residual limb were examined with ideal assumptions that rest of body gait kinematics were restored to normal with the altered limb kinematics. It was observed through static force analysis that by reducing the knee angle progressively throughout stance, effectively realigning the tibia to be directed towards the ground reaction forces, moment transfer within the socket could be decreased significantly. A concept design of an alternative robotic ankle prosthesis was presented in conclusion.

Abstract— The moment transferred at the residuum-socket interface of persons with transtibial amputation can be a limiting factor of both user comfort and activity level. High pressures experienced by the user can be a significant source of pain, and can result in deep tissue damage. Compensation of functionality loss causes an asymmetrical gait which can be a contributor of early onset osteoarthritis in the contralateral intact limbs. It has been shown that the moment transferred with conventional passive prostheses can be lowered in magnitude by aligning the tibia with ground

reaction forces, but this limits the effectiveness of the device. With recent powered prosthetics designed to mimic the missing limb, power can be injected into the gait cycle, but can also be limited by this pressure threshold. This paper shows the results of calculations that suggest that altering the prosthetic ankle mechanism can reduce the socket interface moments by as much as 50%. This supports the development of an active non-anthropomorphic ankle prosthesis having the ability to reduce socket interface moments while injecting substantial power levels into the gait cycle.

2.1 Introduction

With the prevalence of dysvascular disease and the general aging of the US population, it is estimated that the percentage of people living with major lower limb amputations is likely to double from 1 in 500 as of 2005 by 2050 [43,62]. In a 2001 survey it was reported that 51% of amputees experience pain while walking [63,64]. This pain and discomfort can lead to rejection of the prosthesis. This is an indicator that current approach to prosthesis design is not fulfilling the needs of persons with lower limb amputation.

Significant technological advancements over the past decade have made the realization of a new class of intelligent prostheses possible for individuals with lower limb amputation, aiming to compensate for the lost function and power of a missing limb [33,36,65]. The goal in the design of these lower limb prostheses has been to mimic the lost limbs as exactly as possible, assuming that the socket-limb interface to the amputee is rigid and comfortable. Since the socket is supported by soft tissue, the connection to the residuum is far from ideal and results in gait abnormalities [48]. During normal walking, the forces and moments generated in the prosthesis must be transmitted through the socket to the soft tissue of the residual limb. As the tissue compresses, the load is transferred to the residual limb causing uneven distributions that have high pressure peaks, are a source of pain [10], and can cause further damage to the residuum [50]. The pain and discomfort may limit the functionality of the prosthesis in terms of walking speed, stride length, and maximum

push-off forces, requiring the individual to compensate with their intact limb. As a result, they are twice as likely to have pain in their intact knee [48], and seventeen times more likely to have osteoarthritis than age matched subjects with intact limbs [49].

Many health issues faced by persons with lower limb amputation can be attributed to the fact that current lower-limb prostheses available create abnormal loading conditions on the residual limb. The ground reaction force and resulting moments must be transmitted through the socket-limb interface rather than through a skeletal structure as in an intact limb. Ways to reduce the magnitude of the load with an active prosthesis having altered kinematics have not yet been explored. Altering the alignment of the residuum in relation to ground reaction forces throughout stance has the potential to reduce the magnitude of residuum moment loading.

The design principle for lower limb prostheses has always been to replace the form and function of the lost limb as closely as possible [14]. Such an approach does not account for the altered anatomy of the amputee and the connection of the prosthesis to the individual. Large moments caused by loading of prosthetic feet must be transmitted through the socket interface. The most common sockets used are the patellar tendon bearing (PTB) sockets [20]. As a result, abnormal loading conditions on the residual limb compress the tissue against the bone. A simplified perspective is to view the socket interface in terms of three-point bending. Although the contact surface of the socket over the residual limb is continuous, the moment loading creates high pressure areas as seen in three-point bending, illustrated in Figure 2.1. This can be painful and cause further damage to the residual limb [66].

Adding compliance to different sections of the prosthesis is a common approach to addressing peak pressures on the residual limb. The effect of increasing the compliance of the prosthetic foot for reduced socket loading has been studied [14]. This approach was found to also reduce stance

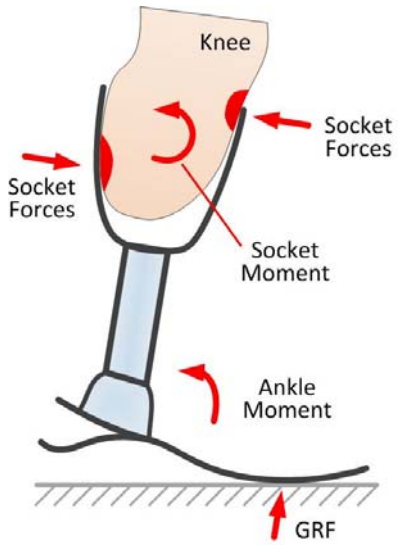

Figure 2.1: Transtibial socket loading during gait with highlighted regions of high pressure.

knee range of motion, as well as the maximum elevation of the person's center of mass during mid to late stance, requiring the user to compensate further with the rest of their body [14,67]. Another method is to add compliance at the socket interface with thicker, compliant silicone gel liners [23]. Added liner compliance reduces peak pressures, but dampens energy return from the prosthesis foot. Thicker liners also introduce higher thermal insulation, causing perspiration that is associated with dermis inflammation and irritation. The user's sense of stability and sensory feedback is decreased, which in some cases can result in higher ground reaction forces and unintentional overloading of the limb [22]. Other studies have been done observing the effects of pylon stiffness on load transfer to the limb [68].

A common method in practice to reduce maximal residual limb pressures in late stance is through static alignment of the prosthesis foot in relation to the residual limb, shifting the prosthetic connection point anterior in the sagittal plane with special hardware, effectively reducing the moment arm during push off [69]. This shift is static throughout the gait cycle however, which decreases push off ability during rollover. It has also been shown that while this decreases the maximum moment during push-off, it increases the negative moment following heel strike [7]. The

approach reduces the socket moment and makes use of the prosthesis more comfortable, however the sound side is still forced to compensate for the decreased performance of the disabled limb.

In this paper, we develop the concept of a non-anthropomorphic active lower limb prosthesis. The approach actively realigns the prosthesis and limb towards ground reaction forces which lowers the moment needed to be transferred, with a slightly altered gait. As a result, it may be possible to inject higher power levels into the gait cycle in order to restore rest of body biomechanics in a manner that is more appropriate for an amputee's altered anatomy. Our preliminary studies have shown that altering the knee angular trajectory during the gait cycle can realign the tibia with the ground reaction forces, lowering the peak moments during gait.

2.2 An Altered Biomechanics Study

Data from one able-bodied, non-amputee subject (29 years of age, 70.2 kg, 1.67 m) was collected and analyzed to examine the possible effects of altering the tibia angular trajectory on mid-tibia moments. Able-bodied data is used for purpose of maintaining able-bodied biomechanics throughout gait in the intact limbs, including the foot to ground angular relations. This satisfies the assumption that rest of body mechanics, foot center of pressure and ground reaction force vectors are ideal and restored to normal. Tibia angular trajectory was then altered with the assumption that the data came from an amputee, and a mechanism between the tibia and foot existed allowing this motion. The resulting mid-tibia moment was calculated through static loading analysis throughout gait. It is noted that with this method, knee and hip moments in the altered limb may be altered as well, however only mid-tibia moment loading is examined due to the correlation with high intra-socket pressures.

The experiment took place in the Biomechanics Laboratory at the University of Massachusetts, Amherst. The data collection used an eight-camera Qualisys Oqus 3-Series optical motion capture system operated by Qualisys Track Manager software (Qualisys, Inc., Gothenberg, Sweden) to

record spatial trajectories of reflective infrared tracking markers placed on the subject at 240 Hz. Horizontal and vertical ground reaction forces were recorded with a floor mounted strain gauge force platform at 2400 Hz (OR6-5, AMTI, Inc. Watertown, MA, USA). Calibration scaling markers were placed at the following anatomical features to reconstruct the bone structure during data processing: 1st and 5th metatarsals, medial/lateral knee joint, medial/lateral ankle malleoli, and the greater trochanters. Four tracking markers were fixed to each foot, shank, and thigh, as well as the hip segment throughout all testing to track the trajectories of each segment. The data were processed using Visual 3D v4 software (C-Motion, Inc, Rockville, MD, USA) to calculate all joint positions, velocities, moments, and power. MATLAB (MathWorks, Natick, MA) was used to analyze and perform all other post-processing calculations.

In Figure 2.2, it can be seen that the calculated moment transferred through the socket-limb interface can be decreased by almost 50%. This decrease in moment assumes that the whole body biomechanics from the affected knee up remain unchanged, as well as the foot rotation in relation to the ground. This corresponds to the center of pressure trajectory used in post-processing. Mid-tibia moment calculations were made by examining the magnitude and direction of the ground reaction force vectors of collected able-body data in relation to mid-tibia with the altered trajectory.

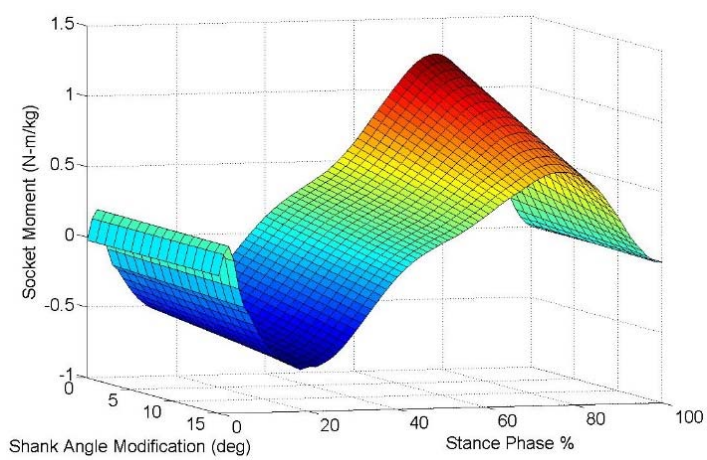

Figure 2.2: Socket interface moment reduction by aligning the shank with the CoP. Peak moments were reduced from 1.25 to 0.64 Nm/kg (a 50% reduction) at 60% of the gait stance phase.

This study represents moments that would be seen at the socket interface of an amputation halfway between the malleoli and knee, and power levels seen in healthy gait were transmitted through an ideal rigid socket, corresponding to an ideal active prosthesis.

2.3 Non-Anthropomorphic Prosthesis Design

2.3.1 Mechanical Design

The purpose of this design concept is alter the tibia angle throughout the stance phase of walking, while maintaining rest of body biomechanics as best as possible, as illustrated in Figure 2.3. When the tibia angle is altered throughout stance, the foot center of rotation translates so that the prosthetic foot trajectory maintains natural rotation in relation to the ground as a healthy foot would during normal gait. This maintains trajectory of the center of pressure. The overall height of 16 cm is comparable to active and semi-active prostheses currently on the market. Lastly, the mechanism is designed to allow different amounts of total translation of the center of rotation between tests, which effects the maximum moment reduction at the socket interface. The tibia shift

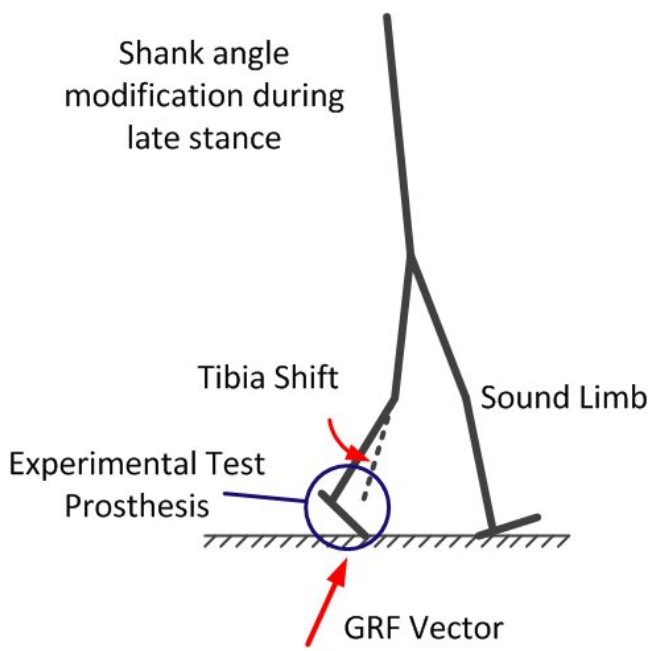

Figure 2.3: Illustration of concept showing shank angle modified during late stance to reduce moment transfer at the socket residual limb interface.

is expressed in terms of the translated distance of the prosthetic ankle's center of rotation in the design section. Between test-subjects, different tibia lengths will result in different amounts of angular shift. When analyzing results however, translational shift will be expressed in terms of degrees of tibia angle shift in order to normalize the data between subjects in future testing.

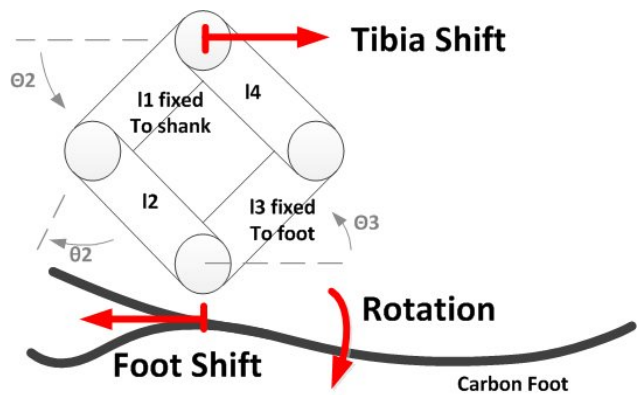

Figure 2.4: Four bar mechanism shown with link lengths l_1, l_2, l_3, l_4 fixed joint angles θ_1, θ_3, used to attain desired rotation and translation of the foot, and dynamic angle θ_2 which dictates the motion of the device.

An optimized actuated four-bar linkage was designed to implement the desired functions. A generic illustration can be seen in Figure 2.4. Links 1 and 2 are fixed rigidly to the shank and foot respectively. The amount of translation of the perpendicular foot rotational axis depends on the length l_2 and amount that this link rotates during actuation. The amount of rotation of the foot depends on the l_1 to l_3 ratio when links 2 and 4 are equal. At the neutral position during standing, the center of rotation should line up on center with the tibia distal/lateral axis to enforce that the foot is in a natural position when not walking and provide natural standing stability. Since one of the design necessities is to maintain foot rotation as it would occur naturally, the flexion during standing and stance of a conventional carbon prosthetic foot is accounted for in the design calculations.

With the design constraints described in the preceding paragraph, link lengths and rigid attachment angles relative to the foot and socket were solved for different amounts of rotational axis translation by minimizing the sum of the link lengths. Link lengths 1 and 3 attached to the

Link Lengths (cm)				Fixed Angles (deg)		Rotational Axis Translation (cm)
l1	**l2**	**l3**	**l4**	**θ1**	**θ3**	
4.50	6.36	6.55	6.36	0.00	22.60	3
4.53	6.36	6.36	6.36	6.81	23.32	6
4.85	6.36	6.36	6.36	21.80	29.69	9

Table 2.1: Design parameter values found to obtain desired axis translation for a 1.67 m tall subject.

socket and foot and are varied, and link lengths 2 and 4 are constant in all three designs. This minimization of link length was done in order to decrease the overall size and weight of the mechanism. Amounts of 3, 6, and 9 cm of translation were chosen for initial testing since they fall into the 5 to 15 degree tibia shift range for subjects less than 1.85 m tall. The same prosthesis will be able to be tested on taller subjects; however less tibia angular shift will be seen. Table 2.1 contains resulting link lengths and rigid attachment angles.

The device as designed for 9 cm of shift can be seen in the top of Figure 2.5 with the major mechanical components labeled. The movement of the linkage translating the axis of rotation during actuation is illustrated in the bottom of Figure 2.5. As the foot rotates, it shifts posteriorly bringing the tibia more in line with the center of pressure.

The links are fabricated components designed to the strength of 7050 aluminum. The links are separated at the pivot points by low friction washers, and have 6mm ID needle bearings that pivot around shoulder bolts. The ball screw nut carrier and thrust bearing carrier are manufactured from cold-rolled steel, and act as the shoulder bolt attachment points for the link 1-2 pivot, and link 3-4 pivot respectively. The ball screw thrust bearing is a single row ball bearing since the actuator will always be under tension in this concept. Connection to the amputees socket is done with a standard pyramid connector, enabling height extension with standard adjustable pylons to accommodate different subjects.

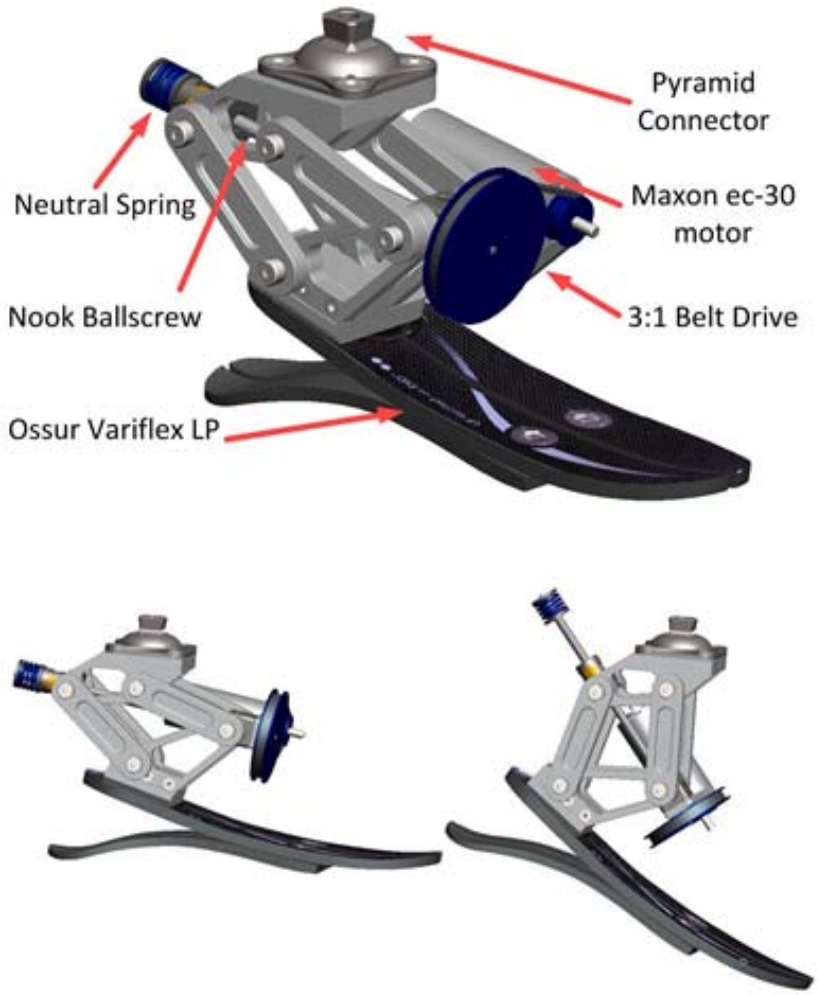

Figure 2.5: The test apparatus mechanical assembly concept is shown with the main mechanical components, demonstrating the altered kinematics.

2.3.2 Actuation

The foot-ankle prosthesis concept is actuated with a ball screw mounted on pivot points centered with the rotational points between links 1 to 2, and links 3 to 4. To avoid imposing a moment on the ball screw, symmetric linkages are on either side of the ball screw in the sagittal plane. The ball screw should only experience tensile stress in this configuration. An off the shelf ball screw diameter of 6mm and pitch of 1 mm was chosen based on loading demands (Nook Industries). The motor is a 200W brushless DC motor (Maxon Motors, EC-30 4-pole) coupled to the ball screw with a belt drive transmission with a drive ratio of 3:1, allowing the maximum needed actuation speed of 7 cm/s. A neutral equilibrium spring is mounted at the end of the ball screw to

support the load during standing and heel-strike to prevent the motor from stalling. The spring has an adjustable equilibrium position to correct for the resulting compression from different subject weights during heel strike and standing.

2.3.3 Sensing

There are three sensors onboard the device for controller feedback. A quadrature encoder mounted on the rear of the motor provides position and velocity feedback. An inertial measurement unit will provide feedback of tibia orientation, and strain gauges are mounted underneath the pyramid connector [33] to identify phase of gait. These sensors will enable state control to be implemented throughout the gait cycle.

2.4 Conclusion

The mechanical design presented in this paper is meant to be a test apparatus to be used in the identification of alternative residuum loading techniques and the effects they have on full body biomechanics, by actively realigning the tibia in relation to the ground reaction force vector during late stance. It can also be used to identify and study the effects of different amounts of gait alterations in order to aid future prosthesis design. Though our calculations suggest that altering the biomechanics can have the potential to improve the comfort and whole body biomechanics, it is completely unknown how much of an alteration would be possible while maintaining walking stability.

Immediate future work involves modeling and simulation of healthy full body biomechanics during a complete gait cycle. The model will consist of a seven link free kinematic chain, with links representing the feet, shanks, thighs, and head arms and torso, all having anthropomorphic length, mass, and inertial properties of a specific subject which biomechanics data can be collected from for model validation. The model will then be altered to simulate unilateral amputee gait with a passive carbon-spring ankle prosthesis and again with the prosthesis described in this paper, in

order to study the effects of the two approaches to prosthesis design on both the moments transferred at the socket residual limb interface as well as whole body biomechanics. These simulations will then be compared to actual biomechanics data of able bodied subjects, and amputee subjects fitted with both conventional passive ankle prostheses, and the prosthesis design described in this paper.

2.5 Acknowledgement

We thank Dr. Joe Hamill and Allison Gruber, University of Massachusetts-Amherst, for their assistance with the biomechanics data collection.

CHAPTER 3:

SIMULATION OF A POWERED ANKLE PROSTHESIS WITH ACTIVE ALIGNMENT

This chapter is adapted from a conference paper titled *Simulation of a Powered Ankle Prosthesis with Dynamic Joint Alignment,* written with second and third authors Professor Brian Umberger and Professor Frank Sup of UMass Amherst. The paper was presented at the Engineering in Medicine and Biology Conference of 2014. The concept of Dynamic Joint Alignment has since been termed "Active Alignment", as it is presented in this document. In this chapter, simulation of gait is introduced, and used to predict how the concept prosthesis would affect gait. An updated concept design of a prosthesis with Active Alignment is presented. A comparison of gait simulations are presented with four different models, representing a subject with intact limbs, and a subject with unilateral amputation utilizing a passive, ideal active, and the experimental prosthesis concept with Active Alignment. In agreement with results presented in Chapter 2, results from this study show that with altered affected limb biomechanics, significantly lower socket moments can be achieved while restoring rest of body biomechanics.

Abstract— This paper presents simulations of a new type of powered ankle prosthesis designed to actively align the tibia with the ground reaction force (GRF) vector during peak loading. The functional goal is to reduce the moment transferred through the socket to the soft tissue of the residual limb. The forward dynamics simulation results show a reduction in socket moment and the impact on the pelvis and affected-side knee. This work supports further research on transtibial prosthetic designs that are not limited to mimicking physiologically normal joint motions to optimize lower limb amputee gait.

3.1 Introduction

A transtibial amputee is connected to their prosthesis through a rigid socket that encapsulates the soft tissue of their residual limb. Moments generated by the prosthesis will be transmitted through the soft tissue of the socket interface, rather than directly to the skeletal structures as in intact-limbs. The highest loading on the residual limb occurs during the stance portion of gait due to the large bending moment, as seen in Figure 3.1. The nature of moment transfer at the socket interface causes an uneven pressure distribution and high pressure concentrations on the anterior and posterior of the limb, which can be painful to the amputee and can cause further damage to the local tissue [50].

Patellar tendon-bearing (PTB) sockets are a common type of socket used for transtibial amputees and are designed to load the more pressure tolerant areas of the residual limb [19,70]; however, high pressure areas remain. This can result in pressure ulcers and deep tissue injury, as well as overloading the sound limb as the amputee develops an asymmetrical gait pattern [8–12]. The overloading of the sound limb may explain why a lower-limb amputee is 17 times more likely

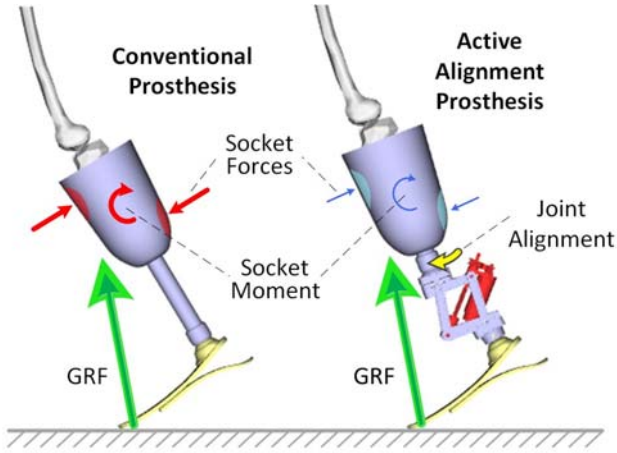

Figure 3.1: Comparison alignment of the GRF vector with the socket for conventional and Active Alignment prostheses.

to have osteoarthritis [49], twice as likely to have pain in their intact knee [48], and report experiencing back pain after amputation [47].

Different methods are used clinically to alleviate the high force concentrations in the socket. Often compliance is added with gel liners to reduce pressures and shear stresses [23]; however, this reduces the amputee's sense of stability and sensory feedback resulting in higher GRFs [22]. The socket is often statically misaligned to the anterior of the foot in an effort to reduce the peak moment transferred during late stance [71], which correlates with a reduction in peak pressures seen in the socket [72]. However, this increases the negative moment seen after heel strike and limits the energy storage and return during push-off [71].

Research on active lower limb prostheses has shown that the unaffected limb of unilateral amputees compensates less when using a powered prosthesis [33,36,65]. However, active prostheses designed to anthropometric constraints are susceptible to the same issues as passive prostheses. The ground reaction forces in the unaffected limb do not change significantly however, showing a slight power burst during very late stance of the affected limb after the second peak, just before push-off [73]. This suggests that the amputee is still compensating with the contralateral limb and is still adjusting their gait to a comfort threshold since the affected side has the same peak ground reaction force during push-off.

Prostheses are usually designed to be anthropomorphic in an effort to replace the form and function of the missing limb [14]. This is done with the assumption that the socket connecting the prosthesis to the residual limb is an ideal, rigid joint, as was modeled by Neptune et al. [74]. However, this idealization is not the case since the weight of the individual must be transferred through compliant tissue of the residual limb within the socket. The result is added degrees of freedom within the socket which affect gait dynamics and efficiency.

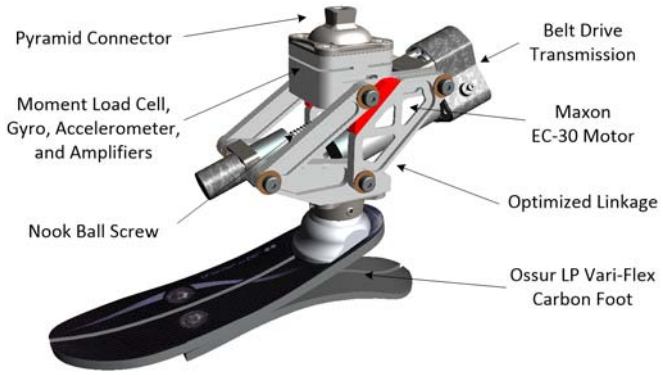

Figure 3.2: Active Alignment prosthesis uses a four-bar linkage with unequal link lengths that both rotate and translate the joint when actuated.

In this paper, a novel active ankle prosthesis is evaluated in simulations which incorporates Active Alignment (AA), while injecting power into the gait cycle. This design, seen in Figure 3.2, has a neutral aligned foot during heel strike, and actively realigns the ankle joint center anteriorly as the foot rotates in a coupled optimized motion. The concept leverages the benefits of different alignments throughout the gait cycle that reduce moments at heel strike and late stance, combined with a fully active prosthesis capable of injecting energy into the stride. A preliminary biomechanics study showed that if the tibia trajectory is altered throughout stance, the peak socket moments can be reduced by up to 50% during late stance [58].

This paper presents a simulation comparison of amputee gait utilizing: a passive carbon spring prosthesis, a powered rotational prosthesis, and the novel design described herein. Sagittal socket moments, joint trajectories and moments, and the trajectory of the pelvis are examined.

3.2 Modeling and Simulation

Gait simulations were performed using the OpenSim simulation platform [75] to simulate and analyze the stance phase of gait of an able-body model, and three modified models seen in Figure 3.3. The OpenSim musculoskeletal model used and modified was ‘gait2354’ [76–78]. Forward dynamics simulations were performed by tracking experimental gait data recorded in the

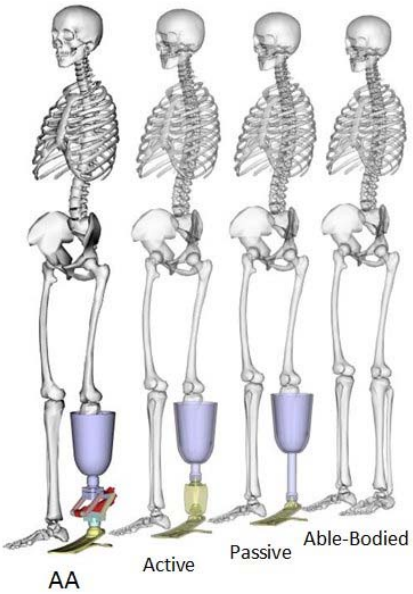

Figure 3.3: Simulation models used for comparison of biomechanics and resultant residuum-socket moments.

Biomechanics Lab at the University of Massachusetts Amherst and was approved the Institutional Review Board.

For the able-bodied model, segments representing the torso, pelvis, thigh, shank, talus, calcaneus/mid-foot, and toes were scaled in both size and weight to match data collected in the biomechanics lab. The subject that the model scaled to was an able-bodied adult male (27 yr, 70 kg, 1.67 m). The model was limited to 11 degrees of motion similar to what was done in [26], with lumbar flexion added for better control of center of mass without affecting hip joint trajectories. The pelvis had two translational and one rotation degrees of freedom, and all joints were limited to 1 degree of freedom rotational motion to constrain the model to sagittal planar motion. Since the main focus was examining the moment transferred through the socket interface, all joints were actuated with ideal torque actuators constrained to physiological limits based on peak muscle forces.

The modified models represented a transtibial amputee with amputation site mid-tibia to represent a typical transtibial amputee. Tibia mass and inertial properties were modified

appropriately. The amputee model was fitted with a passive prosthesis, a pure ankle rotation active prosthesis, and the experimental prosthesis with AA. The connection to the tibia was a rotational joint located halfway between the amputation site and knee joint to represent an estimated center of rotation of the socket joint in the sagittal plane. Translational movements and rotations in other planes were omitted for model simplicity. A high stiffness of 10,000 N-m/deg and damping of 1000 N-m-s/deg was applied to the joint to represent a rigid ideal socket connection [14]. The passive prosthesis was modeled as a rigid socket, shank, and foot. The pure rotation active prosthesis is modeled as a rigid socket and pylon connected to the actuator assembly with a weld joint. The actuator assembly is connected to the foot with a one degree-of-freedom joint allowing only for sagittal rotation. The power of the pure rotation active prosthesis is the same as an able-bodied human ankle. The AA prosthesis is modeled as a rigid socket and pylon connected to the linkage assembly consisting of four links and four joints in a closed chain permitting a single coupled motion consisting of one rotational and two translational components. The coordinated movement is determined by the link lengths and attachment angles to the pylon and foot [58]. All of the prostheses masses and inertial properties were calculated using PTC Creo Parametric CAD software.

A simulation of each model was performed tracking the stance phase of gait from heel strike to toe off of able-bodied biomechanics matching the scaled model. The simulations implemented the Reduced Residual Algorithm (RRA) which is a forward integration tool that applies minimized residual forces to the pelvis compensating for inaccuracies in the model representing the subject and actual biomechanics recorded. In this study recorded ground reaction forces were prescribed to the model rigid feet. Affected knee angle is weighted more heavily to examine the effects on the center of mass height.

3.3 Results

Figure 3.4 presents the simulation results for the knee angle, knee moment, and pelvis height of all four simulations, and socket moments of the amputee models. For the AA model, the knee is more extended during mid-stance. The knee trajectories of the passive and pure rotation active replicate the able-bodied knee trajectories. Knee moments in all four models are close to able-bodied values. The pelvis height trajectories show that the pure rotation active prosthesis and the AA prosthesis come close to matching the able-bodied trajectory while the passive prosthesis model clearly drops in late stance due the lack of actuation at the ankle. The pure rotation active prosthesis model produces the highest socket moment, the passive model is slightly lower, and the model with AA resulted in about 50% lower peak socket moment.

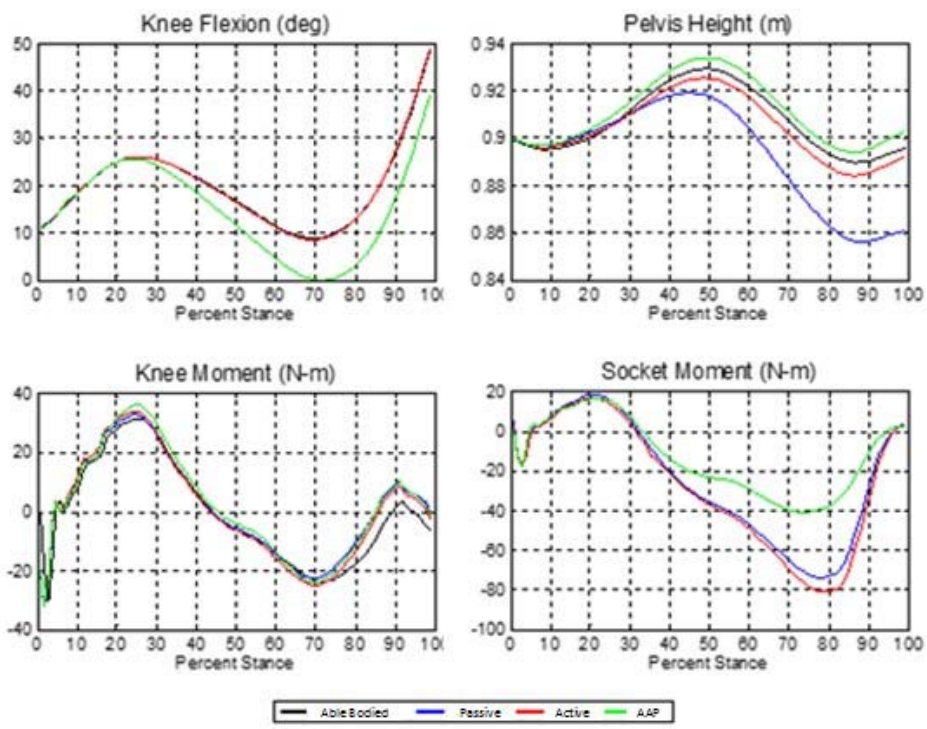

Figure 3.4: Knee angle, knee moment, pelvis height, and socket moment during stance.

3.4 Discussion

The results show a substantial decrease in socket moment in the model that utilizes AA. This suggests that the maximum pressures in the socket would also be reduced, assuming that pressure on the residual limb is related to the socket moment. The knee moments in all three modified models replicate the able-bodied data. The pelvis height doesn't show a large change for the pure rotation active or AA prostheses which gives insight into the body's center of mass trajectory and overall efficiency of gait. Noteworthy for the AA is that the device reduces the socket moment in addition to reducing fluctuations at the pelvis. This suggests that non-physiologically constrained prosthesis designs can be used to restore amputee gait without overburdening the stump-socket interface.

These initial results are limited to the assumptions and simplifications used in the models. In actual amputee gait, the affected joints have altered trajectories to compensate for the deficiencies of the socket-prosthesis system they are using. In these simulation results, the models were programmed to track able-bodied biomechanics. In our approach it does not account for the user's response to loading and the alterations to their gait that they would make to reduce the socket moments. Likewise, the ground reaction forces would most likely be different with the passive prosthesis due to the lack of power and motion. It is assumed that the pure rotation active prosthesis should replicate able-bodied ground reaction forces, for power and motion to be fully restored to the amputee. However, this is not seen in actual amputee gait when a pure rotation active device is used [73]. This may be due to high pressures and a comfort threshold that the amputee may regulate to. Amputee model knee moments are very similar to able-bodied data which would be expected to change with altered kinematics. This may be due to the constraints on the hip angle as well the prescribed GRF which will be addressed in upcoming work for this project.

Future simulation work to optimize the design of the AA device will involve extending the modified models with a multi-segmented, visco-elastic foot (as in [26]) and a foot-ground contact model in order to dynamically predict alterations in the ground reaction force. A more complex

model of the stump-socket interface being developed will also be integrated. The models will then be used in predictive forward dynamics simulations minimizing metabolic cost as in [79] and joint loading (as in [80]) to refine the AA prosthesis design. The prosthesis with AA will then be tested in the gait lab to validate simulations, and evaluate the performance of the AA prosthesis. This will lead to a second generation AA prosthesis design based on both quantitative feedback of gait dynamics and efficiency, as well as qualitative feedback based on the comfort and stability perceived by test subjects.

3.5 Acknowledgements

This work was supported in part by a grant from the National Center for Simulation in Rehabilitation Research.

CHAPTER 4

A ROBOTIC ANKLE-FOOT PROSTHESIS WITH ACTIVE ALIGNMENT

A Robotic Ankle-Foot Prosthesis with Active Alignment is a technical paper published in the June 2016 ASME Journal of Medical Devices with second and third authors Professor Brian Umberger and Professor Frank Sup of UMass Amherst [60]. Following simulation work, the concept was fabricated, bringing the concept to a realization. This paper describes the design process, technical specifications, prototype, benchtop testing, and initial treadmill walking testing with able-body adapters. Results presented in this chapter are significant in that they validate mechanism utility, predicted in simulations and analyses in Chapters 2 and 3.

Abstract— An ankle-foot prosthesis designed to mimic the missing physiological limb generates a large sagittal moment during push off which must be transferred to the residual limb through the socket connection. The large moment is correlated with high internal socket pressures that are often a source of discomfort for the person with amputation, limiting prosthesis use. In this paper, the concept of active alignment is developed. Active alignment realigns the affected residual limb towards the center of pressure during stance. During gait, the prosthesis configuration changes to shorten the moment arm between the ground reaction force and the residual limb. This reduces the peak moment transferred through the socket interface during late stance. A tethered robotic ankle prosthesis has been developed and evaluation results are presented of active alignment during normal walking in a laboratory setting. Preliminary testing was performed with a subject without amputation walking with able-bodied adapters at a constant speed. The results show a 33% reduction in the peak resultant moment transferred at the socket limb interface.

4.1 Introduction

The performance of an individual with lower limb amputation is limited by a combination of their altered morphology, the prosthesis, and the connection between them. Current lower limb prostheses, both active and passive, are designed to recreate the biomechanics of intact limbs [14]. This mimic-type approach assumes the socket connecting the wearer to their prosthesis is a perfect mirror of the intact limb. During walking, however, the prosthesis loads the residual limb at the socket interface, stressing the soft tissue of the limb. This can cause localized pain and tissue damage, as well as injury to the other parts of the musculoskeletal system as the person adapts to and compensates for the device. As a result, persons with lower limb amputation are at greater risk for osteoarthritis, osteopenia, osteoporosis and back pain [47–49,81]. Decline in mobility due to discomfort and deterioration of overall health is common and leads to a more sedentary lifestyle [82]. This further compromises the person's health status through muscle atrophy, decreased bone density and weight gain [81]. A lower limb prosthesis designed to decrease the loads placed on the residual limb has the potential to impact one's mobility in order to sustain a more active lifestyle, without creating health problems associated with high peak load conditions.

Motivated by both the form and function of the lost limb, the design of lower limb prostheses has historically been driven to restore individuals with amputation to a physiologically normal gait with intact limbs [14]. This includes factors such as size, mass, torque, speed, stiffness, range of motion, responsiveness to commands and net positive work ability of an intact limb [83–85]. Differences in physiology of intact and amputated limbs may limit the success of this approach. In an intact limb, the gastrocnemius and soleus muscles generate a majority of the sagittal moment about the ankle joint during push off. The gastrocnemius is biarticular and also acts to transfer energy from the knee to the ankle joint, contributing to whole body angular momentum [55–57]. Examining the paths of the intact gastrocnemius and soleus shows that these muscles counter the

moment transferred through the tibia when a moment is generated about the ankle (Figure 4.1 a). In a limb that has been partially amputated, the bones and muscles are severed and the sagittal moment generated by the prosthesis is transferred at the socket-limb interface through the soft tissue to the bone. As a result of this non-rigid connection, unnatural compressive and shear loading of soft tissue occurs as well as irregular moment loading of bone tissues (Figure 4.1 b). In an evaluation of a commercial powered ankle-foot with healthy joint performance capabilities [83], the altered musculoskeletal anatomy of the affected limb combined with socket movement under loading may have contributed to a decrease in metabolic performance. This was attributed to the recruitment of additional muscles in comparison to healthy controls [13]. Further, it is observed that the ground reaction force (GRF) during push off with a powered ankle-foot compared to passive prosthetic feet shows little improvement, in terms of better resembling that of a person without amputation [37]. It is possible that the socket interface may be fundamentally limiting the effectiveness of a prosthesis, even if the prosthesis replicates the performance of an intact limb locally.

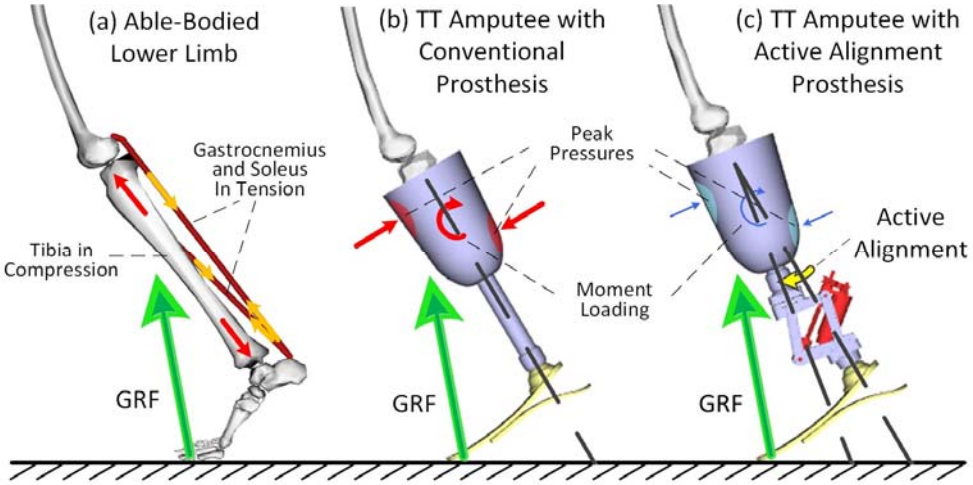

Figure 4.1: The gastrocnemius and soleus muscles in a person with amputation generate a majority of the sagittal moment about the ankle, but also counter the moment transfer through bone tissue, keeping the tibia mostly in compression (a). High peak pressures are observed on the patellar tendon and distal posterior regions of the residual limb when using a conventional prosthesis as a result of high moment transfer through the socket interface (b). The active alignment prosthesis realigns the residual limb towards the center of pressure during mid-stance to reduce moment transfer while producing net-positive work (c).

Different socket designs are used to load the residual limb with varying strategies. Load concentrating sockets such as the patellar tendon bearing (PTB) socket focus the loads in the patellar tendon and distal posterior regions of the residual limb [19,70,86] producing high cyclical peak pressures on tissues that have not evolved to tolerate such loading in a repetitive manner [72]. Other socket designs, such as total surface bearing (TSB) sockets, attempt to distribute the loads over the entirety of the residual limb to reduce peak pressures [21,87]. Even with distributing loading, pain, skin abrasions and scarring due to high inner-socket pressures are still common issues. There have been reported cases where TSB sockets are not always a better option, typically when neuromas or exaggerated bone spurs are present [87,88].

Different methods are used clinically to reduce inner-socket peak pressures. A static alignment of the prosthetic foot to the posterior of the limb reduces the peak sagittal moment generated during push off. This, however, increases the negative moment following heel strike and reduces the center of mass height during roll over [8, 11]. Compliance is often added to the socket with gel liners to distribute large forces [23], but it has been observed that thick liners reduce the sense of stability, sensory feedback and efficiency in energy transfer with increased socket movement [22].

The primary contribution of this paper is a prosthesis design approach that reduces the moment loading at the socket-limb interface, while generating net positive work. The goal is to complement the unique anatomy of a person with amputation rather than try to mimic the morphology and performance of the missing limb segment. Our preliminary biomechanical analyses and simulations have shown that near-normal whole-body gait dynamics can be achieved while also lowering moment loading on the residual limb by actively realigning the limb with respect to the foot prosthesis during gait [59]. Active alignment allows for continuously varying the prosthesis-limb relative orientation throughout stance. It enables the residual limb to be nominally aligned with the foot during heel strike and anteriorly shifted at toe off. This physically reduces the sagittal plane moment arm between the GRF at the center of pressure (COP) and the socket connection during

late stance (Figure 4.1 c). The peak moment per GRF generated is reduced while smoothly transferring power from the prosthesis to the limb during mid stance over a longer period of time, instead of in a sudden burst in late stance. During the realignment, the prosthesis concurrently lifts the body center of mass (COM) for a more natural COM trajectory, reducing the need for rest of body compensation commonly seen in gait post amputation.

This paper presents the design of an experimental, tethered robotic ankle prosthesis with active alignment. The mechatronic system is described including the sensing and control. Experimental results evaluating active alignment are performed using a bench-top setup and walking experiments using able-bodied adapters. The performance, design advantages and disadvantages, and implications of the device on whole body biomechanics are discussed. Lastly, conclusions and closing remarks about the potential design methodology and future works are made.

Figure 4.2: Active Alignment Prosthesis tethered prototype shown with protective covers and foot shell. The prototype was developed to evaluate modified gait mechanics for reduced moment loading of the residual limb and restoration of rest of body biomechanics.

4.2 Methods

4.2.1 Design of Robotic Ankle Prosthesis with Active Alignment

An experimental tethered prosthesis prototype (Figure 4.2) was developed for evaluation of active alignment in a lab environment. An optimized four-bar linkage was used to both rotate and translate the foot relative to the shank using a single actuator, shown in Figure 4.3. During mid-stance, the ball screw actuator develops a tensile force between the joint connecting posterior links and the joint connecting the anterior links. As the actuator contracts, the prosthesis extends and shifts the foot center of rotation to align the residual limb anteriorly towards the CoP. Immediately following toe off, the prosthesis quickly returns to a neutral alignment to provide ground clearance during swing.

The prosthesis linkage design parameters consisted of link lengths (l_1, l_2, l_3, l_4) and rigid attachment angles of link 1 to the shank and link 3 to the foot (θ_{l1}, θ_{l3}) as seen in Figure 4.4. Optimal parameter values were found in [25] and [26] by analyzing recorded able-bodied kinematics and

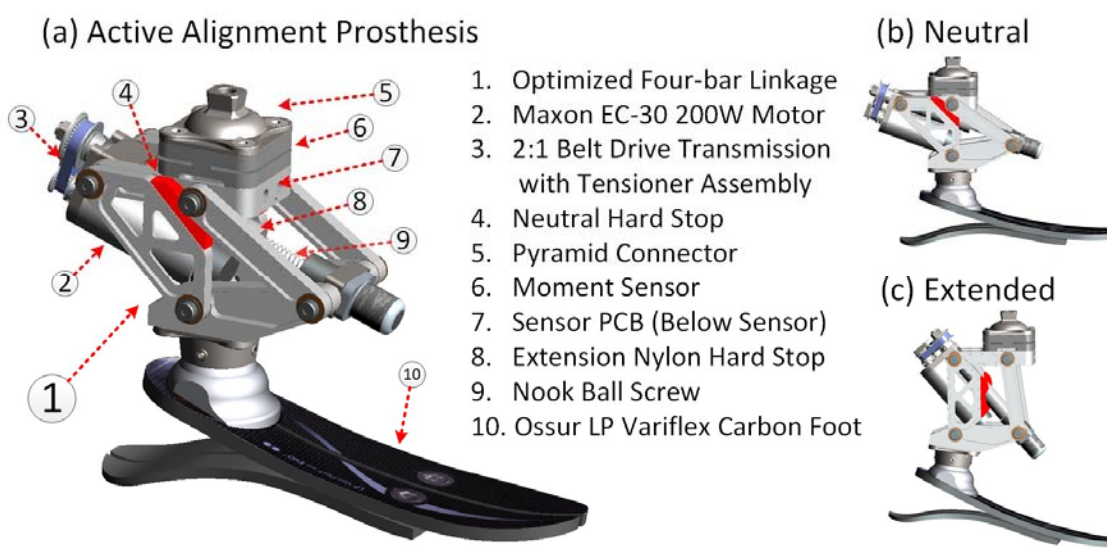

Figure 4.3: A solid model of the Active Alignment Prosthesis is shown. The design is shown without covers, featuring major components (a). The prosthesis model is displayed in a neutral position (b) and fully extended (c) showing the modified kinematics.

calculated kinematics from a model with a unilateral, transtibial amputation and the parameterized prosthesis concept, to minimize the prosthesis height with the following kinematic constraints:

1) In the "*neutral*" position, the active alignment prosthesis was not extended and aligned the model (foot, knee center of rotation and knee angle) with the able-bodied kinematic data in a standing posture. This constraint ensured that the prosthesis would perform as a conventional passive prosthesis when not being actuated.
2) The center of rotation of the affected knee and hip were aligned with able-bodied kinematics at toe off. This constraint was used to realign the rest of body to able-bodied kinematics.
3) At toe off, the knee and the prosthesis linkage were both fully extended. This constraint, was implemented to create a maximum alignment range.
4) Positive prosthesis extension always translated the foot prosthesis both posteriorly and distally relative to the socket, and plantar flexed the foot. This constraint eliminated linkage configurations that would cause the foot to reverse linear or rotational directions to arrive at the correct final alignment during extension.

Assumptions of the model with amputation were as follows:

1) The limb-socket connection was an ideal rigid joint.
2) Joint dynamics of the rest of body (head, arms, torso and unaffected leg) were restored to able-bodied values with the exception of affected limb stance knee flexion, CoP is unchanged from healthy data during walking and the energy storage and return (ESAR) foot flexed an amount calculated by the foot stiffness, body weight and CoP.

Prosthesis kinematic equations were derived, using the moment sensor, with height H_{MS} in relation to the joint connecting proximal links, as the origin. Equations 4.1 through 4.3 describe foot translations x_{foot}, y_{foot} and rotation θ_{foot} as functions of the design parameters and variable linear

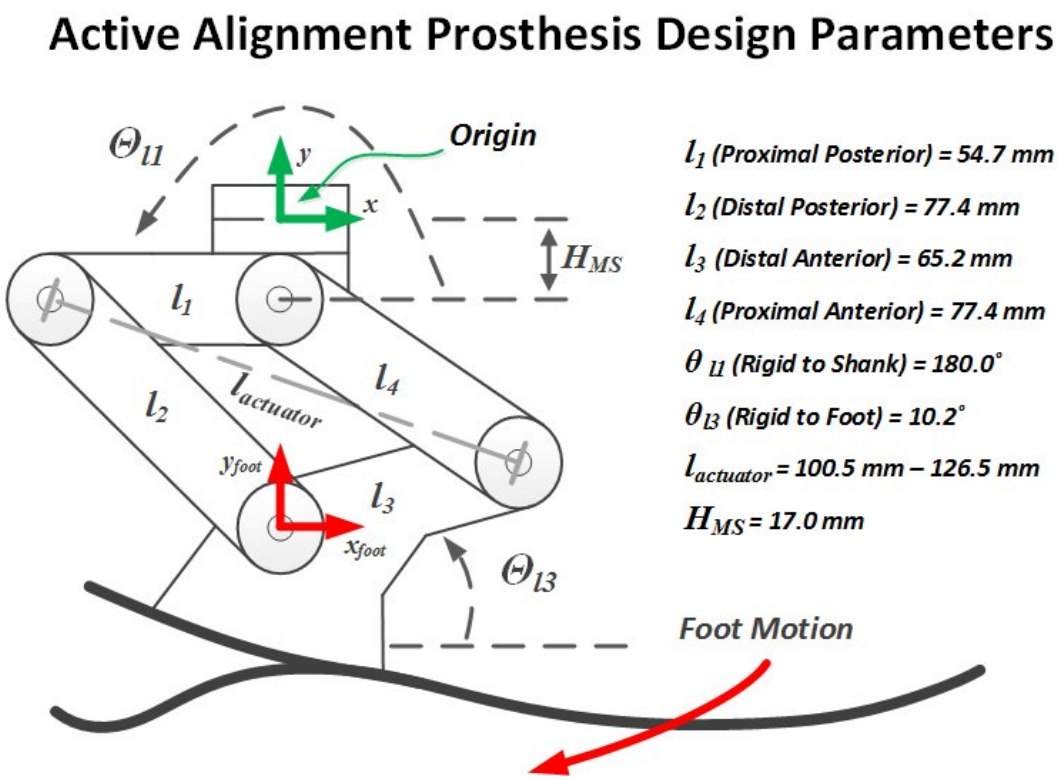

Figure 4.4: A drawing of the four-bar linkage is shown with design parameters with optimal values. The linkage motion directions xfoot, yfoot and θfoot are shown in the shank reference frame as commonly modeled in practice (proximal to distal). The foot motion can be calculated as a function of a variable linear actuator length and the given design parameters. The optimal link lengths given are the distances between joint centers on the links indicated in subscript. The optimal rigid attachment angles, of links 1 and 3 to the shank and foot respectively, are given.

actuator length $l_{actuator}$, which is the distance between the joint connecting posterior links and the joint connecting the anterior links. Design parameters consisted of static link lengths (l_1, l_2, l_3, l_4) and rigid connection angles of links 1 and 3 to the shank and foot (θ_{l1}, θ_{l3}) respectively. The foot translation was described using the motion of link 3 (fixed rigidly to the foot) with the joint connecting the two distal links as the local reference frame. These equations were used to solve for the ideal parameters with the kinematic constraints and assumptions given above. The actuator length was used as an input to attain the kinematics of the foot in relation to the residual limb with specified design parameters.

$$x_{foot} = l_1 \bullet \cos\left(\theta_{l1}\right) + l_2 \bullet \cos\left\{\theta_{l1} - 180 - \cos^{-1}\left(\frac{l_1^2 - l_4^2 + l_{actuator}^2}{2 \bullet l_1 \bullet l_{actuator}}\right) - \cos^{-1}\left(\frac{l_2^2 - l_3^2 + l_{actuator}^2}{2 \bullet l_2 \bullet l_{actuator}}\right)\right\} \quad (4.1)$$

$$y_{foot} = -H_{MS} + l_1 \bullet \sin\left(\theta_{l1}\right) + l_2 \bullet \sin\left\{\theta_{l1} - 180 - \cos^{-1}\left(\frac{l_1^2 - l_4^2 + l_{actuator}^2}{2 \bullet l_1 \bullet l_{actuator}}\right) - \cos^{-1}\left(\frac{l_2^2 - l_3^2 + l_{actuator}^2}{2 \bullet l_2 \bullet l_{actuator}}\right)\right\} \quad (4.2)$$

$$\theta_{foot} = \theta_{l1} - \theta_{l3} - \cos^{-1}\left(\frac{l_1^2 - l_4^2 + l_{actuator}^2}{2 \bullet l_1 \bullet l_{actuator}}\right) - \cos^{-1}\left(\frac{l_2^2 - l_3^2 + l_{actuator}^2}{2 \bullet l_2 \bullet l_{actuator}}\right) - \cos^{-1}\left(\frac{l_2^2 + l_3^2 - l_{actuator}^2}{2 \bullet l_2 \bullet l_3}\right) \quad (4.3)$$

Predictive, forward dynamics simulations were performed in prior work to verify the design [59]. The simulations compared a model modified to reflect transtibial amputation to an intact model tracking able-bodied kinematics. In separate simulations, the modified model was connected to the concept prosthesis, a passive ESAR prosthesis, and an active biomimetic prosthesis for comparison. Simulation results showed that the center of mass trajectory of the modified model when attached to the active biomimetic and concept prosthesis was comparable to that of the intact model, but diverged when attached to the passive prosthesis. The model utilizing the concept prosthesis showed noteworthy reduction of moment transfer at the socket-limb interface in comparison to when attached to both passive ESAR foot prosthesis and active biomimetic prosthesis.

The prototype ankle-foot prosthesis was designed to be actuated by a brushless DC motor (Maxon Motors, EC-30) rated for 200 W at 5.0 Amps nominal current and can be driven up to 15 Amps peak current. The motor was coupled to a 2.5 mm lead 8 mm diameter ball screw (Nook Industries, ECS-08025) with a 2:1 belt drive transmission for a peak linear actuator force of 1.87

kN. The ball screw was centered on opposing anterior and posterior rotational joints of the linkage with trunnion type mounts to prevent a bending moment. Current was supplied to the motor by a driver (Maxon Motors, ESCON 50/5) and supplied by a 40 V DC power supply. All control was performed in MATLAB/Simulink Real-Time Workshop (MathWorks, Natick MA) and communication to the driver and onboard sensors was done using a data acquisition (DAQ) card (National Instruments, PCI-6229) with a 1000 Hz sample rate. All analog signals were processed with a finite impulse response filter with pass and stop frequencies and amplitudes of 30 Hz and 50 Hz and 1 dB and 20 dB, respectively. Analog signals from onboard sensors were sent through a shielded cable which was grounded at the DAQ card and attached to the motor frame on the prosthesis end. The prosthesis was attached to an ESAR prosthetic foot (Ossur, Variflex LP). Neutral alignment hard stops made from urethane rubber with a shore stiffness of 80 (US Composites, POLY-75801) were molded into the lower posterior links to support the upper anterior links at neutral foot alignment. The stops provided support during standing, absorb shock load during heel strike, and limited dorsiflexion of the foot. An extension hard stop machined from nylon stock was placed around the ball screw between the posterior and anterior linkage joints to limit prosthesis extension. Geometry features of the prosthesis links were optimized for weight and a safety factor of two via feature parameterization and optimization using computer aided design modeling (PTC Creo Parametric, Needham MA) and finite element analysis (ANSYS Workbench Canonsburg PA). Prosthesis links were machined from aluminum (AA-6061), and connected with shoulder bolts (grade 8) to the actuator bearing block and ball screw nut block. Needle bearings (QBC Bearings) supported the shoulder bolts and thrust washers were cut from phosphor bronze shim stock (LYON Industries) with thickness of 0.018 inches (0.46 mm) to separate the links and reduce friction. 3D printed protective covers (Stratasys, Rehovot, Israel) prevented insertion of foreign objects and appendages into mechanism pinch-points. All remaining assembly hardware were stainless steel.

4.2.2 Sensing and Control

The prosthesis was controlled using position, inertial and force data from onboard sensors as inputs to a finite state controller and a nested closed-loop controller. Safety was a primary concern during design, and led to control features built into both hardware and software for emergency stops, limits and other features to prevent harm to the test subjects and operators.

To measure the socket moment a low-profile moment sensor was positioned at the prosthesis-socket interface [90]. The sensor was designed to be insensitive to off-axis and direct loading for accurate moment sensing, and to be compact and light-weight as not to add significant height or mass to the overall prosthesis design. Moment loads transmitted through the socket were captured to provide feedback to the controller (Figure 4.5 a). The sensor design was parameterized and optimized with finite element analysis (ANSYS Workbench, Canonsburg PA) to be strain-matched to the foil strain gages used (Vishay Micromeasurements) under maximum loading conditions (combined 120 N·m sagittal moment and 1200 N axial loading). The gages were oriented and wired to cancel out axial and off axis loading. The signal from the bridge was amplified (gain: 99.8) and filtered (50 Hz cutoff frequency) on a custom printed circuit board (PCB) (Figure 4.5 b) before being sent to the data acquisition card (National Instruments, PCI-6229) via tether. Amplifier output had a 0.0-5.0 V range which could be manually zeroed with a precision tuning potentiometer for a

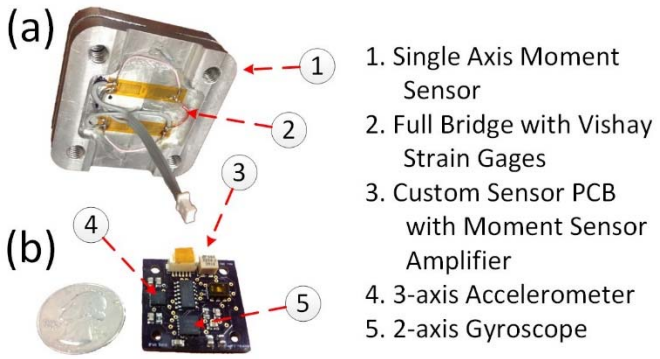

Figure 4.5: The single axis moment sensor is shown with strain gages on the underside (a) and the custom sensor PCB (b) which amplifies the moment sensor signal and measures inertial dynamics.

desired load range offset. The custom PCB also integrated a 2-axis gyroscope and 3-axis accelerometer. The motor was controlled using a current controller built into the driver (Maxon Motors, ESCON 50/5). The driver was given a desired current command which was calculated by other closed loop controllers for position, velocity, or moment control.

The controllers were implemented utilizing a proportional, integral, derivative (PID) feedback loop, which took the standard form of

$$I_M = K_P e + K_I \int e + K_D \dot{e} \quad , \tag{4.4}$$

where I_M was the current commanded to the motor driver, e was the error of the feedback being controlled, and K_P, K_I and K_D were the scheduled proportional, integral and derivative gain parameters. The gain parameters were estimated by using a model of the motor and linkage response utilizing the torque constant provided by the manufacturer to calculate prosthesis force output, taking into account the system mechanical advantage at the different amounts of prosthesis extension used in the benchtop testing. Further tuning was performed manually using the Zeigler-Nichols tuning method [91].

To ensure safety to the user and surrounding people during testing, redundant safety control mechanisms were included in the hardware, software and experiment designs. Both the operator and subject had handheld tethered emergency stop switches that turn off power to the prosthesis in the case of a malfunction. There were emergency stops built into the architecture of the motor controller and in Simulink which stopped operation in the case that over current to the motor was sensed to prevent damage to the hardware.

4.2.3 Device Characterization

Bench top characterization was performed to tune and demonstrate performance of the active alignment prosthesis. Moment sensor output and error were tested and calculated. Step response

was recorded for force and power output, and frequency response was recorded to identify the controllable bandwidth.

To characterize the moment sensor, it was removed from the prosthesis and fixed to a rigid fixture by the base of the sensor (Figure 4.6 a). An arm was fastened to the top of the sensor in order to produce known moments by hanging known masses 0.250 m from the center of the sensor. Applied moments were loaded and unloaded between static measurements of the sensor output voltage to characterize the sensor from -50 to 100 N·m. Negative moments were applied by reversing the sensor in the rigid fixture. The same tests were performed loading the sensor with known moments in the frontal plane to test sensitivity to off-axis loading. Maximum error from coupling of sagittal and frontal plane moments within normal walking load range was calculated. Known axial loads were applied as well ranging from 0 to 1000 N, recording sensor output voltages. The data were fit with linear regression lines and standard errors were calculated. Combined loading was not performed due to limited capability of applying known combined loads, i.e. if axial compression is applied with a known moment, it would not be possible to differentiate between off axis loading contributing to sensor response and coupling between axial and moment loading.

Initial tuning for closed-loop moment control required constraining the prosthesis linkage from movement during actuation such that a moment was present at the proximal end where the moment sensor was located but not at the distal end of the prosthesis. This was to prevent the test setup from being over-constrained. A rigid fixture was bolted to the moment sensor and pinned at the lower posterior link (Figure 4.6 b). In this configuration, a moment could be generated at the sensor that was a product of reaction forces at the pin, accounting for all of the forces in the system. The pinned link had multiple positions at (1%, 33%, 66%, 99% extension) so that performance could be verified through the entire range of motion. Due to spatial constraints on the rigid fixture, smaller extension increments would have required multiple testing fixtures introducing testing

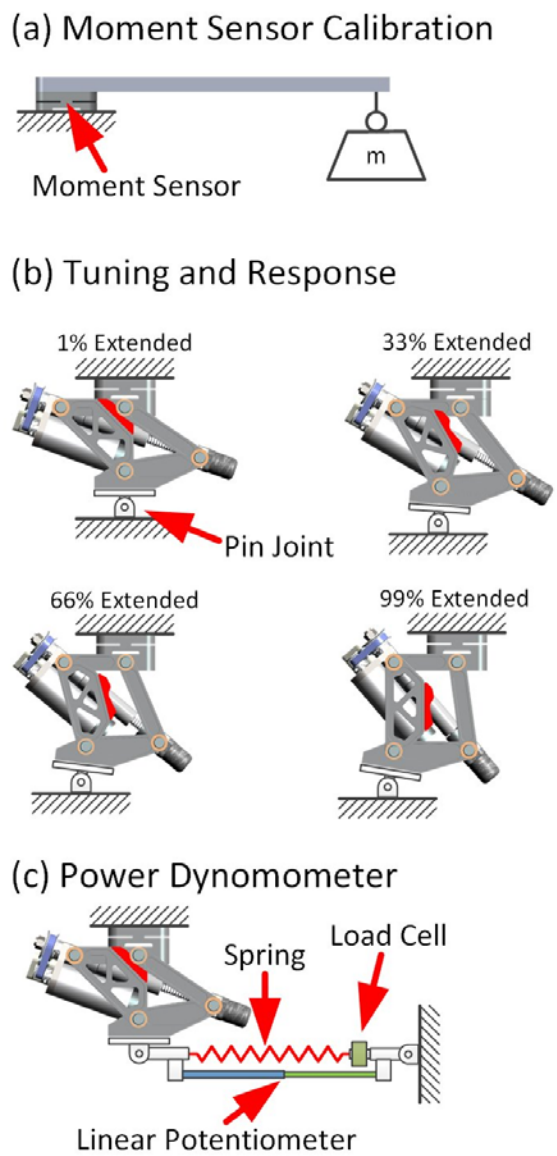

Figure 4.6: Experimental setups used for characterization and initial testing. To characterize the moment sensor the bottom was bolted to ground and a 0.25 m moment arm attached to the top to apply known moments (a). For tuning and step/frequency responses, the prosthesis was mounted rigidly to ground by the moment sensor and pinned to ground at the foot connection for zero moment loading in four increments of extension (b). For power output testing the prosthesis was mounted in a custom dynamometer that bolts the moment sensor to ground and pins the foot connection to a spring in series with a load cell and to a linear potentiometer in parallel to the spring and load cell (c).

inconsistencies and were omitted. Using Ziegler-Nichols tuning method, a PID force controller was tuned for a moment step of 40 N·m. Prosthesis response at all fixed positions were recorded.

After initial tuning, response to maximum current step command was demonstrated in the same rigid fixture used for tuning (Figure 4.6 b). The prosthesis was commanded the maximum current of 15 A, and data was recorded for ten trials at each of four positions throughout the range of motion. Due to the constraints of the rigid fixture, no moment was present at the pinned end of the prosthesis and all forces between the prosthesis and fixture were accounted for, assuming that frictional forces from small movements were negligible.

The frequency response throughout the range of motion of the prosthesis was obtained with the prosthesis mounted in the same rigid fixture used for tuning and maximum force step responses. In this test, the force controller tracked a chirp reference with feedback from the moment sensor to demonstrate closed loop force control bandwidth. The chirp signal command had an amplitude of 10 N·m and offset by 15 N·m so that loading was always positive, as demonstrated by [92], sweeping from 0 to 30 Hz over 120 seconds. The test was performed ten times at each position. Data from individual trials was post-processed, calculating cross power spectral density for amplitude response and phase shift. Data were then averaged over the ten trials for each position.

The power output of the prosthesis was evaluated by using a different characterization fixture, designed to act as a dynamometer. The fixture kept the mechanism fixed rigidly at the moment sensor and had tension springs at the foot attachment end to provide resistance during plantar flexion (Figure 4.6 c). Spring values were chosen to ensure that the motor would operate within its normal operating velocity range, and so the current controller, which was optimized for slower motor speeds at higher currents, could track the given command. The springs were attached to a uniaxial load cell (Omega, lc-202) in series to measure tension, and the load cell was attached to a pinned joint allowing only tension to be measured. A precision linear potentiometer (Omega, LP804-6) was attached parallel to the springs to measure spring deflection and estimate velocity during extension. The prosthesis was given a maximum step command of 15 A for 0.5 s to measure velocity and force output for power calculations. The current was then dropped to 7.5 A, followed

by a ramp of -1.0 A/s to unload the dynamometer without damage occurring to hardware components.

4.2.4 Active Alignment Evaluation

Active alignment for the ankle-foot prosthesis was evaluated with an able-bodied subject, prior to future testing with subjects with lower limb amputation. Able-bodied adapters were fabricated to allow a subject without amputation to walk on the prosthesis for both controller development and demonstration of active alignment (Figure 4.7). The test subject was male, 30 years of age with height and weight of 1.67 m and 69.7 kg, respectively. Testing took place in a lab setting and consisted of treadmill walking at a constant speed of 1.0 m/s. During testing, an overhead safety harness with a locking mechanism was used, as well as parallel bars alongside the treadmill for safety. The magnitude of the socket interface moment during walking was compared between active alignment tests and neutral alignment tests.

An initial walking controller was developed and implemented for early evaluation. A finite state machine monitored data from prosthesis sensors in real time to regulate gains and references

Figure 4.7: Experimental prosthesis able-bodied adapters allow a person without amputation to walk on the prosthesis for preliminary testing. The contralateral limb is attached to a pylon and matching passive ESAR foot prosthesis aligned to match the neutral (retracted) position of the experimental prosthesis. The use of adapters accelerates the controller development and tuning without the need for test subjects with amputation.

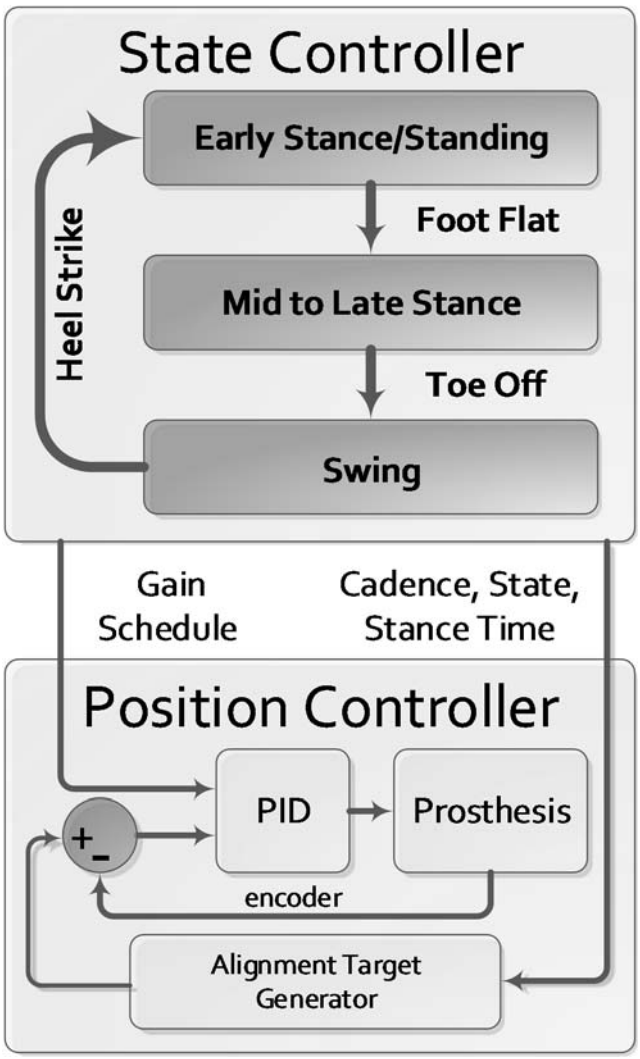

Figure 4.8: The flow diagram of the control methodology used is presented. A finite state controller is used to schedule gains for a PID position controller for each state. A reference target is calculated for each state based on cadence, state and the stance time of the previous step.

used by a position controller throughout all phases of walking (Figure 4.8), similar to [93]. The finite state machine divided walking into three phases: early stance, mid to late stance, and swing, only allowing forward progression through gait when transition events were detected. The transition events consisted of heel strike (HS), foot flat (FF), and toe off (TO), each triggering updates for controller gains and reference targets used by the position controller based on the walking state, cadence, and stance time. Events were detected when moment (M), moment

derivative (*dM*) and angular acceleration (α) of the residual limb exceeded threshold combinations based on recorded walking data when the prosthesis was regulated at the neutral position. For ease of laboratory testing, the controller was automatically activated if mid- to late stance time is less than 0.7 seconds for 4 consecutive steps. Once active, the controller automatically deactivated if late stance time exceeds 1.0 second in order to avoid unwanted deactivation when slowly changing walking speeds.

During early stance from HS to FF (measured global shank angle of zero), a low gain position controller held the foot at a neutral alignment. This prevented extension due to negative moment upon HS. At FF, the gains were increased as the position controller tracked a moving reference. The moving alignment reference, ψ^k, for step k had a derivative, $\frac{d\psi^k}{dt}$, that equaled the target alignment, ψ_{target} (desired maximum extension percent for the current step k), divided by the previous step stance time, t_{stance}^{k-1}, multiplied by an alignment coefficient, $\lambda_{alignment}$, as seen in (4.5). The alignment coefficient, $\lambda_{alignment}$, is the inverse of the intended percent of stance that alignment was to occur. By integrating (4.5), we attained the moving alignment reference, ψ_n^k, in (4.6) for sample *n* during stance. For initial testing, $\lambda_{alignment}$ was set to 2 in order to ensure that the alignment occurred before push off in late stance and the target alignment used was 100% to demonstrate full actuation. When the target alignment was reached, the reference signal became constant until TO was detected. The swing state then gave a neutral position reference and the prosthesis quickly retracted to a neutral position for swing phase foot clearance. With this method, the reference target velocity during stance was a function of walking speed, and the controller quickly adapted to different cadences.

$$\frac{d\psi^k}{dt} = \lambda_{alignment} \frac{\psi_{target}^k}{t_{stance}^{k-1}} \tag{4.5}$$

$$\psi_n^k = \psi_{n-1}^k + \int \lambda_{alignment} \frac{\psi_{target}^k}{t_{stance}^{k-1}} dt \tag{4.6}$$

To demonstrate active alignment able-bodied adapters adapted from [94] and shown in Figure 4.7 were fabricated to allow a person without amputation to walk on the active alignment prosthesis. The adapters were fabricated from modified roller blades (Roller Derby Proline 900) bolted to AA6061 plates, and standard off-the-shelf pyramid connectors. One adapter was attached to the active alignment prosthesis and the contralateral adapter was attached to an un-instrumented pylon and matching passive ESAR foot. During treadmill walking at a constant speed of 1.0 m/s, sensor data were collected for ten steps when implementing active alignment mode, and ten steps when regulating the static neutral alignment throughout stance. During post processing, recorded data were smoothed with a moving average filter with a 10 sample window to remove artifacts and high frequency noise, normalized to body mass, resampled to normalize time to percentage of stance and averaged over the ten steps. Initial testing did not include full body biomechanics data.

4.3 Results

The active alignment prosthesis is an experimental prosthesis built to explore the benefits of altering residual limb kinematics to reduce loading demands, rather than merely mimicking physiological form and function of the lost limb. The experimental prosthesis is 18.4 cm tall and weighs 1.9 kg as tested, including the foot shell. During extension, the foot rotates 10 degrees, translates 54.7 mm posteriorly and 22.7 mm distally. Link lengths and attachment angles are given in Figure 4.4.

The socket moment sensor was tested and calibrated for a range of -50 to 100 N·m (Figure 4.9). The sensor produced a mean of 25.5 mV/N·m applied. All measurement errors were less than 1.55 N·m, and the RMS deviation was 0.53 N·m with pure sagittal moment loading. Off-axis frontal plane moment loading showed a sensitivity of 0.22 mV/N·m, and direct axial loading was not

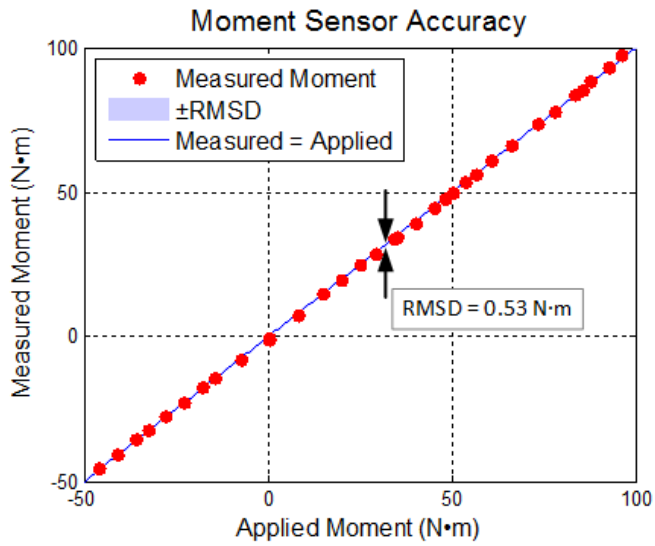

Figure 4.9: Moment sensor accuracy showing the known applied moment in comparison to the moment recorded by the moment sensor, and the RMS deviation as a shaded region.

measurable due to uncertainty of whether the axial loads were perfectly perpendicular to the sensor. Calculated coupling of sagittal and frontal plane moments produced a maximum error of 2.1% with normal frontal moment loading during gait.

Step responses to maximum current command were recorded to examine moment response times. The prosthesis was constrained from movement in four extension positions having different mechanical advantage for ten trials each. Extension positions were 0%, 33%, 66%, and 99%. Peak moment rise times were no more than 60 ms for 90% of the maximum recorded value in all trials. Response when fixed at 66% extension can be seen in Figure 4.10.

The frequency response was evaluated at the same extension percentages of prosthesis travel. In all positions, the prosthesis resonated at 20 Hz, and entered into higher modal frequencies above 22 Hz. Although the standard bandwidth cutoff of -3 dB in magnitude was never seen, the phase shifted rapidly as it became unstable and entered higher modes of vibration. The maximum controllable frequency was measured at 20 Hz for all positions. Figure 4.11 shows the frequency response of the prosthesis extended to 66% with standard deviation that overlaps with the response at all other extension amounts.

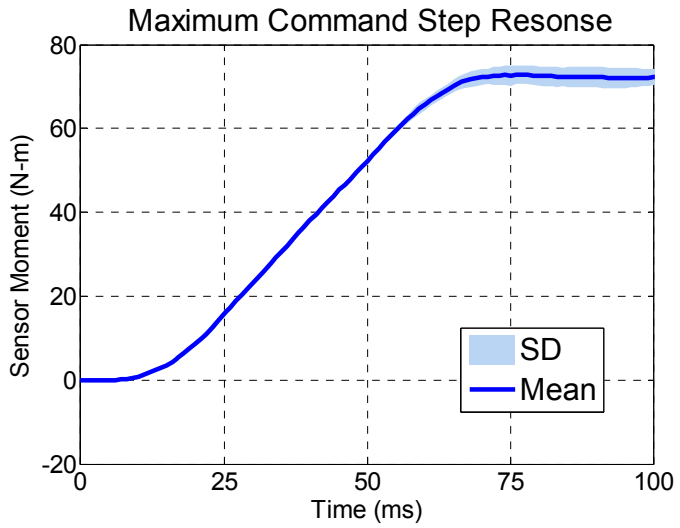

Figure 4.10: Moment generated at the moment sensor of the prosthesis when fixed extended 66% in a bench top jig and commanded a maximum current to the motor. Average rise times at all positions were less than 60 ms for 90% final value, having standard deviations that overlapped.

Peak mechanical power output of the prosthesis was measured to be 511 (±11.3) W, mean and standard deviation. The dynamometer was driven to a linear velocity of 1.10 (±0.02) m/s and measured 460 (±2.65) N at peak power for a mechanical efficiency of 85%. Motor current was saturated at the time of peak power.

Walking test results are shown in Figure 4.12. The plot shows the sagittal plane moment recorded from the moment sensor during the stance phase of walking, normalized to body mass, when walking at a constant velocity of 1.0 m/s. The dataset in red (dashed line) presents the average and standard deviation of the moments from ten steps when the prosthesis regulated at a neutral position, emulating a passive prosthesis. The dataset in blue (solid line) presents the average and standard deviation of the moments from ten steps recorded when implementing active alignment. Average peak moments for regulated neutral alignment and active alignment were calculated to be 1.22 ±0.09 N·m/kg and 0.81 ±0.06 N·m/kg respectively. The results show that the peak moment

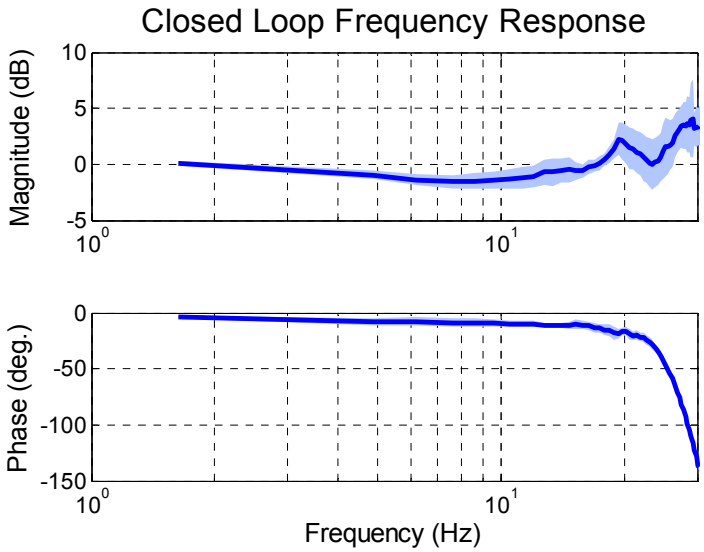

Figure 4.11: Closed loop force control frequency response of the prosthesis extended 66%. Fixed in a bench top characterization apparatus, the system was very stiff and didn't display magnitude cut-off. The prosthesis was observed to be controllable up to about 20 Hz. Shortly after resonating at about 20 Hz, the response exhibited higher modalities and became unstable. Responses in all amounts of extension were similar, having standard deviations that overlapped with the response shown.

during late stance was reduced by 33.6 percent on average when active alignment was implemented.

4.4 Discussion

An experimental prosthesis has been developed to evaluate active alignment in a lab setting. Active alignment shifts the residual limb anteriorly in relation to the foot and center of pressure during mid-stance. The prosthesis reduces the effective moment arm between the ground reaction force and residual limb, while retaining energy storage and release in the foot prosthesis, as well as push off capabilities of an active prosthesis. Peak moment transfer at the socket interface during push off is reduced which is commonly associated with peak socket pressure. The device as developed is experimental and meant only for evaluation of the approach during level ground walking, in order to determine concept validity and feasibility. For this initial study, other activities of daily living are not addressed. Preliminary walking tests reveal that the moment is substantially reduced when active alignment is implemented in comparison to equivalent tests of neutral

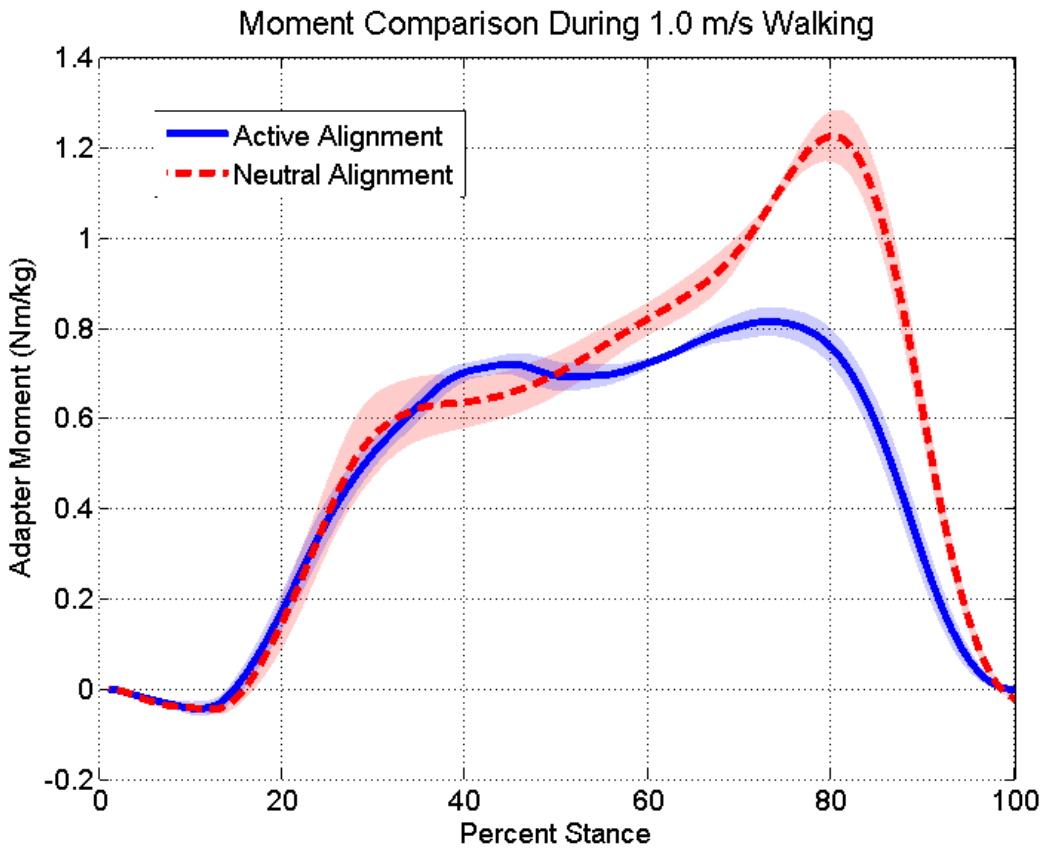

Figure 4.12: Comparison of moments recorded by the prosthesis moment sensor while walking on a treadmill at a constant speed of 1.0 m/s while the prosthesis is regulating at a neutral alignment (red), and actively aligning (blue). Solid lines are means averaged over ten consecutive steps and shaded areas are standard deviations. The recorded data show a peak moment reduction of 33% during active alignment.

prosthesis alignment. These results suggest that implementing the novel functionality of active alignment into future transtibial prosthesis designs may lead to a more comfortable gait for persons with amputation, which could lead to increased mobility and enhanced quality of life.

The experimental ankle prosthesis is based on a four-bar linkage which rotates the foot while translating the foot center of rotation in the shank reference frame for active alignment. There are other mechanisms that can achieve active alignment, such as multiple degree of freedom prismatic joints in series; however, this linkage was chosen for simplicity and it needs only a single actuator. The four-bar linkage also acts as a variable ratio transmission. The mechanical advantage of the

device increases while the linear actuator pulls the anterior and posterior link joints closer in proximity. This increases the end effector to linear actuator force ratio as the prosthesis extends. In late stance, a greater linkage force is needed to overcome the larger reaction moment generated in the foot. The variable ratio feature is advantageous, as it enables more force to be generated by the actuator as the demand increases.

The link lengths and attachment angles of the prosthesis linkage are optimized based on able-bodied walking biomechanics and simulations of corrected biomechanics when a limb is missing. The constraints chosen to design the linkage were based on the assumption that active alignment can restore biomechanics (joint forces and trajectories) to near normal values in the rest of the unaffected body, starting at one joint removed from amputation. It must be noted that the design constraints and modeling assumptions used are ideal. They are considered to be initial design criteria made in order to realize a new paradigm of prosthesis design, with the understanding that future work may require us to refine our approach. Future constraints will be based on findings from biomechanics analysis of gait while persons with amputation use the prosthesis prototype, testing validity of the assumptions.

The linkage is driven by a high power motor coupled to a pulley transmission and ball screw. Characterizations of performance were completed on the actuator and custom moment sensor. The moment sensor is seen to have a high linearity and repeatability having an RMS deviation of 0.53 N·m between measured and actual applied moments when applying and releasing loads ranging from -50 N·m to 100 N·m. This is within the range that is normally observed during normal walking for an able-bodied person having up to 83 kg of body mass. In order to accommodate larger persons a redesign would be required of the pulley transmission with a higher reduction ratio. The linkage acting as a variable ratio transmission is observed to be advantageous due to the increase in moment demand as stance progresses during walking. This has the potential to allow smaller motors to be used assuming that the control strategy times the alignment to begin when loading demand is low.

The prosthesis was found to be controllable up to 20 Hz throughout the entire range of motion demonstrating adequate bandwidth for normal walking speeds where cyclic loading is normally observed to be an order of magnitude less.

Preliminary tests performed to emulate gait of individuals with amputation utilized able-bodied adapters, which effectively elongated the shank. The tests reveal that the peak sagittal moment generated is on average 33 percent lower with active alignment in comparison to neutral aligned walking tests. It is also seen that after foot flat, when the prosthesis is actuating, the moment is slightly higher than normal (Figure 4.12). This may be a result of positive work performed by the prosthesis during that time, however work was not evaluated in this study. There are many unknowns about walking stability and the true dynamic interaction of the device and residual limb that may be clarified in future work including full body biomechanical analyses on persons with amputation. However, while observing an able-bodied subject walk with adapters there was no noticeable instability throughout gait, including when the device actuated during single supported stance and retracted following toe off. Although complete biomechanics analyses were not performed during preliminary testing, the gait did appear reasonably normal despite the extended shanks. The test subject was able to adapt very quickly to both the prosthesis adapters and the active alignment. The subject also reported that they were easy to walk on. Future biomechanics studies involving test subjects with amputation will examine center of mass trajectory, work performed by the contralateral limb, net positive work generated by the prosthesis and subject metabolic cost.

The preliminary prototype is heavy, weighing 1.9 kg; however, the focus of this prototype is to study the effects active alignment has during walking in a lab setting. Future iterations of the device will need to be lighter and could show more promise in reducing metabolic cost and compensation by the rest of body. The moment sensor only accounts for a portion of the dynamics and does not provide insight to the linear force components being transferred or center of pressure. A multi-axis load cell or pressure sensors in the prosthesis heel and toe would give insight to the center of

pressure and effective moment arm in real time. This would allow for more sophisticated control approaches that rely on complete dynamics being known and used for feedback. Additional future improvements will include a more compact design, improved cosmetics, a dedicated embedded system with a battery pack, and control methodologies that allow different activities throughout the day in a normal setting.

Although initial walking tests performed by a subject with intact limbs appear to be successful, it is unclear at this time how subjects with amputation will react to modified stance kinematics, and if there are limits to kinematic modifications that will be perceived as stable. This is mainly due to the limited knowledge of the socket-limb kinetics. The assumption that only stance phase knee flexion will be modified may be false, and changes to the hip joint trajectories may also be modified if the person feels they need to better support themselves during the active limb alignment. It is anticipated that an adaptive controller which gradually increases the amount of alignment from step-to-step as a subject begins to walk will be beneficial and more intuitive to use. This will allow a more natural transition into an altered gait as the subject gains confidence in the modified mechanics.

4.5 Conclusion

In this paper, a tethered ankle prosthesis prototype was designed for evaluating active alignment during walking in a lab environment. Initial walking tests show a peak moment reduction of 33 percent at the prosthesis connection when active alignment is implemented, in comparison to neutral prosthesis alignment. These results demonstrate that active alignment may be implemented in powered lower limb prostheses to improve loading conditions for a more comfortable gait for persons with amputation.

Future work involves developing an improved adaptive control methodology to slowly increase the amount of realignment with each progressive step as a person gains confidence in the new

device and modified gait mechanics. Full body biomechanical analysis on persons with amputation will follow for evaluation in a lab environment, giving insight to design requirements to be applied in future prosthesis designs realizing active alignment. Additionally, more work is needed to find optimal prosthesis kinematics and kinetics that can restore rest of body biomechanics with tolerable limb loads.

4.6 Acknowledgement

This work was supported in part by grants from the National Science Foundation (IIP-1439683 and IIS-1526986) and National Center for Simulation in Rehabilitation Research (NCSRR, Stanford University).

CHAPTER 5

A CONTROL STRATEGY FOR AN ACTIVE ALIGNMENT TRANSTIBIAL PROSTHESIS

This chapter is taken from a paper presented the ASME 2015 Dynamic Systems and Control Conference (DSCC), written with second author Professor Frank Sup of UMass Amherst and published in the conference proceedings [61]. Here we outline a basic control strategy used to demonstrate Active Alignment with a real-time adaptive controller. The controller is able to adapt on a step by step basis to account for the users walking speed. Results from this chapter demonstrate usability of the device in a laboratory environment.

Abstract— This paper presents a control approach for an experimental transtibial prosthesis (Figure 5.1) that can actively realign the residual limb in relation to prosthetic foot during the stance phase of gait. The realignment objective is to inject positive power into the gait cycle while actively reducing the magnitude of the sagittal moment transferred to the residual limb. The altered gait dynamics of this new type of prosthesis require a control approach that coordinates its function with a user's gait cycle. This paper overviews the mechanical design of the prosthesis development, the proposed finite-state adaptive controller, and presents experimental results for constant cadence walking and adaptation while changing walking speeds.

5.1 Introduction

Amputees are faced with a physical challenge that compromises their ability to maintain health and mobility. When using a prosthesis to overcome their altered physiology, an amputee must adapt to the resulting system in order to ambulate to the best of their abilities. Commercial and experimental prostheses to-date have aimed to restore an efficient gait by replacing the lost limb

Figure 5.1: Experimental tethered robotic prosthesis with active alignment, shown with covers installed (top) and removed revealing mechatronic internals (bottom).

with passive and active components that are optimized for energy storage/return and added power [2]. These devices improve gait, however, they have not yet restored efficiencies to able-bodied norms. Further, other health problems related to loading of the residual limb are still prominent with passive prostheses such as increased back pain, pressure ulcers and early onset osteoarthritis in the intact limb [10,48,50,95].

The residual limb consists of remaining bone surrounded by muscle, tendons and other soft tissue [96]. For an amputee, the ground reaction forces are transmitted through the soft tissue on the residual limb. This interface has a significant impact on the amputee's ability to transfer load

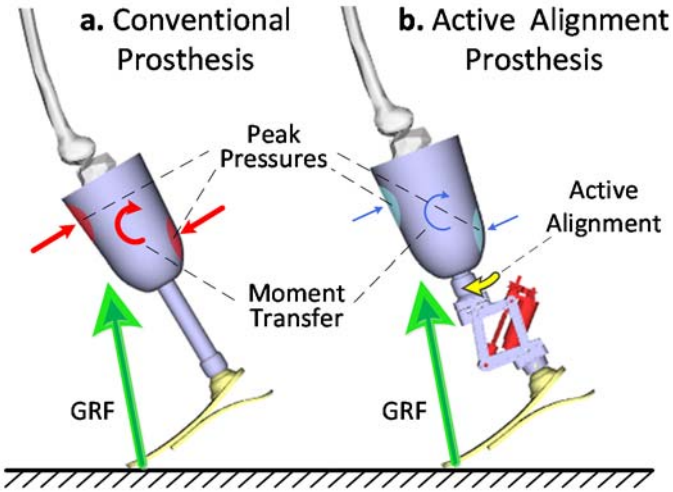

Figure 5.2: During gait, large sagittal moments from ground reaction forces acting on the prosthetic foot must be transferred through the socket interface, resulting in high pressure concentrations on the residual limb (a). The active alignment prosthesis aligns the limb with the center of pressure during mid to late stance, reducing the moment while transmitting power (b).

to the ground and passive whole body motions resulting from residual limb movement within the socket. Additionally, an amputee's discomfort from high pressures on the residual limb result primarily from the large sagittal moments generated during late stance [51] (Figure 5.2 a.).

Another important post-amputation difference is that the gastrocnemius muscle is normally biarticular, acting across both knee and ankle joints; healthy coupling of joint forces enables effective energy transfer [55,56] and contributes to whole body angular momentum [57]. The coupled forces are not present when the gastrocnemius muscle is severed, resulting in less effective energy transfer between the intact knee and prosthesis. Likely, additional muscles are needed to compensate which leads to increased metabolic energy costs for amputees [37,44,45]. The combined loss of functionality renders the amputee unable to produce and transmit forces as an able-bodied person would and results in an inefficient gait.

State-of-the-art robotic prosthesis technology focuses on restoring gait efficiency by replacing the lost limb with a device that best replicates the biomechanics lost. The commercial BiOM

consists of an actuated one degree of freedom (DOF) pin joint ankle driving an energy storage energy return (ESER) foot [83,97]. While it has been shown to be capable of healthy performance and to add power to the stride, whole body walking mechanics still show little increase of ground reaction forces and whole body angular momentum compared to walking with passive devices [37]. Another device developed at Michigan Technological University explores the impact a multi-DOF ankle joint in the sagittal and frontal planes to aid turning and walking on uneven terrain [98].

It is clear that there is a loss of efficient energy transfer between the amputee and prosthesis during walking. Even with newer robotic prostheses having the capability to produce healthy mechanics, and good fitting sockets having little movement, amputee gait still appears to have limits that stem from the amputee physiology and the connection of the prosthesis to the residual limb. An asymmetric gait may always be the result of a loss of functionality.

Previously, the authors presented the concept to design active lower limb prosthetic devices with additional coupled DOFs that act to reduce loading of the residual limb [58]. Rather than aiming to replicate normal biomechanics, this new approach seeks to explore alternative ankle mechanics designed via simulation to redirect loading during gait. Walking kinetics are intentionally altered, aligning the residual limb in relation to the center of pressure (CoP), while increasing net positive work (Figure 5.2 b.). This paper presents a control approach and preliminary results for a previously developed ankle prosthesis with active alignment. A prototype device has been developed and shown in Figure 5.1. A control methodology is presented for intuitive and natural interaction with the amputee. Experimental results are obtained that show the effectiveness of the device and controller using an able-bodied adapter.

5.2 Methods

This paper realizes a robotic ankle prosthesis design concept previously presented by the authors, that has the capability to shift center of rotation (CoR) of foot during stance in order to

Figure 5.3: Experimental prosthesis able-bodied adapters allow a non-amputee to walk on the prosthesis for preliminary testing, controller development and tuning without the need for test subjects.

realign the residual limb in relation to the CoP [58,59]. The prosthesis is optimized to reduce moment transfer to the residual limb and restore rest of body biomechanics to healthy conditions. Based on this concept, a tethered prototype was built that consists of a four-bar linkage in series with an ESER carbon foot (Ossur Variflex LP), driven by a DC motor (Maxon EC 4-Pole 30mm, 200W) coupled to a 2:1 belt drive that actuates a ball screw. As the linkage extends, the foot rotates and the CoR is shifted to the posterior. This dynamically reduces the effective moment arm which the ground reaction force acts at. The result of the altered kinematics is reduced peak moments during late stance while energy is injected into the gait cycle.

To develop a control methodology and tune parameters, an able-bodied adapter was designed and fabricated. Two adapters allow a non-amputee to walk on the test prosthesis with minimal ankle movement, emulating a socket connection. The use of adapters reduces time needed for test subjects, greatly cutting development time. The adapter design was adapted from [94] and is based on a modified in-line skate boot (Roller Derby Proline 900) which is stiffened with an aluminum foot plate in order to attach a standard adjustable female pyramid connector. The prototype prosthesis is connected to one adapter and an aluminum pylon, and a passive ESER foot (Ossur

Variflex LP) is attached to the contralateral adapter. Using common clinical prosthesis alignment techniques [99], the neutral alignments of boot adapters, prosthesis, pylon and feet were adjusted until little effort was needed to maintain balance and walk comfortably. The user was able to walk normally without the use of a handrail or crutch.

Treadmill walking trials took place in the Mechatronics and Robotics Research Laboratory at the University of Massachusetts Amherst. The test subject is a healthy male non-amputee, 1.67 m and 70 kg in height and weight. The subject was tasked to walk with the able-bodied adapters on a treadmill with an overhead safety harness. Trials consisted of constant and varying walking speeds ranging between 1.0 to 3.0 m/s. The subject walked both while the prosthesis was passive (not powered) and active using the walking controller described in Figure 5.4.

5.3 Controller

The walking control strategy uses a finite state controller that schedules gains for different phases of gait as shown in Figure 5.4. The transitions occur at heel strike (HS), foot flat (FF) and toe off (TO) which are detected in the main walking control loop. Event detection is based on fixed thresholds of feedback from the prosthesis moment and inertial sensors. The state loop can only progress in a forward manner. Each state utilizes a feedback controller that tracks a static or dynamic target alignment reference, and has the capability to adjust target references on a step by step basis based on estimated cadence and inertial feedback.

Event thresholds were determined by first collecting sensor data while walking on the prosthesis at different speeds from 0.5 m/s to 1.5 m/s. To prevent unintentional extension due to foot rebound and inertia when entering and during swing phase respectively, a low gain position controller was utilized to regulate the prosthesis at a neutral position with zero percent extension. Examining the data, it was determined that moment, moment derivative, sagittal angular velocity and angular acceleration could be used to identify events in real-time. At HS for all walking speeds,

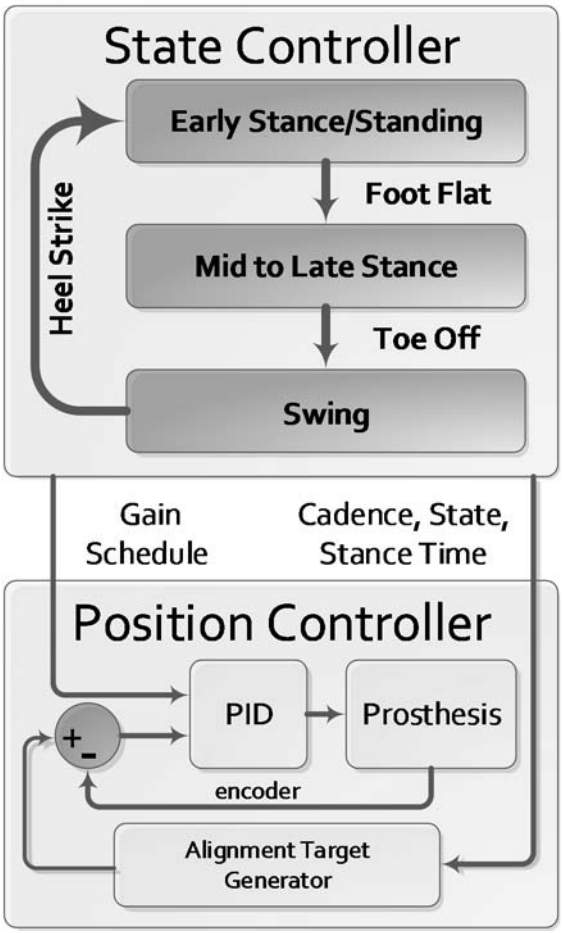

Figure 5.4: A flow diagram of the control methodology is shown. A finite state controller is used to schedule gains for a PID position controller for each state. A reference target is calculated for each state based on cadence, state and the stance time of the previous step.

the moment and moment derivative were both observed to be negative, and angular velocity and acceleration were observed to be above 50 deg/s and 2000 deg/s2. FF was detected with positive moment and moment derivative, and TO was detected when the moment dropped below 5 N-m and the moment derivative was negative.

Upon HS, the finite state controller enters early stance mode. During this mode, low gains are scheduled to the position controller, which regulates the actuator at zero percent extension. Although the user's bodyweight is supported by bushings within the prosthesis, this controller stiffens the device and prevents extension when a negative moment is generated during early stance.

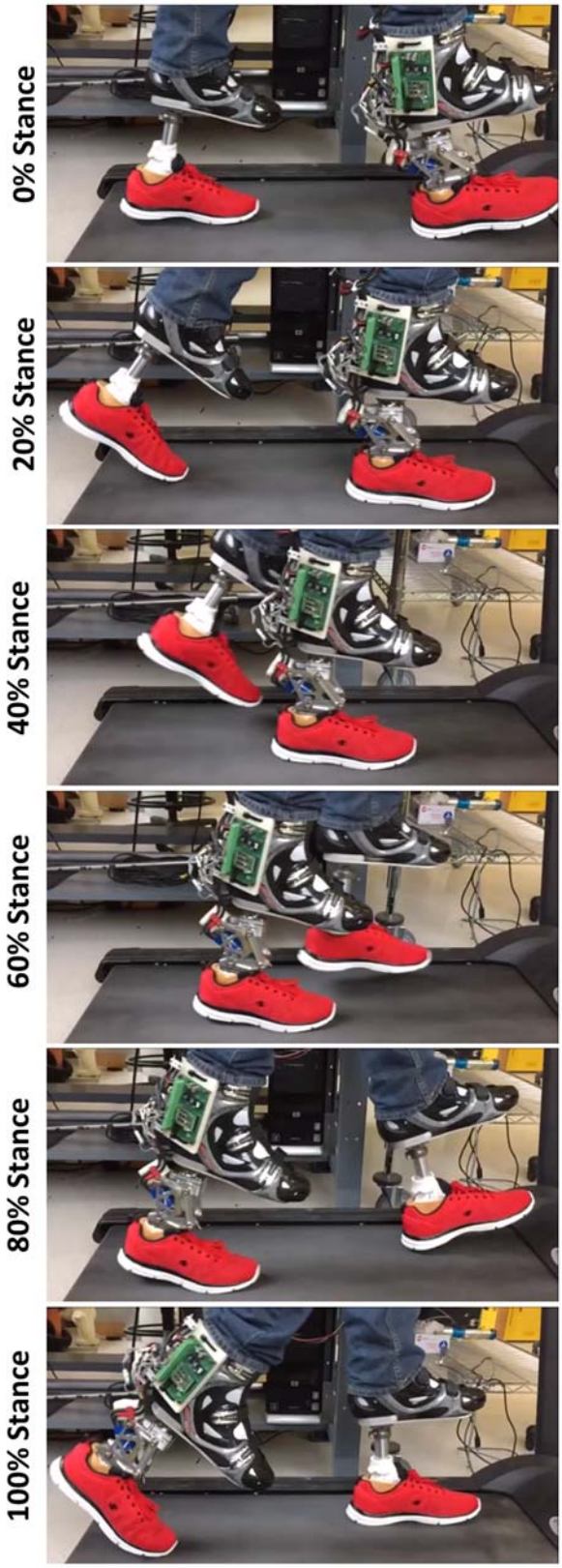

Figure 5.5: Able-body adapter implementation during treadmill walking showing active alignment different phases of gait.

When FF is detected, the state controller enters a mid-to-late stance phase. The mid-to-late stance phase schedules high gains to the position controller which tracks a moving target. This enables the alignment to adapt to the user's cadence on a step by step basis. During alignment, a moving target is implemented in order to distribute power input throughout mid-to-late stance. This prevents a large power burst in late stance. The target generator has an adjustment component that updates the target alignment rate at each step which is proportional to the calculated cadence. When the prosthesis is within five percent of a predetermined final alignment value, gains are scheduled for better damping and the target becomes static to prevent stalling the motor at the end of the prosthesis range of motion. This also enables the capability to prescribe different amounts of total alignment for late stance.

5.4 Results

The objective of this work is to evaluate the dynamic performance and finite-state control approach of the Active Alignment foot-ankle prosthesis. Figure 5.5 shows a time sequence depicting the stance phase during active prototype control during an experiment. At heel strike the foot is fully retracted and impact is absorbed by the ESER foot and the linkage is supported by rubber bushings within the prosthesis. By 60 percent, the ankle has started to actuate and is nearly fully extended by 80 percent when the peak moment is experienced.

Figure 5.6 presents a comparison of the moments measured at the boot coupling while the prototype is active (powered) and in the neutral position (unpowered) while walking at 1.0 m/s, which corresponded to a cadence of 100 steps/min. The shaded region represents plus and minus one standard deviation for the ten captured steps for each condition and provides a measure of the stride variability. In the neutral alignment, the prototype acts as a passive ESER prosthesis and exhibits a pattern similar to that observed in amputee gait [71]. The maximum observed boot moment connection is 1.2 Nm/kg which is higher than observed in amputees (0.8 Nm/kg), but can be attributed to the increased stride length (longer limb segments) and altered dynamics while using

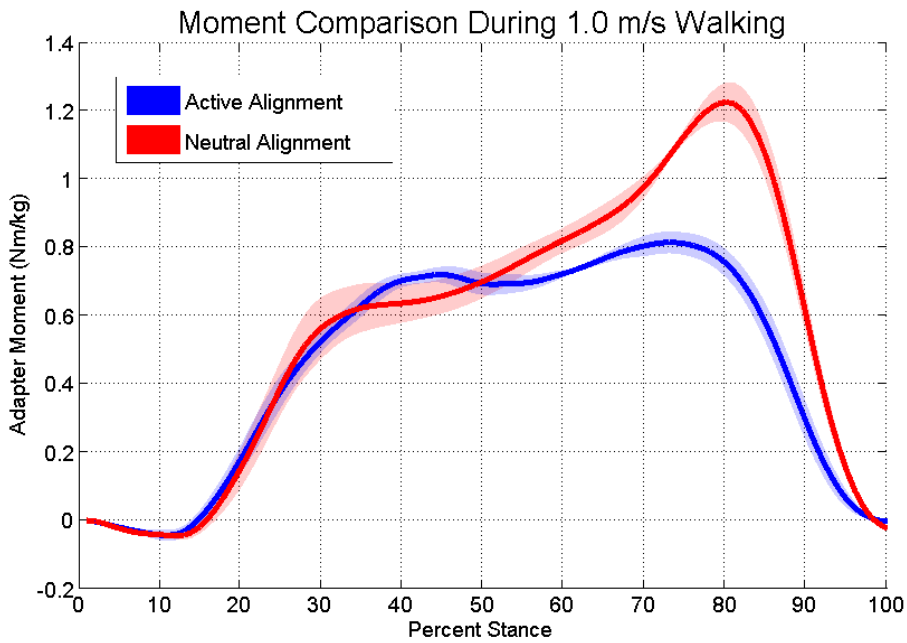

Figure 5.6: Comparison of moments recorded by the prosthesis moment sensor while walking on a treadmill for 10 steps at a constant rate of 1.0 m/s while the prosthesis is regulating at a neutral alignment (red), and actively aligning (blue).

the able-bodied adapters. Up to about 40 percent of stance the neutral and active responses closely align, however there is a small increase in the moment transfer when the active prosthesis is engaged, and power is introduced. It is observed that the active alignment reduces the magnitude of the moment in late stance. Further, the peak magnitude is reduced to 0.8 Nm/kg, a 33 percent reduction.

Figure 5.7 presents data from a single trial showing the prosthesis alignment rate and moment transferred to the boot adapter while changing walking speeds from 1.3 m/s to 0.9 m/s. Examining the data, it can be seen that as the cadence slows, peak alignment target rate (red line) adjusts and decreases as the target generator reduces the rate of moving targets during late stance. As the treadmill slows down, peak moments are seen to be reduced as the test subject slows down not needing to push-off as hard due to the changing speed. The moment increases slightly at the end of the trial when the treadmill speed becomes constant and the subject has to increase push off to

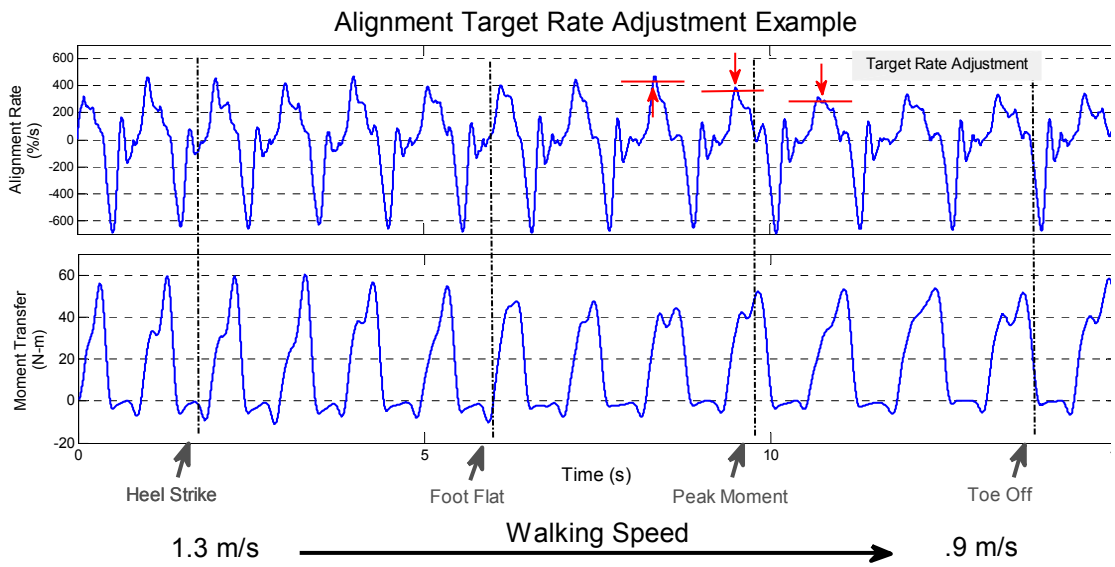

Figure 5.7: Shown is treadmill walking while reducing from a fast pace of 1.3 m/s to a medium pace of 0.9 m/s. Data is from a single trial showing the prosthesis alignment rate (top) and moment transferred to the boot adapter (bottom). At foot-flat, the controller begins to align the residual limb. At late stance, the alignment is complete, and the effective moment arm is reduced before peak ground reaction forces and peak moments occur. As the walking speed changes, the controller regulates the alignment target rate on a step by step basis based on previous steps in an iterative learning fashion. At toe-off the controller quickly aligns the prosthesis to a neutral position during swing.

maintain velocity. Although moment is changing due to user input, the controller doesn't alter its generated target at a constant velocity since it is based on cadence.

5.5 Discussion and Conclusion

The actuation and control approach presented distributes the actuation throughout mid-to-late stance instead of providing a burst of power at the end of stance as seen in biomimetic approaches of prosthetic design, and in healthy human gait. The extended actuation time reduces dynamic loading on the limb, and requires a smaller motor and peak actuation power. A significant result of this work is that it provides a new solution to the dynamics of bipedal amputee walking. Further exploration is required to fully map the design parameters of the prosthetic ankle to the overall gait performance of the amputee.

Additional future directions include a focus on improved gait detection to avoid missing recognition of heel strike. During walking, this could result in a fall. Further development of event detection should be performed for a more robust controller. The cadence adaptation is observed to quickly change the target alignment rate as the user changes speeds, however the magnitude of the target alignment was fixed in all trials to the maximum prosthesis extension. This has the possibility of being parameterized and should be adjusted as well in future work. Transitions from standing to walking mode was observed to be abrupt. This could be made more natural by making the adaptation a function of steps taken since standing, as well as adjusting the target alignment. Future work includes further development of the controller to make it more robust in event detection and have better adaptive capabilities, and analysis of full body biomechanics including linear forces at the socket joint. Prior to testing in a gait lab with test subjects, trials will be conducted on a treadmill in order to tune the controller parameters further, and allow the test subject to become accustomed to walking on the device.

5.6 Acknowledgement

Supported in part by a grant from the National Center for Simulation in Rehabilitation Research.

CHAPTER 6

AN APPROACH FOR WHOLE BODY INVERSE KINEMATICS AND INVERSE DYNAMICS INCLUDING THE RESIDUUM-SOCKET INTERFACE UING MARKER-BASED MOTION CAPTURE

This chapter highlights our approach of performing whole body biomechanics analyses on marker and force data collected from persons with lower limb amputation. Current standard practices of performing inverse kinematics analyses are designed for tracking body segments with experimental markers on each segment with a kinematically constrained model. Modeling transtibial amputation, segments of the effected limb consist of the thigh, residuum and prosthesis socket which surrounds the residual tibia. Markers cannot be placed on the tibia, and assumptions of the residuum-socket interface must be made to maintain a constrained model. Previous studies have either modeled this interface as a rigid connection increasing tracking error, or was ignored altogether. Our approach allows tracking of all body segments with the accuracy seen in analyses of persons with intact limbs, and gives insight to the mechanics of the residuum socket interface. Additionally, it enables the separation of evaluating socket performance and prosthesis mechanism performance. This chapter is written with intent to be submitted to the Journal of Computer Methods in Biomechanics and Biomedical Engineering with second author Ryan Wedge of UMass Amherst, third author Professor Brian Umberger of UMass Amherst, and Professor Frank Sup of UMass Amherst.

6.1 Introduction

Modern marker-based motion capture techniques combined with musculoskeletal modeling and computational analysis have become standard tools for studying normal and pathological gait

biomechanics. Current techniques are limited when used to analyze the biomechanics of gait in people with lower limb loss due to the inability to place tracking markers on the residuum inside of the socket. Additionally, movement of the residuum within the socket is often omitted from musculoskeletal modeling analyses due to a lack of experimental data on the dynamics of the interface, even though significant motion inside the socket has been documented [17,100–103]. Here, we present an approach for quantifying gross motion and resultant loads at the residuum-socket interface as part of a whole-body inverse kinematics (IK) and inverse dynamics (ID) analyses. Our perspective is that this approach will lead to a more comprehensive understanding of gait biomechanics in persons with lower-limb amputation and also provide direct insights into the mechanics of the residuum-socket interface.

Most previous kinematic studies of persons with lower limb amputation have not been whole body analyses, have not used a traditional IK approach, and do not use information from IK or ID studies for the residuum-socket connection. Those that were IK based used early methods where segment positions were calculated sequentially without joint constraints. These methods included a direct method where a frame transform for each segment was determined from vectors between markers attached to the limb [104,105], or a segmental optimization method where error between experimental and model reference marker data was minimized in a least-squares routine [106–109]. Often the studies were only conducted for sagittal plane motion in two dimensions [102,110–114]. Lastly, the residuum and prosthesis socket were lumped together as a single segment, since motion of the residuum within the socket from only marker data was entirely unknown.

Current marker based IK methods estimate the underlying bone positions by utilizing a global least-squares optimization of all segments in a model with joint constraints, as first described by Lu, et al. [115]. In this method, the global error between experimental and model reference marker coordinates for all segments is minimized at every time step of the experimental data to determine the position and orientation of every segment concurrently. This method is beneficial in that all

segments are kinematically constrained to each other with the joint locations and degrees of freedom (DOF), and subsequently requires fewer markers to reconstruct segment movements (e.g. an IK analysis can be performed with a model containing a chain of three kinematically constrained segments with tracking markers on only distal segments). Use of this method with a musculoskeletal model of a person with a prosthesis, combining the residuum and socket into a single segment, will increase the global marker error and reduce accuracy of the calculated kinematics throughout the entire body. However, if the residuum and socket are modelled as

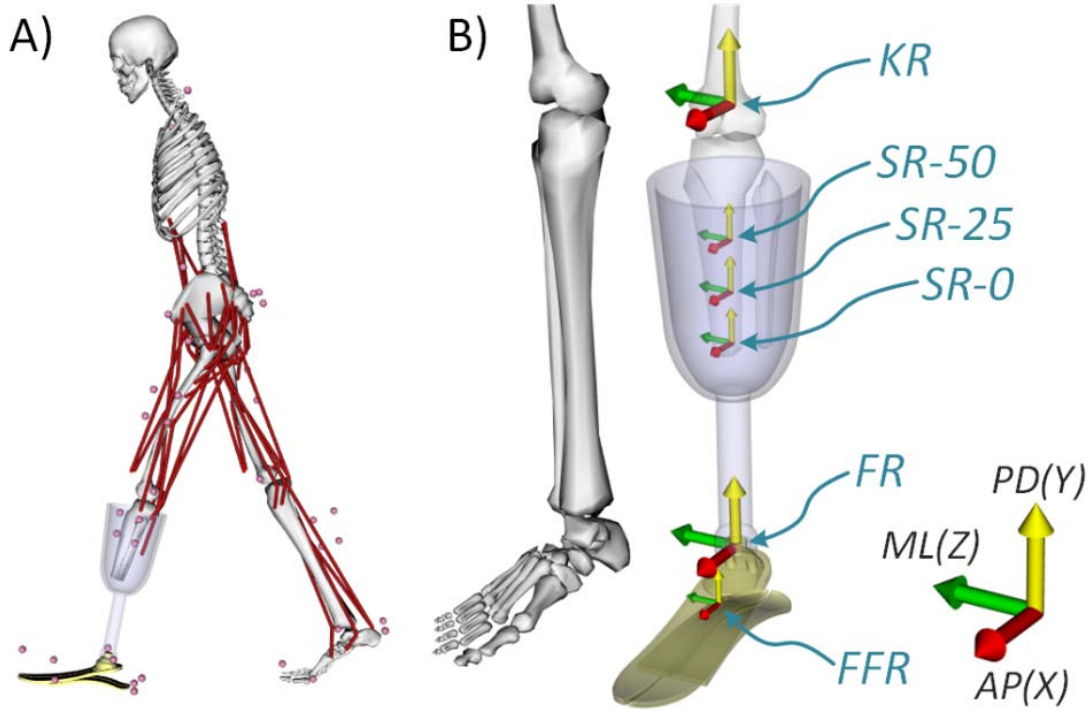

Figure 6.1: A) A generic model with transtibial amputation was created by modifying the gait2354 model provided by OpenSim. B) Socket-limb model showing the different socket reference frames (SR-0, SR-25 and SR-50) used for the constrainable 6 DOF joints. Each reference frame uses the conventions of anteroposterior (AP), proximal-distal (PD) and medial-lateral (ML) for the X, Y and Z axes respectively. KR is the knee reference frame location and orientation in the femur body. The socket reference frames are defined in the socket body, which are used to study the effect of residuum-socket joint placement along the PD axis on calculated residuum-socket mechanics. FR is the foot attachment reference frame in the socket body, and FRR is the foot flexion reference frame is the location of a 1 DOF joint used to express lumped foot flexion motion.

separate segments, constrained with select DOF at the connecting joint, it may be possible to estimate residuum movement within the socket without the need to have markers directly on the residuum and also reduce global marker error. It is clear that a part of the analysis is missing, as motion of the residuum within the socket is well documented [100,101] and should be accounted for.

Sensing techniques used to record residuum motion within a prosthesis socket include planar ultrasonic [116], radiological [103,117,118], and fluoroscopic methods [119]. These methods however, are complex, require costly equipment and sometimes expose the subject to potentially harmful radiation, making these methods impractical for routine gait analyses. More recently, three-dimensional X-ray techniques have been employed to monitor the residuum-socket interaction [101], but are still susceptible to the downfalls of prior methods. A research prototype has been developed to measure axial bone movement in relation to the socket [120], but it does not capture the entirety of limb movement within the socket.

We propose that a whole-body IK analysis utilizing a least-squares global optimization method with a constrained musculoskeletal model (including a residuum-socket joint) can be performed to estimate the residuum-socket kinematics and also track whole-body movements with a degree of accuracy comparable to similar analyses of persons without amputation. By leveraging the global least-squares method's dependency on joint constraints, DOF can be added between the residuum and socket segments, and the model can remain kinematically constrained. Known marker locations attached to the socket and thigh provide enough information to calculate the location and orientation of both socket and thigh bodies. Assuming that all motion between the residuum and socket exists in select, predominant DOF, the global optimization should converge to positions and orientations of all body segments with an accuracy that is seen if an unconstrained joint were present between the residuum and socket.

In this paper, a full body model with unilateral transtibial amputation was developed in OpenSim [75,121]. The joint between the residuum and prosthesis socket has maximally 6 DOF. Each individual DOF can be constrained providing the residuum-socket joint with anywhere between 0 and 6 DOF. Additionally, the joint reference frame origin is modifiable axially along the residual tibia and socket body segments. Experimental walking data of a test subject with unilateral transtibial amputation were collected. A global least-squares approach was used to perform IK analyses with the model in different configurations followed by ID analyses. The effects that the residuum-socket DOF combination and joint location have on IK marker error was examined, and the resulting residuum-socket generalized motions and forces for each model configuration are reported. The results and discussion evaluate the residuum-socket model performance for whole-body IK analyses when using the global least-squares method.

6.2 Methods

6.2.1 A Generic Musculoskeletal Model with Unilateral Transtibial Amputation

A generic model with a left transtibial amputation (Figure 6.1 A) was created by modifying the gait2354 model provided with OpenSim [75,121]. All bodies distal of the affected tibia were removed and the left tibia body segment (which includes the fibula) was transected by modifying mass, inertia and the graphical depiction to represent an amputation at 50% of the limb. A generic socket body segment was connected to the transected tibia body via a joint having 6 independently constrainable DOF. The socket joint was defined such that motion in each joint DOF would be expressed in the socket reference frame. It is assumed that the joint center of rotation (COR) is located along the proximal-distal axis of the socket and tibia segments, however it is apparent that the COR location may affect the calculated motions when the joint is partially constrained. To examine the impact of this, three variations of the model were constructed (Figure 6.1 B) to study the kinematic and dynamic sensitivity to changes in reference frame location along the proximal-distal axis. The first socket reference frame (SR-0) is positioned at the most distal point of the

modified tibia segment. The second socket reference (SR-25) is positioned 25% closer to the knee joint reference frame (KR) than SR-0, and the third (SR-50) is positioned 50% closer to KR than SR-0.

An ankle-foot prosthesis was connected to the end of the socket body segment at the foot reference frame (FR). This was placed in the socket segment such that the prosthetic foot was properly aligned with its correct anthropometric placement. Although some forward dynamics studies have incorporated prosthetic foot models containing many segments to simulate flexion throughout the prosthetic foot [26], the ankle-foot flexion defined in this model is lumped into a single DOF pin joint at the foot flexion reference frame (FFR). A lumped flexion parameter has the advantage of being computationally efficient, while adequately accounting for the relative displacements of the tracking markers during motion capture.

After defining all kinematic constraints in the modified model, mass and inertial parameters were calculated for the new bodies at their respective joint location with computer-aided design modeling tools, and added to the model. All muscles distal of the amputation site in the generic model were removed with the exception of the biarticular gastrocnemius, which was reattached to the posterior tibia.

6.2.2 Experimental Procedures

Assessments of IK with the proposed model and its variations were made for a single subject. Motion data were collected during over-ground walking using an eleven-camera optical motion capture system (Qualisys, Inc., Gothenberg, Sweden) to track reflective infrared markers attached to the test subject at 240Hz. Ground reaction forces were recorded at 2400 Hz using three flush-mounted strain gauge force platforms (OR6-5, AMTI, Inc. Watertown, MA, USA). The test subject was a healthy male with a left, unilateral transtibial amputation (Table 6.1).

Metric	*Value*
Height (m)	1.88
Mass (kg)	104.3
Gender	Male
Amputation	Left Transtibial
Activity Level	K-4
Prosthesis	Ossur Variflex
Residual/Intact Limb	0.44
Preferred Walking Speed	1.26

Table 6.1: The test subject information is presented, highlighting key attributes.

Markers were placed on the test subject for model scaling and motion tracking. Scaling markers included left and right acromion process, iliac crest, anterior superior iliac spine (ASIS), posterior superior iliac spine (PSIS), greater trochanter, lateral and medial femoral condyles , lateral and medial malleoli, first metatarsal head, 5th metatarsal head, and tip of the second toe. Markers on the left prosthesis were matched with the intact side. Tracking markers included acromion processes, iliac crests, ASISs, PSISs, toes, clusters of four markers on the thighs, right shank, and socket, and clusters of three markers on heels of the shoes.

Marker trajectory and ground reaction force data were first collected with the subject standing in a static pose for model scaling purposes. Marker trajectory and ground reaction force data were then collected for normal level over-ground walking at the subject's preferred speed, which averaged to be 1.26 m/s (Table 1). A successful experiment trial was defined as one where the subject stepped fully onto the three force platforms in a sequential pattern with alternating feet, but without looking down in an attempt to target the platforms, which could affect gait patterns. Walking speed was measured with photogates 6 m apart. Three successful trials were recorded so that ensemble averages could be calculated.

6.2.3 Model Scaling

Prior to scaling the generic model with the OpenSim scaling tool, the residuum in the model needed to be pre-scaled in order to properly reflect the specific level of amputation and to account for the lack of scaling markers on the residuum . Using physical measurements of the subject, the residuum (lateral femoral epicondyle to the distal end of limb) was determined to be 0.44 times the length of the intact limb (lateral femoral epicondyle to lateral malleolus). Each of the socket reference frame origins were altered to reflect this ratio, and maintain correct placement within the tibia body frame. Residuum and prosthesis inertial and mass properties were scaled in the model to reflect the residuum to intact limb length ratio.

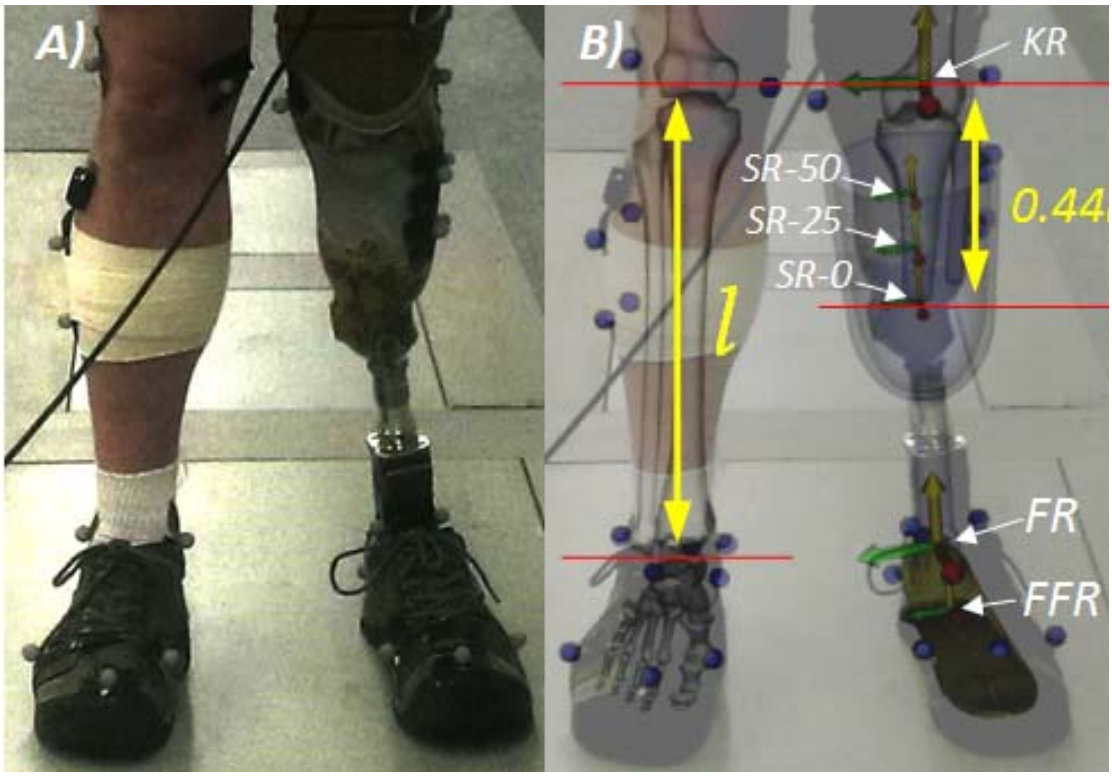

Figure 6.2: (A) Test subject standing for the standing calibration pose. (B) A graphic of the scaled model with amputation is overlaid on image A, in the same loaded pose. KR is the affected knee joint reference frame, SR-0, SR-25 and SR-50 are the socket-limb reference frame variations, FR is the foot prosthesis reference frame, and FFR is the foot flexion reference frame. The residual limb is approximately 0.44 times the length of the intact limb. The socket reference frames are attached to the socket-pylon body, and their position is defined by their proximity to the affected knee joint and length of residual limb when in a neutral unloaded position.

After pre-scaling the residuum, the model was scaled using the OpenSim scale tool. Normally, each body would be scaled to a ratio of distance between experimental markers to distance between virtual model markers placed primarily at joint centers of rotation. Since experimental markers could not be mounted to the residual tibia body, the prosthesis and residual tibia bodies were scaled proportionally to the intact limb. All six coordinates in the residuum-socket joint were allowed to be unconstrained during scaling, in order to accurately align the model with experimental data. A close-up of the scaled model can be seen in Figure 6.2, overlaid on an image of the test subject posing for the static calibration experimental data.

6.2.4 Data Post Processing

Marker data for each trial were post-processed, calculating IK and ID for the three model reference frame variations and for the 6 residuum-socket joint DOF configurations for a total of 18 different model configurations shown in Table 6.2. The *Rigid* joint configuration constrained all 6 DOF. With respect to the socket reference frame shown in Figure 6.1 B, the *Flex* configuration constrained all DOF with the exception of socket flexion/extension (rotation about the medial-lateral axis) and the *Pist* configuration constrained all DOF with the exception of socket pistoning (translation along the proximal-distal axis). The *Flex/Pist* configuration combined free coordinates of *Flex* and *Pist* and the *4-DOF* configuration combined the free coordinates of *Flex/Pist* with the added coordinates of adduction/abduction and residuum-socket rotation (rotations about the anteroposterior and proximal-distal axes, respectively). Pistoning and flexion/extension were considered to be the most clinically relevant displacement; however, we included the two additional rotational coordinates for two reasons. First, our own experience is that some subjects exhibit visible angular displacements about one or both of these axes. Second, including these DOF might further improve global marker tracking during the inverse kinematics analysis. Lastly, a *6-DOF* residuum-socket joint configuration was included to compare the unconstrained case with the other configurations and to examine the convergence of model marker tracking error with increased

model complexity. With the exception of the *6-DOF* configuration, anteroposterior and medial-lateral translational movements in the socket reference frames were constrained since the residuum segment would be kinematically under-constrained otherwise, and further these were considered to be the least clinically relevant motions.

Average IK marker error root mean square (RMS) error values were calculated across all trials, residuum-socket reference frame variation, and joint DOF configuration. Marker error results were then normalized to the *Rigid* model configuration to show percent error reduction in other model configurations. IK and ID data were normalized to percent stride for each trial, reference frame variation and residuum-socket joint configuration. Averages and standard deviations were then calculated across trials for each residuum-socket joint placement, and joint configuration. The results were inspected and the kinematically constrained residuum-socket joint configuration with the greatest error reduction was identified.

Socket-Limb Joint Configuration	Free Rotational Coordinates			Free Translational Coordinates		
	AP(X)	PD(Y)	ML(Z)	AP(X)	PD(Y)	ML(Z)
Rigid – Welded						
Flex - Flexion Only			•			
Pist – Pistoning Only					•	
Flex/Pist - Flexion and Pistoning			•		•	
4 DOF - Full Rotation with Pistoning	•	•	•		•	
6 DOF - Full Rotation and Full Translation	•	•	•	•	•	•

Table 6.2: Socket-limb joint configurations, showing free coordinates for the accompanying configuration and description.

6.3 Results

RMS marker errors averaged across trials are presented in Figure 6.3 for each residuum-socket reference frame variation, and each joint configuration. The normalized results showed model marker error RMS generally decreasing with increasing model complexity. The *4-DOF* joint configuration had a 25% reduction in marker error RMS compared with the *Rigid* configuration. However, there was no further reduction in the marker error RMS for the under-constrained *6-DOF* joint configuration, relative to the *4-DOF* condition (Figure 6.3). Actual average marker error values were reduced from 1.70 ±0.18 cm (rigid) to 1.27 ±0.13 cm (*4-DOF*). While the number of DOFs did affect the marker tracking error, the location of the socket reference fame had little effect on the marker error RMS (Figure 6.3). Based on these results, subsequent kinematic and kinetic results are presented based on the *4-DOF* model.

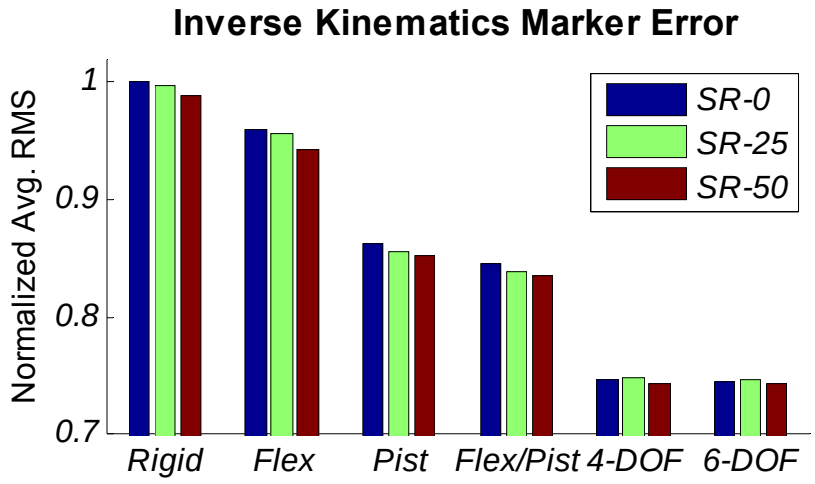

Figure 6.3: Inverse kinematics model marker error RMS, averaged across preferred speed walking trials for each model variation tested, is presented normalized to the *Rigid* model marker error RMS with the *SR-0* frame, which exhibited the largest error value of all models. *SR-0*, *SR-25* and *SR-50* are the socket reference frames located 0%, 25% and 50% proximally from the distal tip of the limb. Actual average error RMS values ranged from 1.27 cm to 1.70 cm. The fully-constrained 4-DOF socket-limb joint reduces marker error by 25 percent, about the same as the under-constrained 6-DOF joint.

Average preferred speed kinematic and normalized kinetic results are presented in Figure 6.4 for the affected limb with energy storage and return (ESR) prosthesis and contralateral intact limb for the *4-DOF* model (dark and light solid lines respectively). Complementary *Rigid* model results for the affected and intact limbs are included to highlight the differences in calculated movements and forces (dark and light dashed lines respectively). These data show an asymmetric gait commonly seen in persons with lower limb amputation [110]. Comparing the *Rigid* and *4-DOF* model results, offsets can be seen throughout the gait cycle, most notably in the affected limb. The calculated prosthetic foot, affected knee and affected hip kinematics each differed maximally over 5 degrees. Calculated kinetics differed maximally about 0.1 N-m/kg in the affected limb.

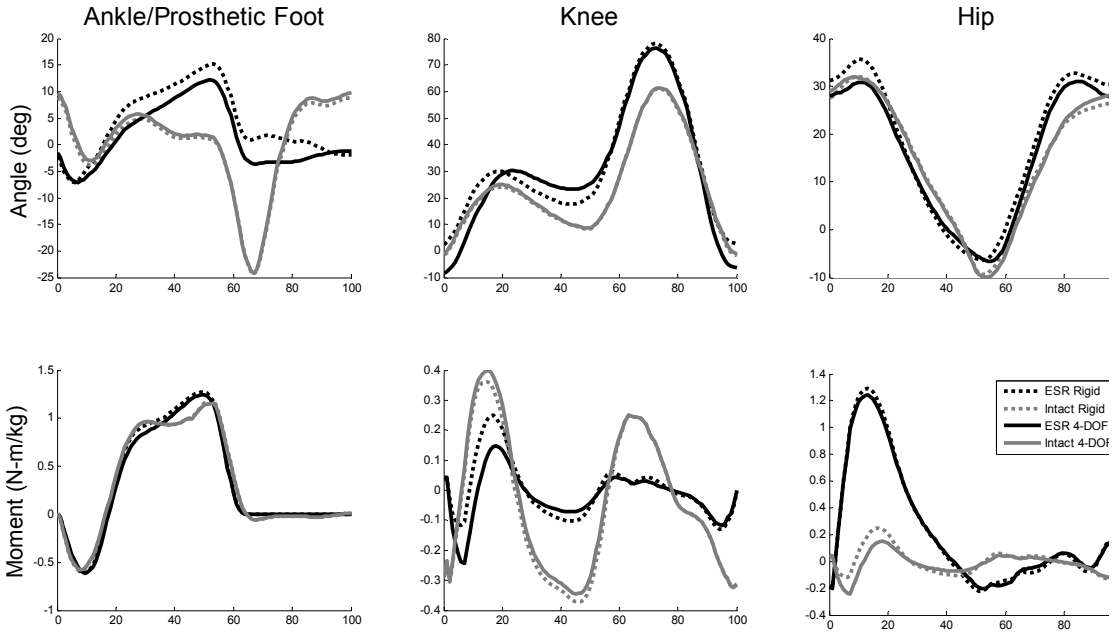

Figure 6.4: The resultant average kinematic (top) and kinetic (bottom) data are shown for the ankle/prosthetic foot (left), knees (middle) and hips (right). In each plot, the dark solid lines are average data for the amputated limb with a 4-DOF socket model, the light solid lines are average data for the contralateral intact joint, the dark dashed lines are average data for the amputated limb calculated with a rigid socket model, and the light dashed lines are average data for the contralateral intact joint.

The average normalized ground reaction forces (GRF) are shown in Figure 6.5 for the affected limb with an ESR ankle/foot and the intact limb. These data show higher peak vertical and horizontal forces in the intact limb, agreeing with data found in the literature [110].

Figure 6.6 presents the *4-DOF* residuum-socket joint kinematics results, comparing across socket reference frames. All results for each coordinate exhibit similar patterns across reference frame variations. Pistoning shows compression of the residuum inside of the socket immediately after heel strike, having peak magnitudes between 23 and 27 mm. Throughout stance, the pistoning values remain fairly constant until a slight oscillation in magnitude at toe-off after 60% stride. The magnitude then slowly decreases throughout swing until it returns to the neutral position after 90% of the stride. An offset of about 4 degrees between different reference frame data sets is most noticeable during the first and last 10% of stride. Flexion/extension shows residuum rotation relative to the socket, about the medial-lateral axis of the socket reference frame. Although all data

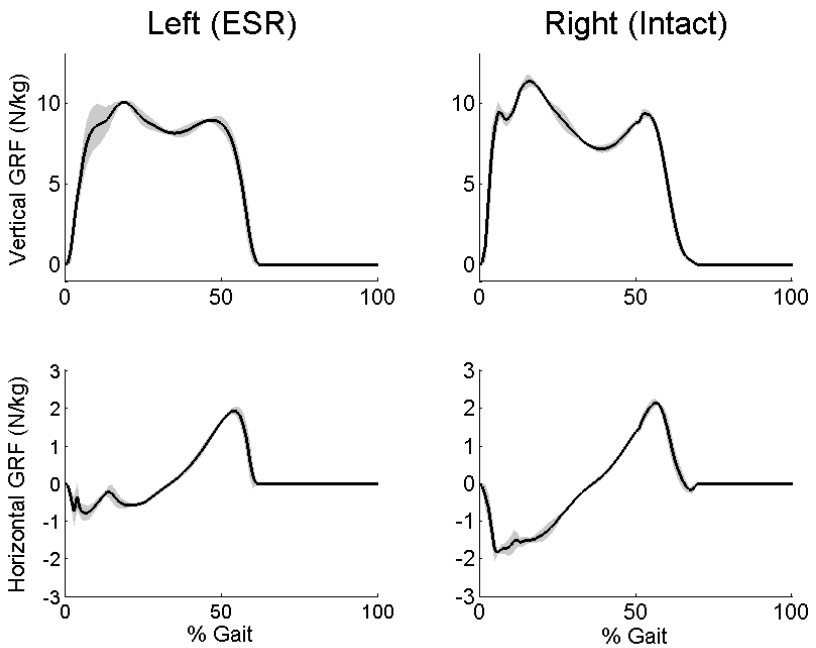

Figure 6.5: Average vertical (top) and horizontal (bottom) ground reaction forces (GRFs) are shown for the affected amputated left side with ESR (energy storage and return) foot/ankle prosthesis, and the right intact foot.

sets show similar patterns, the peak magnitudes vary maximally by about 10 degrees just before and after heel strike. Axial rotation shows residuum movement about the proximal-distal axis in the socket reference frame. This appears to be most consistent across datasets, however the standard deviation increases throughout stance. There is a slight offset in axial rotation magnitude throughout mid to late stance. Abduction/adduction, residuum rotation about the anteroposterior axis in the socket reference frame, also exhibits similar patterns across datasets with moderate offsets in the magnitude value. Abduction/adduction has the smallest range of rotational movement of 3 to 7 degrees depending on the reference frame, while flexion/extension range varies from 11 to 29 degrees. Axial rotation has a fairly consistent range of about 25 degrees.

4-DOF residuum-socket joint kinetic results for preferred speed trials are shown in Figure 6.7, corresponding to the kinematic data presented. Pistoning force exhibits a pattern and peak magnitude that closely resembles the vertical ground reaction force, with very little difference between reference frame positions. Flexion/extension moments have sharp oscillations about zero early in the stance phase, following the impact of the foot with the ground. The peak magnitude of the flexion/extension moment in mid-stance varied 33 N-m maximally depending on reference frame locations, with the moments converging to the same value at toe off. The axial rotation moment averages show consistent patterns throughout stride, however the standard deviation during stance is noticeably larger during late stance. Abduction/adduction moment shows the same pattern exhibited by flexion/extension moment with a slight offset through mid to late stance and convergence at toe off.

6.4 Discussion

The results of this study demonstrate the utility of including the residuum-socket joint in whole-body gait analysis of people with limb loss. The residuum-socket joint is modeled as having 4 DOF, which is a more realistic generalization than current practices of modeling it as a free or rigid joint.

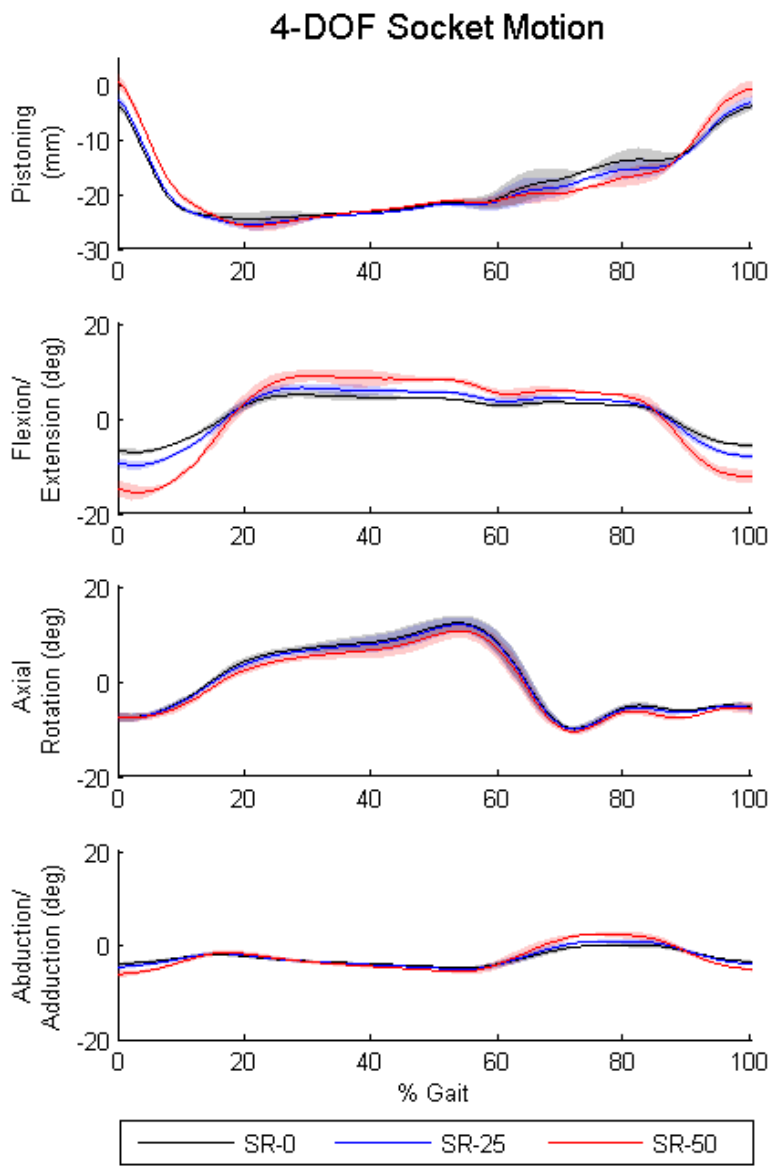

Figure 6.6: The inverse kinematics for preferred speed walking are shown for the 4-DOF socket-limb model, and compared across the different reference frames defined.

This approach allows for more accurate IK calculations of whole body movements, and yields insight on residuum-socket mechanics.

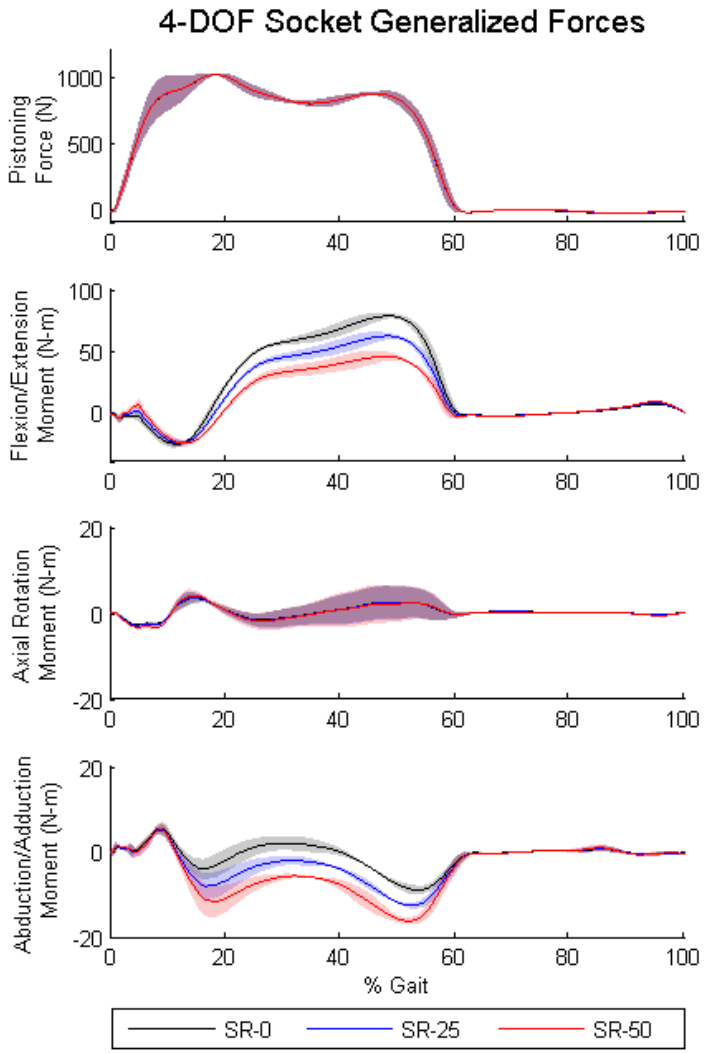

Figure 6.7: The inverse dynamics are shown for the 4-DOF socket-limb model for preferred speed walking trials, for comparison across different reference frame variations.

Examining IK marker error (Figure 6.3), error convergence shows that a *4-DOF* residuum-socket model should allow calculation of whole-body mechanics (not including the residuum-socket joint mechanics) as accurately as using an unconstrained residuum-socket joint. Differences in RMS values across socket reference frames in the *rigid* configuration are due to a slightly altered model marker placement during scaling, even though markers were weighted the same (i.e. the marker locations in reference to the different socket reference frames change with a calibration pose with non-zero positions/rotations of the residuum-socket joint). This difference due to scaling

most likely alters the error in all joint configurations. Studying marker error reduction alone makes it difficult to conclude whether one reference frame is a better fit for a residuum-socket model over another when using this method.

For the residuum-socket motions calculated from IK (Figure 6.6), it is seen that each coordinate exhibits similar patterns when compared to results calculated in a different reference frame. Some noticeable attributes and differences among the data stand out. Pistoning motion is offset between reference frames at the beginning and end of the stride; however, pistoning shows agreement across reference variations from mid to late stance suggesting that reference frame placement has little influence on pistoning motion calculations when the limb is loaded. Socket flexion/extension is the most inconsistent between reference frames, revealing that this coordinate is highly sensitive to reference frame placement. Axial rotation movement is consistent regardless of reference frame, and the large magnitude indicates that this coordinate may play an important role in calculating socket mechanics. This substantial motion will be missed in experimental or simulation analyses that treat the residuum-socket interface as rigid. Data offsets were most apparent in flexion/extension and abduction/adduction, and were mainly caused by the static center of rotation. Although the offset magnitudes differ between datasets, it was apparent that there is less difference between datasets SR-0 and SR-25 (socket reference frame placement at 0% and 25% proximal from the limb distal tip respectively) than between datasets SR-25 and SR-50 (socket reference frame placement at 25% and 50% proximal from the limb distal tip). This may indicate that the actual center of rotation, while likely not a fixed point, is dynamic within the distal 25% of the residuum. This is consistent with the idea that the COR is not likely at extremum points of the residuum. Further, it can be argued that since joint motions throughout the body are commonly approximated when studying gross motion, such as the knee joint being almost always approximated as a fixed point midway between the femoral epicondyles, it is acceptable for the residuum-socket joint to be approximated this way as well.

More prominent features were found when examining the generalized forces calculated from ID analyses (Figure 6.7). Like the average coordinate data, similar patterns were seen across all average force data. The pistoning force greatly resembles the vertical ground reaction force and shows little deviation across data sets. This implies that pistoning force is not sensitive to the reference frame selection. In all three rotational coordinates, a slight oscillation is apparent during initial loading. This may be caused by the subject balancing on the unactuated residuum-socket joint with little reaction moment to stabilize against. The recorded horizontal ground reaction forces (Figure 6.5) were also seen to agree with this assessment. After the first 5% of stride, the patterns and values of the coordinate forces generally agree with existing data reported in other studies [122,123]. The apparent difference in ID results across datasets during mid to late stance is most apparent in flexion and adduction moments. This sensitivity is due to the GRF vector acting about the socket reference frame with a moment arm altered proportionally to the change in reference frame position. This indicates that flexion/extension and abduction/adduction moment patterns can be estimated, however the magnitudes are effected by the choice of reference frame placement. Axial rotation moment data was estimated consistently across datasets, however the high standard deviation indicates that this coordinate varies greatly on a step to step basis. High axial rotation standard deviation for the trials may be a result of the counter moments being generated only by sheer forces and tissue deformation within the socket (i.e. no structural boney hard stop), giving the subject less control of the counter moment for stability. Although the axial rotation moment magnitude is low during stance in comparison to other coordinates, axial rotation may play a key role in some locomotion strategies considering the large movement range. It is possible that this subject twists their residuum into the socket during late stance for increased joint impedance in an effort to better support high axial forces and flexion moments, however the local kinematics and kinetics may just be a result of whole body dynamics acting through an under actuated joint.

Requiring only marker based motion capture data is a significant advantage of this proposed methodology, as it aligns with current global least-squares IK methods [115]. The methodology does not require additional imaging systems, such as ultrasound, MR or radiological, that add complexity and are cumbersome to incorporate into routine gait analyses. It also does not introduce any more risk to the subject that other methods might (e.g. radiation) when tracking residuum motion within the socket. The most notable improvement over previous methods is that our approach should yield more accurate joint kinematics and moments throughout the body by more accurately representing the topology of the affected limb, while at the same time yielding insights on mechanics of the residuum-socket interface.

The major limitation of this method is that translational movements in the anteroposterior and medial-lateral directions must be constrained statically in order to keep the joint fully constrained for a marker based global optimization IK analysis, even though it is clear that the residuum-socket joint has 6 DOF in actuality. If the joint was modeled with 6 DOF in this type of analysis, it would be under constrained and would provide no insight into residuum-socket mechanics. The 4 DOF residuum-socket provide a window into the residuum-socket interaction, but causes actual anteroposterior and medial-lateral translational movements to be accounted for in the free coordinates. This simplification of the model introduces a source of error in free coordinate calculations, even though the actual anteroposterior and medial-lateral movements are likely to be small in comparison to clinically relevant coordinate movements. When examining flexion/extension and abduction/adduction reaction moments, it is clear that the calculated values greatly depend on the location of the socket-residuum reference frame in the proximal-distal axis of the residuum. It may be argued that even though the center of rotation is realistically moving dynamically throughout the distal region of the residuum, our approach allows a more realistic estimate of where the actual COR is, compared with the approximation at the distal tip of the limb that is required in moment sensor studies seen in the literature [71,122].

6.5 Conclusion

A *4-DOF* residuum-socket model, as described, produces calculations of whole body motions comparable to an IK analysis using a fully unconstrained residuum-socket joint, while providing insight into residuum-socket mechanics. The patterns of generalized movements and forces within the socket estimated with this method should, in most cases, describe the actual movements and forces of a residuum within a prosthesis socket, with error occurring in the magnitude of calculations. Error in calculated residuum-socket mechanics at this point is not quantifiable without experimental validation. However, the benefits of having the knowledge of generalized socket-residuum motion and force patterns outweighs the presence of error since the current methods for performing whole body IK analyses lower limb prosthetic gait utilize either a rigid or unconstrained free residuum-socket model. An additional important outcome is the ability to separate socket fitment and prosthesis performance. When analyzing data with previous methods, it is lumped together and all results focus on the performance of the prosthesis without regard to the performance of the socket fit.

Future work should include applying this method to existing motion capture datasets in an effort to build a database of residuum-socket mechanics. Validation of the model will be performed with additional imaging equipment to calculate the accuracy lost to constraining two translational degrees of freedom. Modeling the correlation between residuum-socket forces and movements to be used in predictive simulations will also be explored.

6.6 Acknowledgement

This work was supported by NSF National Robotics Initiative grant, IIS-1526986, and by a pilot grant given by the NCSRR OpenSim team at Stanford University.

CHAPTER 7

EVALUATION OF A ROBOTIC ANKLE PROSTHESIS PROTOTYPE WITH ACTIVE ALIGNMENT

7.1 Introduction

Following lower limb amputation, a person's gait is a function of their overall health, prosthesis, and the connecting interface at the residual limb [1]. High loads are borne by soft tissues at this interface [3,4], and often are a source of discomfort, further damage to the limb and can lead to further problems throughout the rest of the individual's body [8–12,37,44–50]. For this reason, simply designing a prosthesis to replicate the lost form and function of the limb as it would be found naturally may be insufficient for restoring gait. Daily activities such as standing and walking can become incredibly challenging, causing activity levels to decrease. This often leads to further deterioration of overall health.

Active Alignment is a novel design feature in a robotic transtibial prosthesis prototype developed in Chapters 2-5. Active Alignment utilizes active components and an optimized mechanism to realign the residual limb in relation to the ground reaction force (GRF) during mid to late stance. The prosthesis alignment in relation to the center of pressure is continuously adjusted in an effort to reduce both moment transfer to the limb and associated peak pressures while power is injected into the stride. If the loading demand on the residual limb decreases, it is hoped that an individual stays active longer, maintaining health.

In this chapter, the prosthesis performance and its effect on gait mechanics is evaluated in a comprehensive biomechanics study. In the following section titled Methods, experimental procedures and data post-processing are detailed. Results are then presented, covering entire-body

biomechanics, GRFs, center of mass trajectories, residuum-socket mechanics, prosthesis performance, and intra-socket pressures during gait. After results, the findings and implications on prosthesis design are discussed.

7.2 Methods

7.2.1 Prosthesis Hardware and Controller Updates

During early testing of the prosthesis prototype, many parts of the prosthesis prototype system were modified for durability and enhanced performance, and also to address design oversights. The modified prosthesis is shown in Figure 7.1.

The original moment load- cell was redesigned after multiple failures of strain gages in the full bridge. The original load cell was designed for AA-6061 and marginal strain gage safety factor for minimal weight and maximum load cell response respectively. After multiple failures, it was determined that the strain gauges were inadvertently over-stressed, even though the load cell itself appeared to be intact. However, since the material of the original design is aluminum, there is also a chance that the load cell body had begun to fatigue from high cyclical loading seen in gait. To address this problem, the load cell was redesigned to be made out of SS-304 and a maximum von Mises stress below the material endurance limit of 240 MPa. A sensor characterization as described in Chapter 4 was performed, and the new load cell sensitivity was found to be 29.1± 0.57 N-m/V.

Shoulder bolts that were used for assembling the mechanism linkage bent during repetitive testing, causing the mechanism to become less efficient. Eventually one of the bolts sheered during testing. A design revision to the ball screw and nut carrier assemblies, which the shoulder bolts screwed into, involved adding a pocket for the shoulder to insert into in order to relieve a stress concentration where the shoulder begins. The bolt material was also changed from stainless steel to hardened alloy steel with a tensile strength of 965 MPa, which is twice the strength of the stainless hardware used originally.

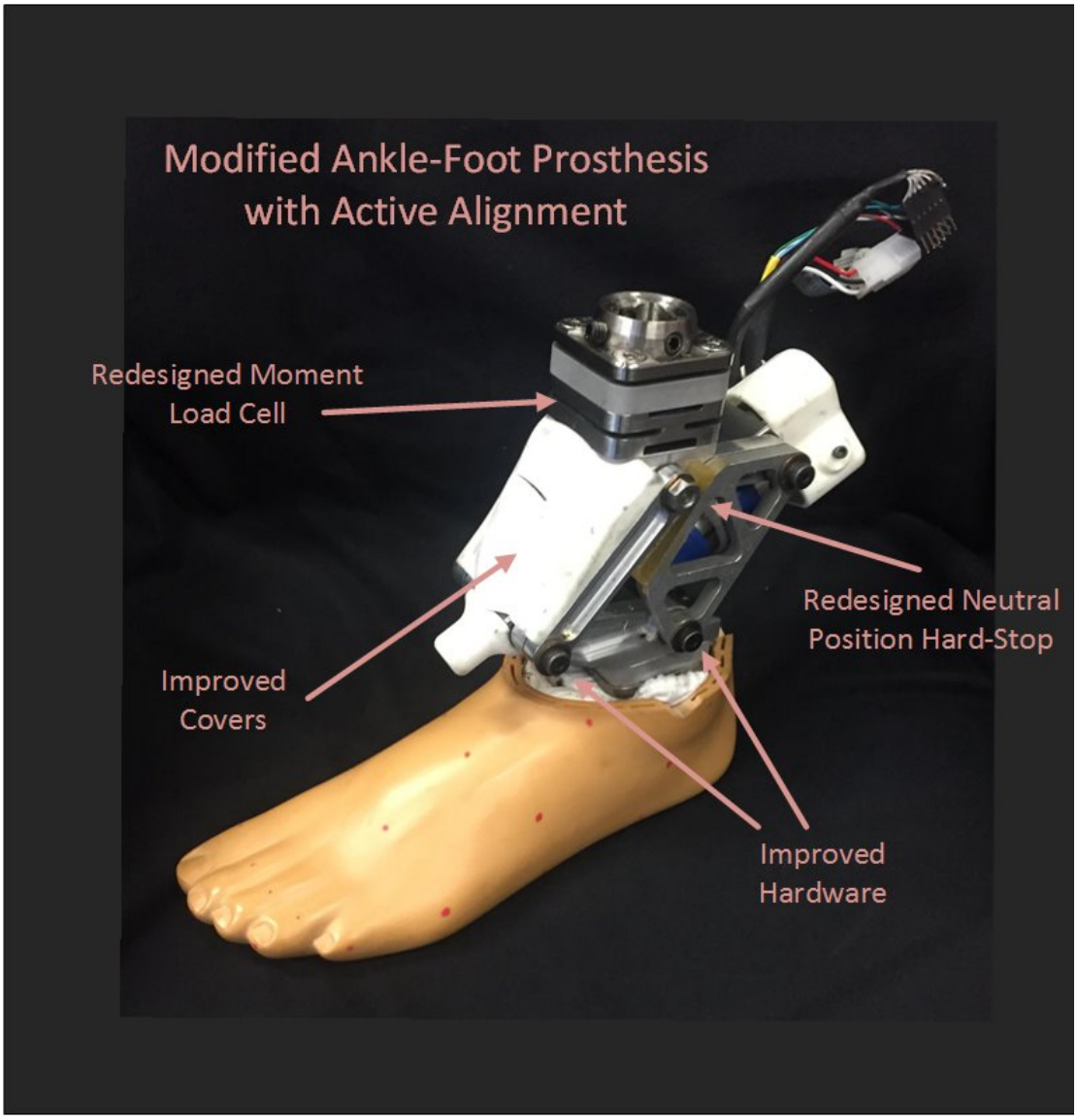

Figure7.1: The modified prosthesis is shown with redesigned neutral position hard-stops, new hardware and redesigned load cell.

Modifications were made to the prosthesis neutral position in order to increase the neutral position mechanical advantage. The maximum prosthesis vertical GRF output is shown in Figure 7.2, showing an increase with mechanical advantage as the prosthesis mechanism extends. During early testing, it was found that since the controller starts actuating after the center of pressure moves past the ankle center, there was just enough neutral position force output capability to actuate the ankle for a 70 kg user. While this is not an issue for subjects below 70 kg, testing with heavier users

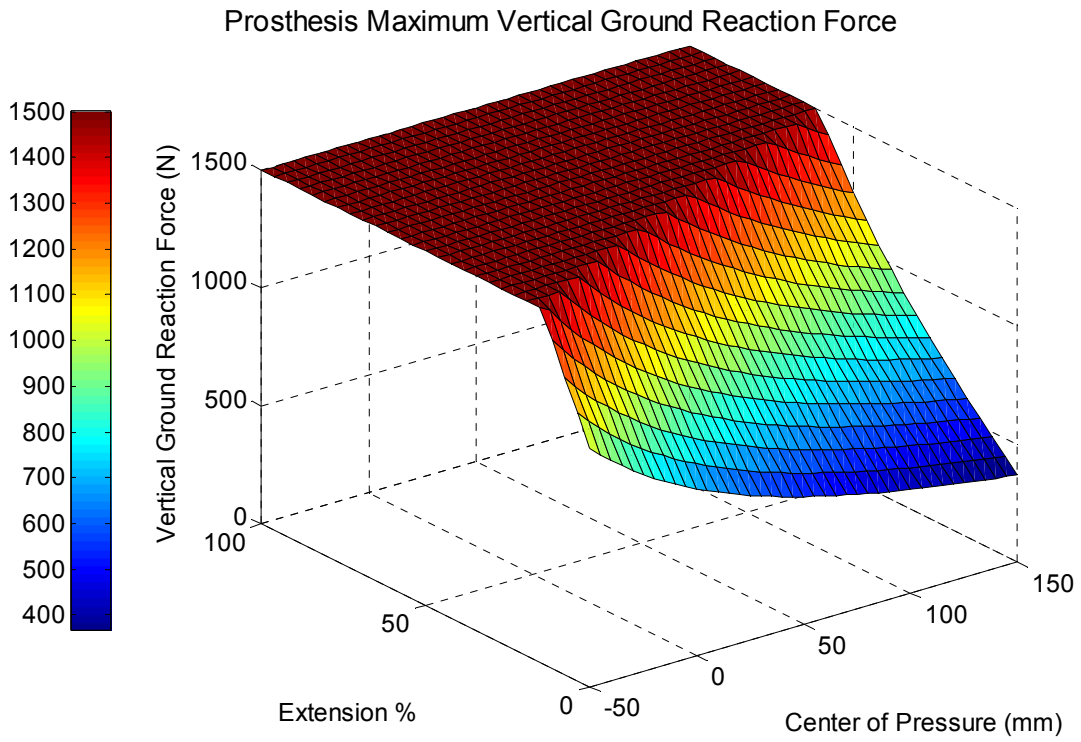

Figure 7.2: The maximum force output of the prosthesis is presented, used to determine how to modify the prosthesis.

often resulted in overloading the motor and motor driver, causing the motor controller to shut down. To resolve this issue the prosthesis neutral position was adjusted so that actuation begins at 25% extension. This resulted in both positive and negative effects. On one hand, the maximum neutral position mid-stance vertical GRF with the modification is now increased from about 600 N to approximately 1100 N at the neutral mechanism position. However the negative impact from this adjustment is twofold. First, the neutral position adjustment shifts the neutral foot position to the posterior without additional hardware, increasing the dorsiflexion moment seen in early stance. This can be corrected by the prosthesis static alignment adjustment by angling the mechanism pyramid connectors, however this increases height of the mechanism, limiting the range of users that can use the prosthesis when properly aligned. Second, the actuator range of motion is reduced by 25% of the original design, limiting the effect Active Alignment originally designed for. These

negative effects must be taken into account in the next design iteration, but do not invalidate the utility of the design.

Multiple modifications were made to the controller to improve prosthesis performance. Firstly, event detection for the walking state controller has been modified to be less dependent on moment. Throughout early testing and studying sensor outputs throughout gait, sagittal jerk magnitude (derivative of acceleration magnitude) recorded from the accelerometer was found to be a reliable trigger to detect heel strike. Layered logic statements were incorporated into the controller to allow moment thresholds or jerk magnitude thresholds to trigger state changes. The second controller modification implemented was the mapping of linkage mechanical advantage to the controller gain schedule, based on actuator encoder feedback. This made the controller response more consistent and allowed it to be critically damped throughout prosthesis extension. Lastly, the walking state controller is designed to actuate only if an event is detected, however false positives are frequent if the controller is active and the person is just standing. To address this, the walking state controller was nested in another state controller, which detects whether or not the test subject is walking by identifying consecutive successful steps. Successful steps are identified by timing the entire gait cycle where all walking events are detected, and enters walking mode if the gait time is less than a gait time cycle threshold and all walking events are detected for two consecutive steps. To enter standing mode, the controller detects if the gait cycle time is less than a threshold lower than the entry threshold to prevent exiting walking mode prematurely, or if an event is skipped representing an abrupt stop. In standing mode, the controller regulates at the neutral position. It was found that even though testing is performed in a laboratory environment, usability of the device increased by eliminating the need to externally turn the walking controller on and off. Additionally, since the prototype prosthesis is tethered and controlled by a desktop PC, modifications were made to the tether and the PC was mounted on a rolling cart. This allowed a test subject to walk across through

a data collection area for motion and force capture while a laboratory technician followed with the tethered controller and power source.

7.2.2 Experimental Procedures

All biomechanics testing took place in the Kinesiology Department Biomechanics Laboratory at the University of Massachusetts, Amherst. A K-4 activity level test subject was recruited for prosthesis evaluation testing. Subject data can be seen in Table 7.1. The subject had already walked on the device in 3 previous experiments, and was comfortable and stable walking on the prosthesis without an overhead harness during the tests. All testing in this evaluation consisted of steady state walking at the subjects preferred speed while data were collected. Data recorded during this test session included tracking experimental markers attached to the subject's limbs head and torso through 3 dimensional space, recording GRFs, and recording pressure on load bearing surfaces of the residual limb.

Metric	*Value*
Height (m)	1.83
Mass W/Passive Prosth	73.16
Mass W/Active Prosth	74.28
Gender	Male
Amputation	Left Transtibial
Activity Level	K-4
Prosthesis	Ability Dynamics Rush 87
Residual/Intact Limb	0.59
Preferred Walking Speed	1.32

Table 7.1: Test subject data.

Prior to testing, the subject was fitted with infrared reflective tracking markers on their head arms and torso for both model scaling and motion tracking. Scaling markers, placed at bony anatomical landmarks, consisted of left and right acromion process, iliac crest, anterior superior iliac spine (ASIS), posterior superior iliac spine (PSIS), greater trochanter, lateral and medial femoral condyles , lateral and medial malleoli, first metatarsal head, 5th metatarsal head, and tip of the second toe. Markers on the prosthesis were matched with the intact contralateral limb. Tracking markers included acromion processes, iliac crests, ASISs, PSISs, toes, four marker clusters on the thighs, right shank, and socket, and clusters of three markers on heels of the shoes. At this time, the subject's socket was also instrumented with 3X4 grid array capacitive pressure transducers on the limb tibial tubercle and mid posterior region (Figure 7.3), connected to a wireless transponder worn on the hip. Measurements of the subject's residual limb were also taken at this time.

During testing, marker trajectories were calculated in real-time via measurements taken from an eleven-camera optical motion capture system (Qualisys, Inc., Gothenberg, Sweden) at 240 Hz, and ground reaction forces were recorded at 2400 Hz using three flush-mounted strain gauge force platforms (OR6-5, AMTI, Inc. Watertown, MA, USA) integrated into the Qualysis Track Manager software. Pressure was recorded with a Novel Pliance pressure measurement system (Novel, Inc.,

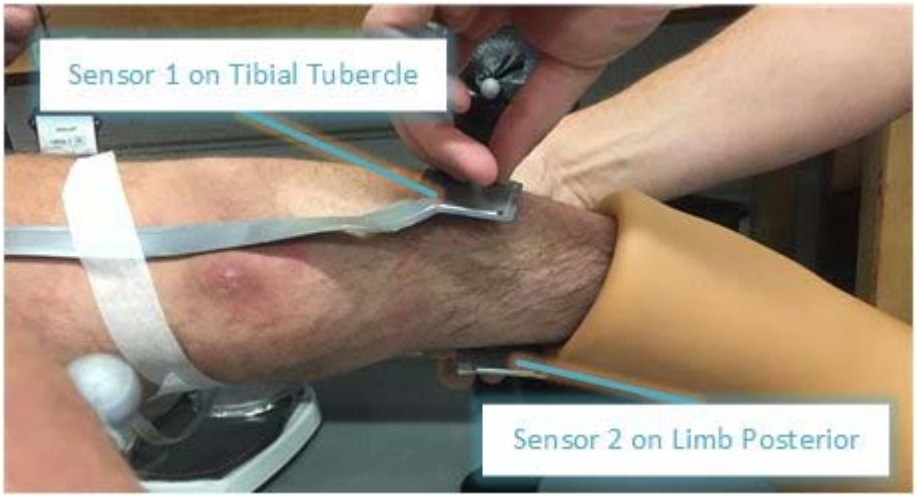

Figure 7.3: The subject's residual limb is shown with pressure sensors being mounted on the tibial tubercle and limb posterior.

Munich Germany) shown in Figure 7.4. To synchronize pressure data with marker and GRF data, a custom RF trigger (Figure 7.4) was designed to wirelessly send a logic high signal to the data collection board on the first frame, to be used during post-processing.

Prior to experimental trials, static calibration trials were performed to establish scale factors and subject weight (Figure 7.5). The subject first stood on the force platform closest to the center of the data collection area in a normal standing pose where all limbs were straight, and arms extended out laterally. Marker and force data were recorded for ten seconds with the subject standing as still as possible. The same protocol was then repeated with the subject standing in a

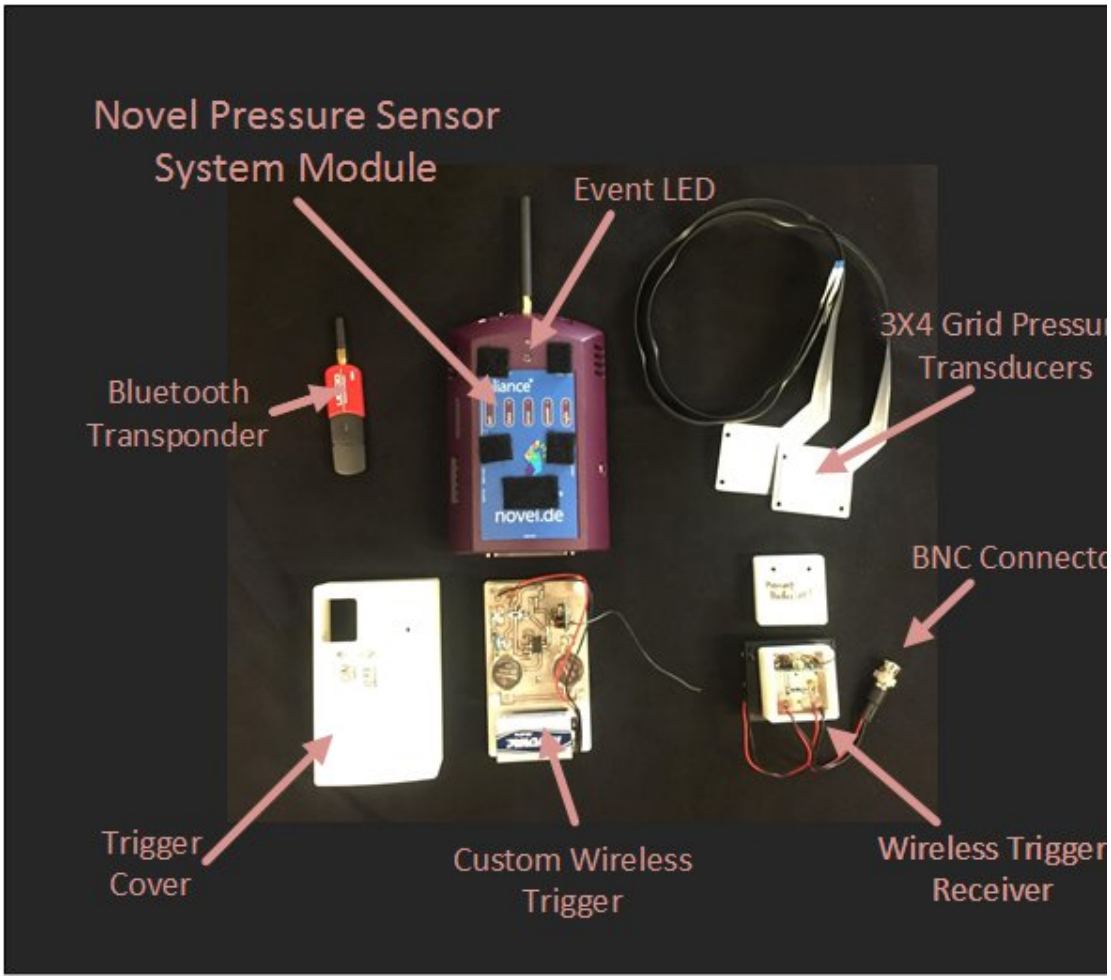

Figure 7.4: The novel pressure system used to record intra-socket pressures is shown with two 3x4 grid capacitive sensors and the custom RF data synchronization trigger.

flexed pose where all limbs were slightly bent, to better establish joint centers of rotation during scaling.

Test trials for this evaluation consisted of normal walking at the subjects preferred speed. To establish a preferred speed baseline, the subject was tasked to walk through the data collection area 5 times measuring speed with photogates spaced 6 m apart. After establishing a baseline, the subject performed the same task while wearing their daily use prosthesis while all data was recorded until 3 successful trials were completed. A successful trial was considered one in which the subject was within 5% of their preferred speed, and struck all 3 force platforms without targeting. The subject

Figure 7.5: The subject is shown posing for a static standing calibration trial, where marker positions are recorded to be used for model scaling during data post processing.

was then outfitted with the Active Alignment prosthesis, and statically aligned to match the passive prosthesis based on walking observations and subject feedback. The alignment coefficient, described in Chapter 4, was manually tuning in increments of 0.1 to extend the prosthesis 100% before toe off and to minimize actuator stall during toe off. The alignment coefficient requires different tuning based on walking style, which varies from subject to subject as well as test conditions (i.e. treadmill vs runway). After a brief period of acclimation, and another set of static calibration trials, the subject repeated the walking trials until 3 successful trials were completed.

7.2.3 Data Processing

Two generic musculoskeletal OpenSim models for a person with left transtibial amputation were used, one with a generic passive prosthesis and the other with the modified Active Alignment prosthesis, both including the 4-DOF socket joint developed in Chapter 6. The models were pre-scaled to match the residual limb length, detailed in Chapter 6.

To scale the models to the subject identically, a model matching algorithm was developed (Figure 7.6) to avoid error introduced by manual scaling of each model. The passive model was first scaled manually, by altering the calibration model markers through the OpenSim GUI and using the OpenSim scale tool, which scales each segment to a distance measurement ratio based on experimental scale marker positions recorded in the static calibration and marker placement on segments in the model. The tracking markers were then placed automatically by using a MATLAB optimization routine that iteratively adjusted the model marker positions and then performing an IK analysis through the API, reducing the optimization cost c in (7.1). This function minimizes the sum of marker errors, which is the Euclidian norm of the vector between marker m experimental position $E(x,y,z)_m$ and model position $M(x,y,z)_m$ for each frame n of the IK results, plus passive prosthetic foot flexion *flex* in the last 10 percent of gait multiplied by a weighting factor W. Using this method to place the model markers, tracking error RMS was reduced to 4.9 mm. After markers were placed, both scale factors and marker placement from the passive model were used to modify

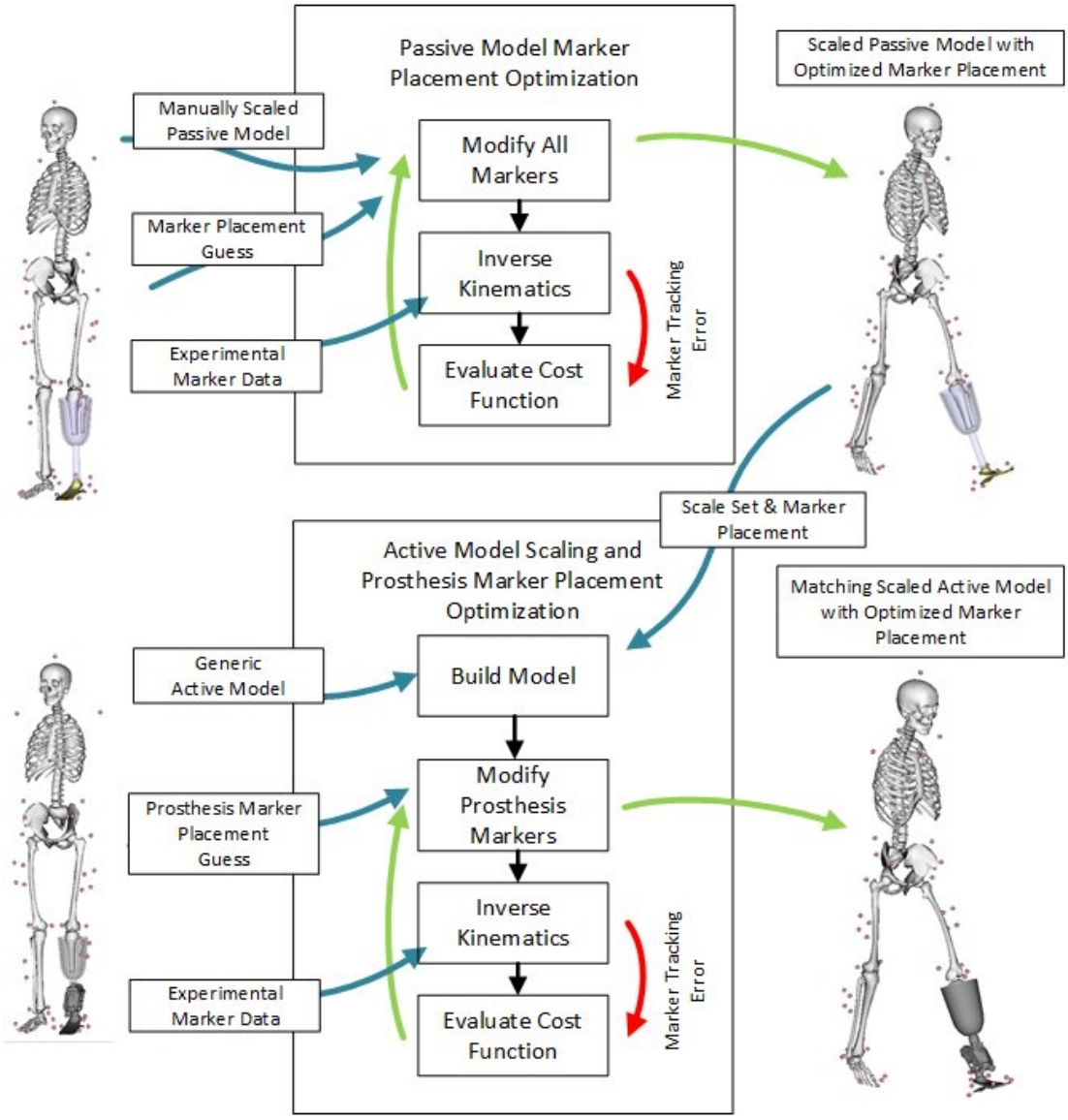

Figure 7.6: The workflow of the model matching algorithm is presented. After manually scaling a passive model, it is loaded in the script with a marker set placement guess and experimental marker data from a single walking trial. The first optimization loop minimizes marker error and prosthetic foot unloaded flexion by performing an inverse kinematics analysis and adjusting marker placement throughout the model with the exception of the sternum tracking marker. The second stage of the algorithm takes the scale set and optimized marker placements, and applies them to the generic active model. A second optimization loop then minimizes marker error on the prosthesis only since the rest of the model is identical to the passive model. After optimizing the marker placement with this method, average marker RMS for inverse kinematic analyses is about 5 mm.

the active model so that it was identical with the exception of the prosthesis. A similar optimization was then performed on the active model prosthetic limb markers only, with the added penalty of

the prosthesis actuator deviating from 0 displacement on the first and last frames. This optimization reduced tracking error RMS to 5.7 mm.

$$C = \sum_{n=1}^{n_{frames}} \sum_{m=1}^{m_{markers}} \sqrt{\left(Mx_{nm} - Ex_{nm}\right)^2 + \left(My_{nm} - Ey_{nm}\right)^2 + \left(Mz_{nm} - Ez_{nm}\right)^2} + \sum_{n=n_{frames}-.5*n_{frames}}^{n_{frames}} W_1 flex_n \quad (7.1)$$

Post processing data included calculating inverse kinematics followed by inverse dynamics for all trials using OpenSim tools through the MATLAB API. Center of mass (COM) trajectory was calculated, followed by joint power. Prosthesis power was estimated using the computed muscle control tool, since inverse dynamics could not separate forces exactly in a closed loop kinematic chain. Ground reaction forces were and pressure data were imported and filtered with a moving average window. All datasets were then averaged across trials, and standard deviations were calculated.

7.3 Results and Discussion

Comprehensive results are presented and discussed in this section, highlighting comparisons of walking mechanics when the test subject uses a daily use prosthesis and the experimental prototype with Active Alignment. Measures include ground reaction forces, joint level kinematics, kinetics, power and work, total power and work summed across healthy joints, intra-socket pressure, center of mass trajectory, and active prosthesis power contribution. In the following data presented, ESR represents data from the amputated limb using a passive energy storage and return prosthesis, and Intact ESR represents data from the contralateral intact limb. Similarly, AAP represents data from the amputated limb fitted with the Active Alignment prosthesis, and Intact AAP represents data from the intact contralateral limb from the same data set. All curves represent averaged data.

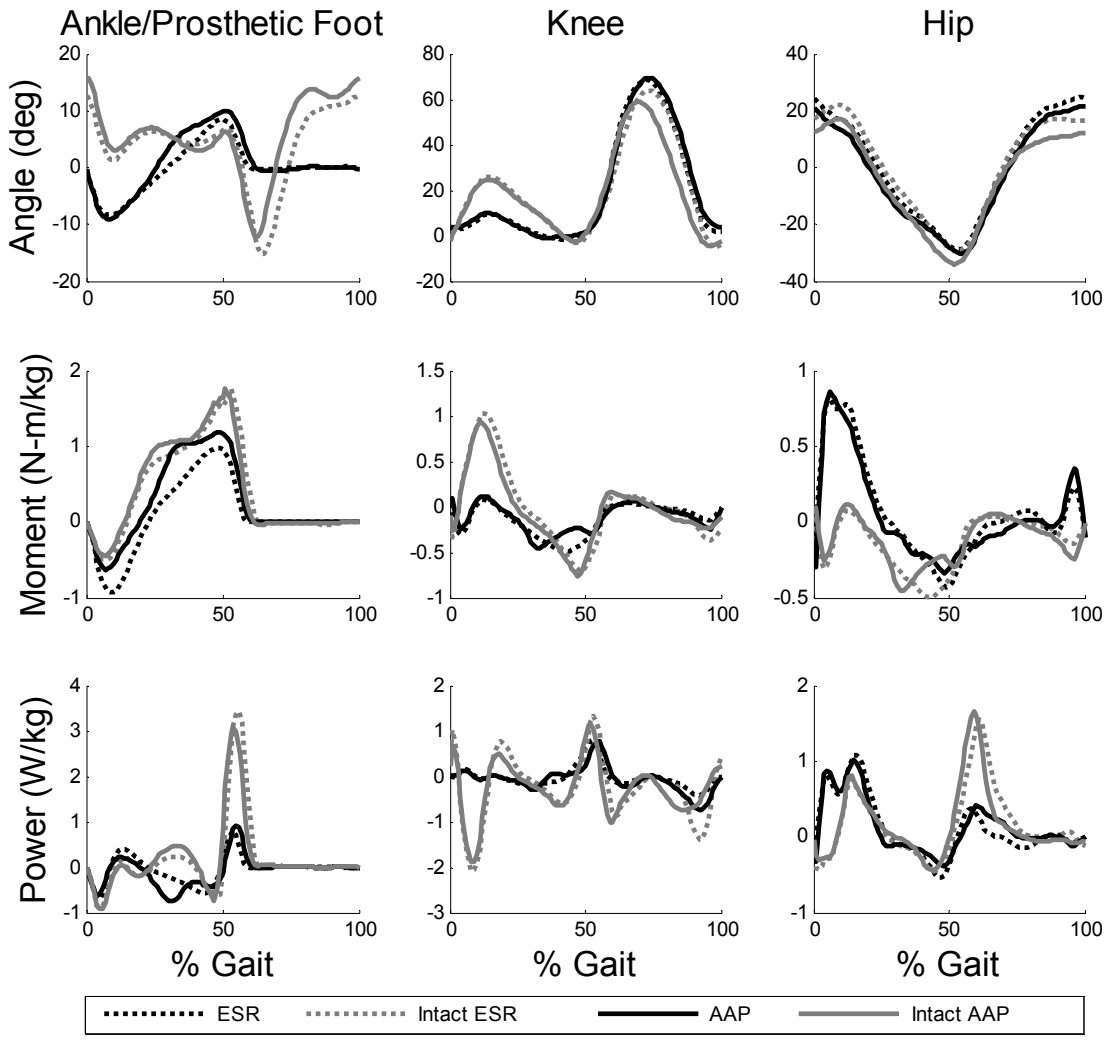

Figure 7.7: Average sagittal plane biomechanics data are presented for the ankle, knee and hip joints. ESR represents data from the limb with amputation using a passive energy storage and return foot, and Intact ESR represents data from the contralateral limb. AAP represents data from the limb with amputation using the active alignment prosthesis, and Intact AAP represents data from the contralateral limb. The prosthesis data shown for the prosthetic foot in the AAP case only includes the passive foot attached to the active prosthesis.

Figure 7.7 presents the calculated inverse kinematics generalized motions, inverse dynamics generalized forces and power for the ankle, knee and hip joints in the sagittal plane. On the ankle plots, the prosthetic foot flexion coordinate is shown with intact ankle data as presented in the literature. Prosthetic foot mechanics in the AAP case represents the flex foot only, not including robotic ankle mechanics. In this figure, the kinematic data are shown on the top three plots. The

main observations that can be taken from these three plots are that the prosthetic gait is very asymmetric in nature, and differences between passive and active trials throughout the body are subtle. The biggest change is in the intact knee and hip joints, which are altered due to Active Alignment as simulated in earlier studies. Inspecting joint moments and power, it is clear that there are no major changes to how the person is walking, and the added motions and forces of the Active Alignment ankle prosthesis introduce small deviations from the user's normal prosthetic gait. The motion and force patterns all represent gait data that are seen in the literature.

Figure 7.8 shows average ground reaction force data of experimental trials. It is seen on the prosthetic left side that there is an increase in vertical force on heel strike, and mid-stance when the prosthesis realigns the limb. However, reduced vertical GRF during late stance before toe off suggests that the subject pushes off less with the active prosthesis. Peak horizontal ground reaction forces on the prosthetic side are increased with the active prosthesis, indicating the subject is

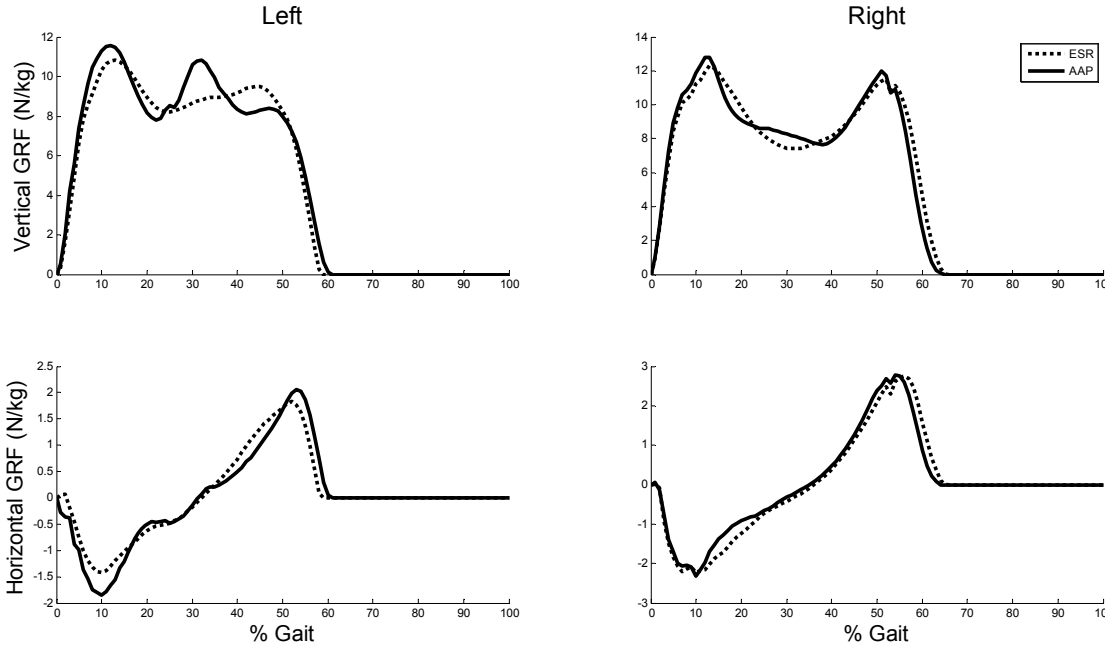

Figure 7.8: Average normalized ground reaction forces are shown for trials where the test subject used the passive energy storage and return (ESR) foot prosthesis and the active alignment prosthesis (AAP).

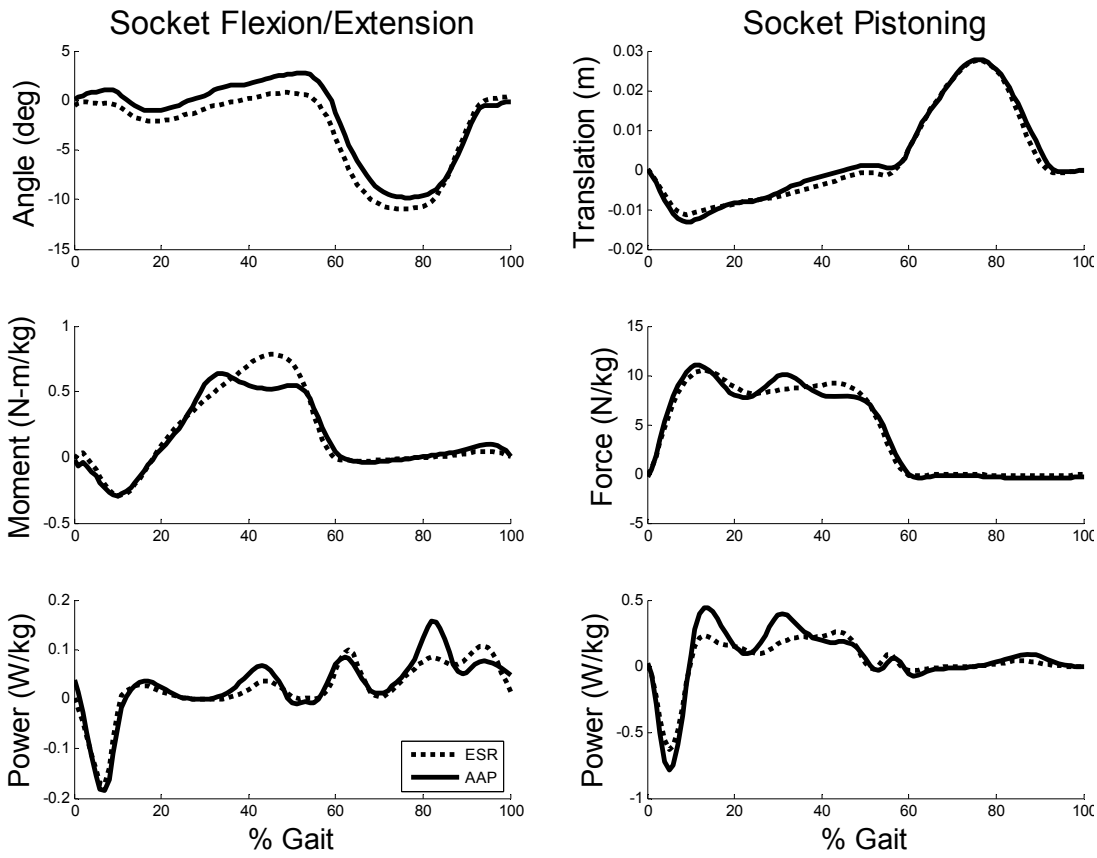

Figure 7.9: Socket mechanics plots with average normalized sagittal plane generalized socket movements, forces and power are shown for trials where the test subject used the passive energy storage and return (ESR) foot prosthesis and the active alignment prosthesis (AAP).

landing harder, and able to sustain support from the prosthesis slightly longer during roll-over. The intact right side shows little difference in peak values for horizontal and vertical forces, but shows less stance time on the active limb when using the active ankle prosthesis. Interestingly, the affected limb shows a longer stance percentage with the active ankle, which suggests that the active ankle reduces the loading demand on the residual limb.

Figure 7.9 presents generalized motions forces and powers for socket flexion/extension, and pistoning, which are the two most clinically relevant coordinates in the socket joint. The most notable feature of these plots is the reduction of peak socket moments during late stance, as

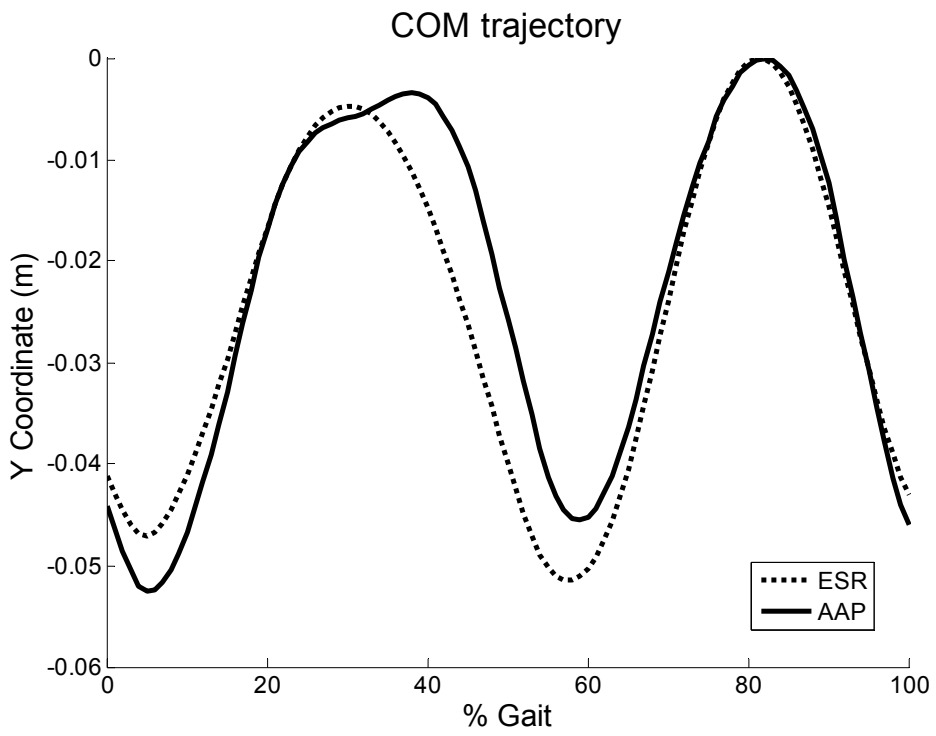

Figure 7.10: The COM trajectory during gait is shown zeroed to the second peak, seen during contralateral stance. Trial averages where the test subject used the passive energy storage and return (ESR) foot prosthesis are represented by the dashed line, and trial averages from the active alignment prosthesis (AAP) are represented by the solid line.

predicted in earlier work, which is associated with peak intra-socket pressures. Pistoning force resembles GRFs presented in Figure 7.8 as expected, and near zero net power is generated throughout gait which is expected of a passive joint.

The center of mass (COM) trajectories are shown in Figure 7.10, zeroed with the second peak seen during mid stance of the intact contralateral limb. This allows for comparison of the COM trajectories, negating the effect that a heavier prosthesis will have on center of mass as well as differences caused by alignment of prosthetic devices. It is observed that the active alignment prosthesis drops the center of mass lower after heel strike and before actuation, indicating the prosthesis height may have not been adjusted the same as the passive prosthesis height. The center

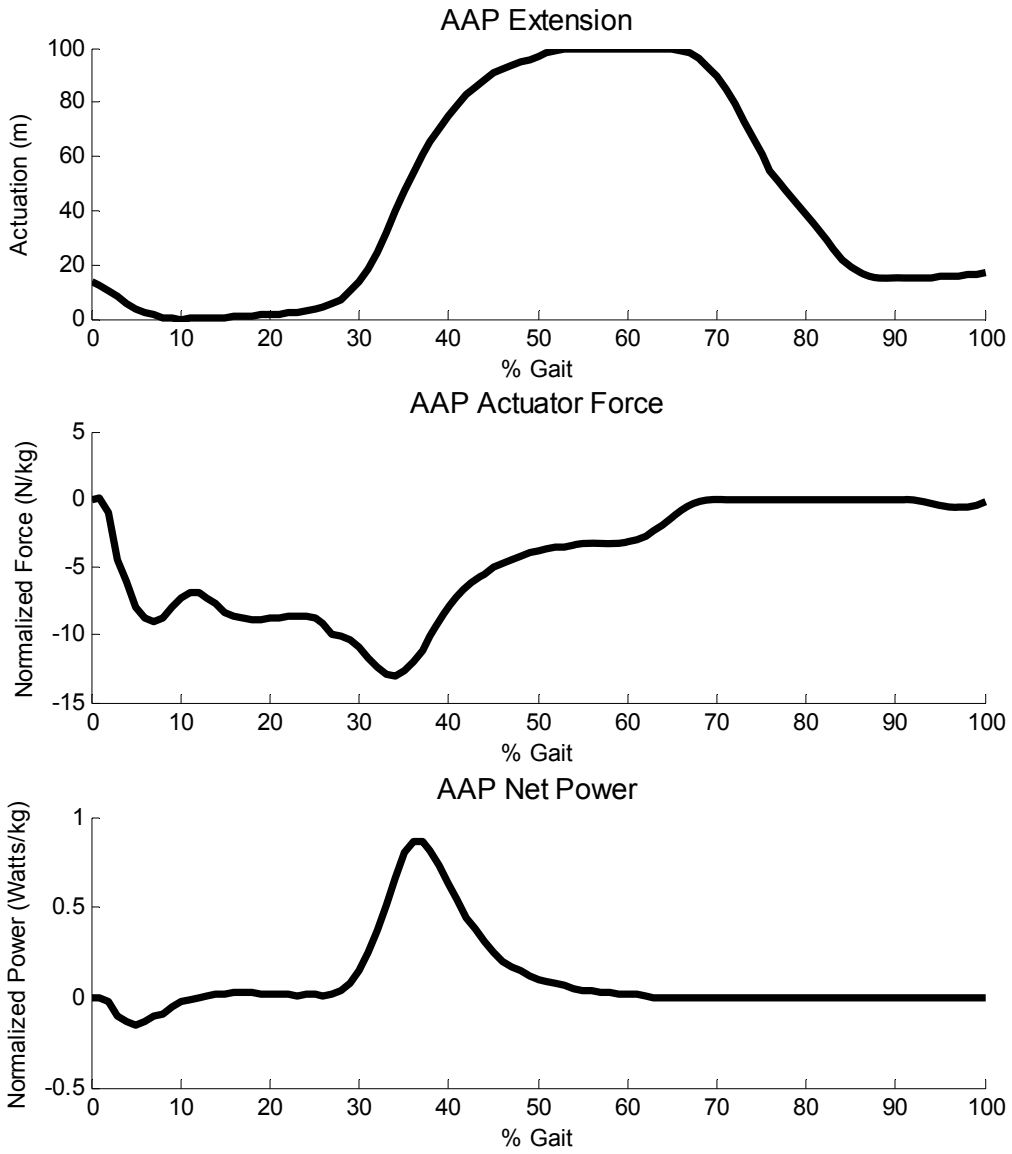

Figure 7.11: Prosthesis, average extension, actuator force and power data are shown for the active alignment prosthesis.

of mass then peaks slightly higher with the active prosthesis, showing that the prototype is effectively injecting power during stance and performing net positive work to lift the subject.

In Figure 7.11, the prototype prosthesis actuator mechanics are shown during gait. The top plot displays the ball screw position, which quickly contracts to extend the prosthesis. The middle and lower plots present the prosthesis force and power. Force and power for the experimental prosthesis

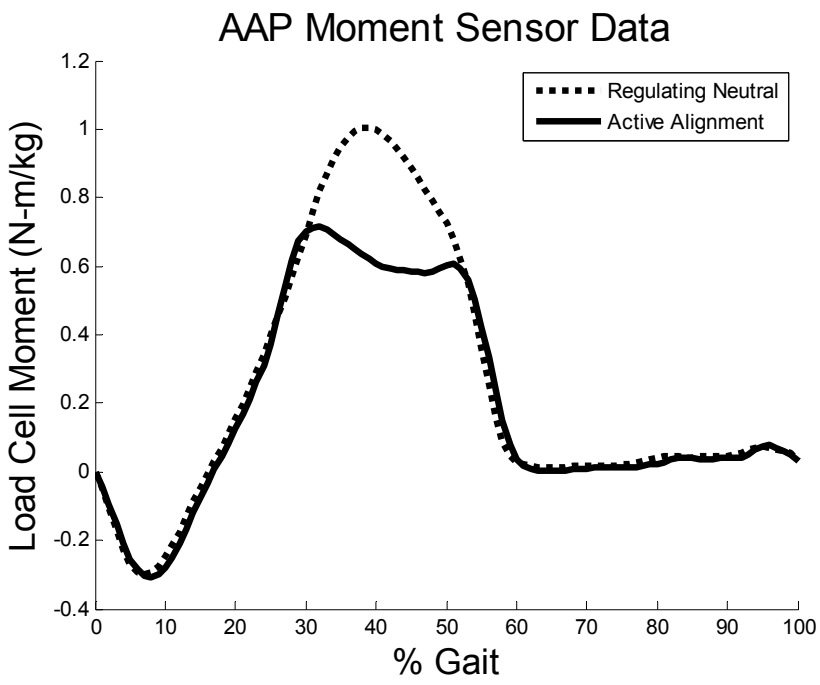

Figure 7.12: Average moment sensor data from 5 steps are shown while the experimental prosthesis regulates a neutral position, and employs active alignment.

were estimated with a computed muscle control, forward dynamics simulation algorithm, which tracked calculated IK results with a scaled model of the subject wearing the prosthesis prototype. This method was used in order to avoid problems encountered when applying standard ID methods to a closed kinematic chain, i.e. four bar linkage with a linear actuator, which would result in false joint moments at every joint in the prosthesis where actuators don't actually exist. CMC was performed using a point to point force to represent the actuator ball screw, resulting in force and power calculations that are a lumped sum of all force contributors in the prosthesis, including friction losses and static loading of the hard-stops. For this reason, the data that are shown for power can be considered prosthesis net power, which is positive during mid stance.

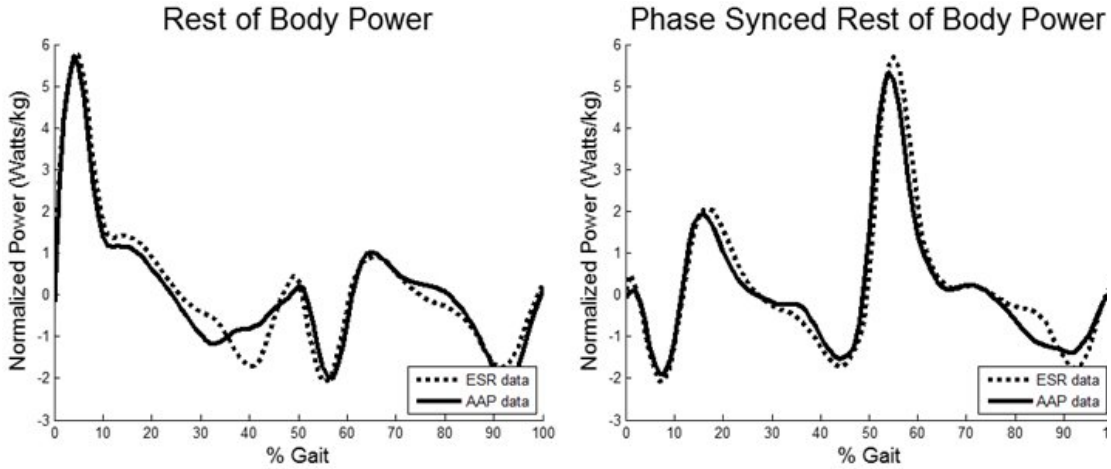

Figure 7.13: Combined intact joint power is presented showing the natural power flow (left) and phase synced (right). The phase synced plot aligns the stance and swing phases of the limbs. Each plot displays the sum of calculated power from all biological joints as it occurs throughout gait (left) and aligning the stance and swing phases of the limbs (right). Examining the left plot, peak power generation and absorption does not change between cases, but in the phase synced plot, the average peak is reduced at every peak when Active Alignment is employed. This indicates that with active alignment, power demand is distributed differently across joints.

Figure 7.12 shows average data recorded from the experimental prosthesis moment sensor when the prosthesis regulates a neutral position compared to employing Active Alignment. This data agrees with moments calculated for the residuum socket interface seen in Figure 7.11.

The normalized, average rest of body power is presented in Figure 7.13 in two plots. Rest of body power is the sum of power generated by the intact ankle, both knees, and both hips. The plot on the left shows power summed across all intact joints as it is generated naturally throughout gait, revealing the net power flow needed to generate locomotion. This highlights how asymmetrically power is generated, showing a greater reliance on the intact limb to ambulate. The plot on the right of Figure 7.13 shows phase synced summed power of the intact joints, which aligns left and right limb stance and swing phases. Phase synced summed power reveals a 6.6% reduction in peak power generation when Active Alignment is employed, which can mostly be attributed to the decrease in peak intact ankle power during intact push off (Figure 7.7). The reduction seen in the phase synced

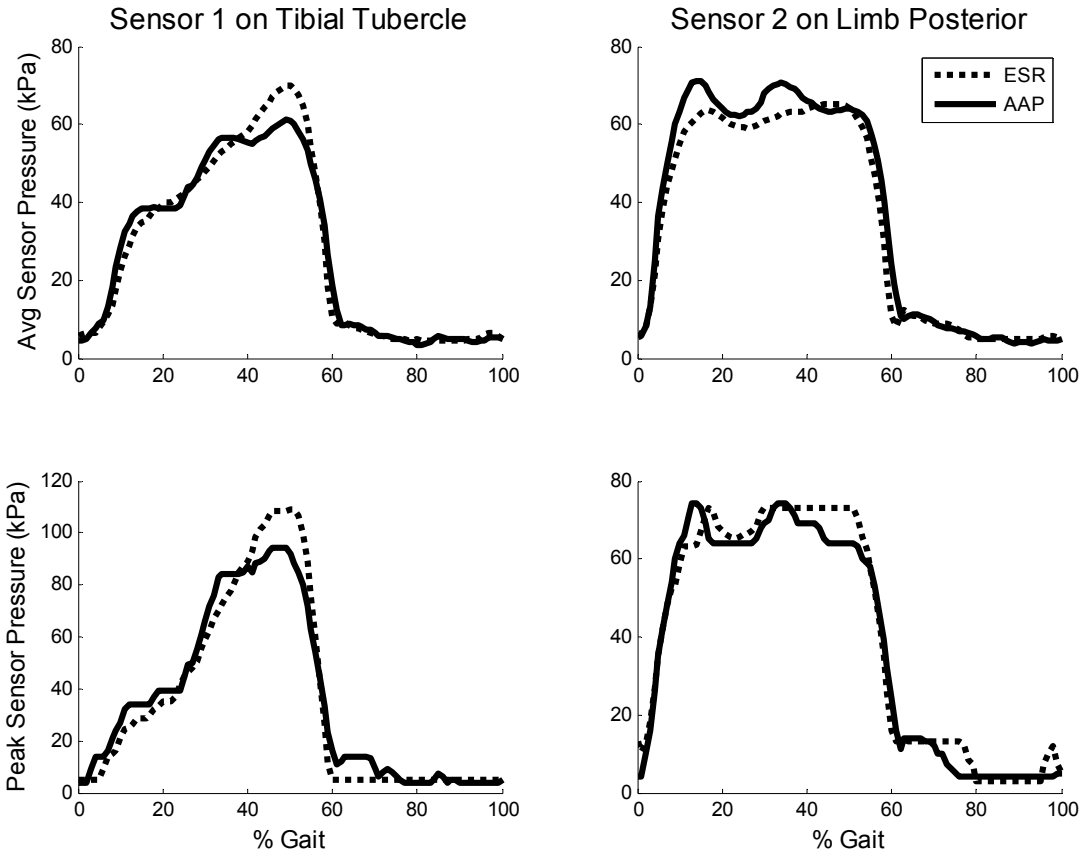

Figure 7.14: Average and peak pressures are shown for the tibial tubercle region, and mid posterior region of the residual limb throughout the gait cycle.

plot indicates that total power needed to ambulate may be distributed differently across joints (decrease in intact ankle power and increase in intact hip power during push off seen in Figure 7.7), but the amount of power does not change. Table 7.2 presents the maximum power generation, maximum power absorption, net work and net positive work during gait for the individual biological joints and summed across joints. Data for each joint are mean and SD of the specified measure for when the subject used their daily use passive prosthesis compared to the experimental prosthesis. Net positive work remained consistent between test conditions, however a 25% reduction in average net work was seen, indicating an increase in average net negative work in rest of body when using the experimental prosthesis. This may be attributed to multiple factors,

Biological Joint	*Prosthesis Used*	*Max Power Generation (W/kg)*	*Max Power Absorption (W/kg)*	*Net Work (J/kg)*	*Net Positive Work (J/kg)*
Intact Ankle	Passive	3.636 ±0.044	-0.987 ±0.063	0.213 ±0.030	0.352 ±0.005
	Active	3.590 ±0.129	-1.009 ±0.073	0.219 ±0.034	0.362 ±0.011
Affected Knee	Passive	0.879 ±0.037	-0.446 ±0.041	-0.028 ±0.007	0.092 ±0.012
	Active	0.865 ±0.213	-0.768 ±0.021	-0.086 ±0.013	0.088 ±0.009
Intact Knee	Passive	1.528 ±0.144	-2.219 ±0.035	-0.307 ±0.021	0.211 ±0.003
	Active	1.427 ±0.236	-2.127 ±0.524	-0.343 ±0.041	0.173 ±0.049
Affected Hip	Passive	1.144 ±0.083	-0.573 ±0.093	0.137 ±0.011	0.248 ±0.014
	Active	1.213 ±0.031	-0.046 ±0.040	0.167 ±0.015	0.258 ±0.010
Intact Hip	Passive	1.693 ±0.217	-0.643 ±0.030	0.196 ±0.006	0.305 ±0.002
	Active	1.906 ±0.047	-0.510 ±0.087	0.208 ±0.036	0.312 ±0.027
Summed Total	Passive	n/a	n/a	0.212 ±0.039	1.208 ±0.019
	Active	n/a	n/a	0.165 ±0.067	1.192 ±0.059

Table 7.2: Peak power generation, absorption, net work and net positive work are shown for all biological joints when using the active prosthesis and the daily use passive prosthesis. Data are mean ±SD. Active and passive data cannot be proved significantly different with the sample size used.

including the added mass of the experimental prosthesis and increased power of the active prosthesis. The subject also may not have been entirely acclimated to the prosthesis. It is feasible to expect less power absorption in the biological joints given more time for the user to adapt to the robotic ankle.

Figure 7.14 presents data that are from the pressure transducers on the tibial tubercle and residuum mid-posterior. These findings are perhaps the most significant of all results presented. It is clearly shown that both average and peak pressures on the tibial tubercle are decreased by over 10% when the active alignment prosthesis is used. Average pressure on the limb posterior increased during early stance following heel strike, however peak pressures on the posterior are not increased.

Lastly, when the subject was asked to describe level of effort and comfort, they stated that it was easier to walk with the experimental device, and that they felt they would have more endurance

while walking on it. This is despite the device weighing more than twice that of their daily use device. They specifically said that it was less demanding on their residual limb, and that the load bearing tissues felt less stressed.

7.4 Conclusion

This chapter presents a single demonstration as a preliminary evaluation of the robotic prosthesis prototype with Active Alignment. After a brief background, prototype modifications were discussed. The methods were then presented highlighting modeling, data collection and data post-processing. The results were then presented and discussed.

The findings in this chapter provide strong evidence that the prosthesis is able to inject net positive power into the gait cycle while reducing loading demand on the residual limb. Stance support time is increased in the affected limb and reduced in the intact limb when Active Alignment is used. Average net work in biological joints is reduced by 25%, while net positive work is consistent between test conditions indicating increase in total power absorption during gait. Peak pressures on the residual limb were reduced by over 10%. With minimal training, stance time increased on the effected limb and decreased on the healthy contralateral limb, providing a more symmetric gait. Additionally, the user stated that it was easier to walk with the powered prosthesis, and that they felt they had more endurance despite the prototype being over twice as heavy as the user's daily use prosthesis. Overall, the prosthesis did not fundamentally change or disrupt the subjects gait in order to achieve the intended pressure reduction on the residual limb. It is feasible to think that greater improvements would be seen if the subject were allowed more time to adjust to the prosthesis, and if improvements to the controller and hardware were implemented.

Although the results presented are far from those of simulations used in the prosthesis development, it is clear that there is potential that is worth further investigation and optimization. It may be found that further effects are seen if the user is allowed to acclimate to the modified gait

kinematics over a longer period of time. Additional modifications to the prosthesis that enable the full range of motion may further improve results. Lastly, we point out that the model used in the original design assumed an ideal rigid socket interface. A more realistic model and truly predictive simulations would enable a better optimized prosthesis design.

CHAPTER 8

SUMMARY, CONCLUSIONS AND FUTURE WORK

8.1 Summary

This dissertation aims to attain a better understanding of the role of residuum-socket mechanics on prosthetic gait, and to determine whether prosthesis design approach with criterion defined by this interaction can yield an alternative prosthetic gait with positive attributes. Through a synergistic amalgamation of computational studies, device design, evaluation and refinement, prosthetic gait mechanics were analyzed in silico and in a controlled laboratory environment to evaluate the effects of a concept prosthesis with Active Alignment. The most noteworthy findings and key contributions are discussed in this chapter.

First, the concept of Active Alignment was developed through a series of systematic analyses and simulations. It was shown that with ideal assumptions used in the design of physiologically normal prosthetic devices, when applied to simulations of virtual prototypes with altered kinematics, it was theoretically possible to reduce the loading demand on the residual limb and simultaneously improve gait mechanics with additional power from the active prosthesis. A complete design was then detailed, including mechanics and electronics for the realization of a prototype prosthesis.

Next, modeling methods were developed for evaluating whole-body biomechanics of persons with lower limb amputation. It was shown that the accuracy of whole body inverse kinematic solutions for prosthetic gait could match the accuracy seen when performing the same analysis on non-prosthetic gait, even though it is not possible to place tracking markers on the residual limb. This was achieved with a 4-DOF residuum socket joint model, also giving previously unattainable

insight to residuum-socket mechanics. Additionally, the development of the 4-DOF socket joint is the first step to achieving a model that can be used for realistic predictive simulations in future work.

Lastly, the prosthesis design was evaluated with the new modeling and evaluation techniques. It was demonstrated that the prosthesis prototype injects positive power into prosthetic gait, decreases power demand from the rest of body joints, and reduces the loading demand on the residual limb. Peak pressures on the residual limb were reduced by over 10%, compared to pressures observed when the user wore their daily use prosthesis. With minimal training, a more symmetric gait emerged as the subject used the device. Qualitatively, the user stated that it was easier to walk with the active prosthesis despite the device weight being twice that of their daily use prosthesis. The user also stated that they felt they had more endurance.

In summary, the results presented in this dissertation offer key insight about the role and limitations of residuum-socket mechanics on prosthetic gait. Our study has determined that prosthesis design can leverage insight into load transfer limitations of the residual limb, allowing for the optimization of prosthesis kinetics for an improved, more efficient gait.

8.2 Conclusions

Lower limb prosthesis technology has recently surged in advances in the past decade due to developments made in the field of robotics. Until now, traditional design criterion has always revolved around normal local morphology and functionality of an intact limb without regard to the loading interface. In this dissertation, it is demonstrated that kinetics of a prosthesis mechanism can be altered from the norm to redirect loading in a more efficient manner. In detail, the key contributions of this dissertation are summarized below:

- Whole body marker based inverse kinematics solutions of persons with lower limb amputation can achieve similar accuracy seen when performing the same analysis on

data from persons with intact limbs, even though markers cannot be attached to the residual limb. This is achieved with a 4-DOF socket model, and by leveraging the kinematic constraints required for a global IK solution.

- Alternative prosthesis designs that deviate from normal morphology and functionality can improve prosthetic gait. Power can be introduced into prosthetic gait with an alternative active prosthesis while simultaneously decreasing peak limb pressures and limb loading demand as well as improve gait symmetry.

In conclusion, the results of the computational studies, modelling methods, design and evaluation presented in this dissertation illuminate new possibilities for the design of robotic, lower limb prostheses. Through systematic simulation, design, modeling and evaluation, it was demonstrated that gait can be improved with alternative devices, while simultaneously reducing load demand on the residual limb. We expect that the findings presented will help to direct the design of future lower limb robotic prostheses.

8.3 Future Work

The work presented in this dissertation represents the first step forward in a new paradigm of prosthesis design. Future work involves further testing of the device, improvement of the current prototype, and then designing a second generation prototype ankle prosthesis with Active Alignment. More specifically, the future work that should be addressed is detailed below based on the findings presented in this dissertation.

8.3.1 Potential Improvements for the First Generation Prototype

In regards to improvement of the current prototype, control methodologies should be first improved upon in an effort to guide the design of second generation prototype. These controller improvements include both software and electronics hardware. Following advancements in control methods and design, certain aspects of the mechanism may be revisited.

Throughout the development of the prototype prosthesis, impedance based control was not explored since the linkage both rotates and translates the end effector but the only force feedback attainable is moment transfer to the prosthesis socket. Implementing impedance control may be able to be addressed in two ways. The first method would involve designing a new 3-axis load cell that senses moment in addition to linear force components in the sagittal plane. The second approach would be to treat the ankle as many different rotational ankles at discrete points of articulation, regulating the rotational impedance based on only moment and position feedback. Machine learning algorithms should also be explored in an effort to improve event detection, and also tune controller gain parameters more systematically.

Regarding controller hardware improvements, there are two issues that should be addressed to improve reliability, and usability in a laboratory environment. Routing of analog signals should be limited in order to reduce system feedback noise. Low voltage analog signals are easily corrupted from both ambient noise in a laboratory environment, and also from high-frequency/high-power signals being sent to the motor on the prosthesis itself. The inertial sensors and load cell amplifier should be changed over to modules with digital signal outputs, which could all be transmitted over the same sensor bus to the controller. The second major modification to controller hardware would be to develop an embedded controller pack, to rid the need for a desktop PC for the prototyping phase of development. Recent progress has been made with development kits such as the Raspberry Pi and Beagle Bone Black, enabling programming of the kits wirelessly from MATLAB Simulink models. Such a development kit combined with a dedicated peripheral handler board, motor driver and battery pack in a contained package would enable faster prototyping, and less complicated testing procedures. Further, it would allow testing to be performed outside of a laboratory environment.

8.3.2 Design of a Second Generation Prosthesis Prototype

The prototype presented in this dissertation used forward dynamics physics based simulations and ideal models to track able body kinematics. A comparison of simulation results presented in Chapter 3 to experimental results presented in Chapter 5 reveals that there are clear drawbacks to the methodology presented. These pitfalls must be overcome in order to accurately predict prosthetic locomotion with a virtual prototype.

State of the art modeling and predictive simulation techniques in development will be the main utilities used for designing the next generation ankle prosthesis with Active Alignment. This will include advanced residuum-socket impedance models based on experimental data, and simulations driven by optimal control techniques that utilize direct collocation optimization methods. Robotic device designs can also be simultaneously optimized in these predictive simulations, if proper objective functions are identified.

Without question, ignoring traditional design criterion for lower limb prosthetic devices introduces a new paradigm of what prosthetic devices should do, and an entire new realm of possibilities of what the prostheses can be. Clearly, if all criterion were ignored, one could design a robotic assistive device that eliminates the need for the user to perform any work at all. At a certain point however, there must be compromise between practicality, rehabilitation and utility. Therefore, a truly effective robotic prosthesis, that could potentially assume any form or functionality, should be designed to restore rest of body biomechanics to eliminate any user compensation as best as possible, but not impede user day to day activities.

BIBLIOGRAPHY

[1] Gailey, R. S., Roach, K. E., Applegate, E. B., Cho, B., Cunniffe, B., Licht, S., Maguire, M., and Nash, M. S., 2002, "The Amputee Mobility Predictor: An instrument to assess determinants of the lower-limb amputee's ability to ambulate," Arch. Phys. Med. Rehabil., **83**(5), pp. 613–627.

[2] Pitkin, M. R., 2010, Biomechanics of Lower Limb Prosthetics, Springer Berlin Heidelberg, Berlin, Heidelberg.

[3] Sanders, J. E., Bell, D. M., Okumura, R. M., and Dralle, a J., 1998, "Effects of alignment changes on stance phase pressures and shear stresses on transtibial amputees: measurements from 13 transducer sites.," IEEE Trans. Rehabil. Eng., **6**(1), pp. 21–31.

[4] Seelen, H. a. M., Anemaat, S., Janssen, H. M. H., and Deckers, J. H. M., 2003, "Effects of prosthesis alignment on pressure distribution at the stump/socket interface in transtibial amputees during unsupported stance and gait," Clin. Rehabil., **17**(7), pp. 787–796.

[5] Boone, D. A., Kobayashi, T., Chou, T. G., Arabian, A. K., Coleman, K. L., Orendurff, M. S., and Zhang, M., 2013, "Influence of malalignment on socket reaction moments during gait in amputees with transtibial prostheses.," Gait Posture, **37**(4), pp. 620–6.

[6] Wolf, S. I., Alimusaj, M., Fradet, L., Siegel, J., and Braatz, F., 2009, "Pressure characteristics at the stump/socket interface in transtibial amputees using an adaptive prosthetic foot.," Clin. Biomech., **24**(10), pp. 860–5.

[7] Boone, D. a, Kobayashi, T., Chou, T. G., Arabian, A. K., Coleman, K. L., Orendurff, M. S., and Zhang, M., 2012, "Influence of malalignment on socket reaction moments during gait in amputees with transtibial prostheses.," Gait Posture.

[8] Chadderton, H., 1978, "Prostheses, pain and sequelae of amputation, as seen by the amputee.," Prosthet Orthot Int., **2**(1), pp. 12–14.

[9] Nielsen, C., Psonak, R., and Kalter, T., 1989, "Factors affecting the use of prosthetic services," J Prosthet Orthot., **1**(4), pp. 242–49.

[10] Dillingham, T., Pezzin, L., MacKenzie, E., and Burgess, A., 2001, "Use and satisfaction with prosthetic devices among persons with trauma-related amputations: a long-term outcome study," Am J Phys Med Rehabil., **80**(8), pp. 563–71.

[11] Bilodeau, S., Hébert, R., and Desrosiers, J., 2000, "Lower limb prosthesis utilisation by elderly amputees," Prosthet. Orthot. Int., **24**(2), pp. 126–132.

[12] Beekman, C. E., and Axtell, L. a, 1987, "Prosthetic use in elderly patients with dysvascular above-knee and through-knee amputations.," Phys. Ther., **67**(10), pp. 1510–6.

[13] Herr, H. M., and Grabowski, a. M., 2012, "Bionic ankle-foot prosthesis normalizes walking gait for persons with leg amputation," Proc. R. Soc. B Biol. Sci., **279**(July 2011), pp. 457–464.

[14] Pitkin, M. R., 2010, Biomechanics of Lower Limb Prosthetics, Springer Berlin Heidelberg, Berlin, Heidelberg.

[15] Silverman, A. K., and Neptune, R. R., 2012, "Muscle and prosthesis contributions to amputee walking mechanics: a modeling study.," J. Biomech., **45**(13), pp. 2271–8.

[16] Lilja, M., Johansson, T., and Oberg, T., 1993, "Movement of the tibial end in a PTB prosthesis socket: a sagittal X-ray study of the PTB prosthesis.," Prosthet. Orthot. Int., **17**, pp. 21–26.

[17] Convery, P., and Murray, K. D., 2001, Ultrasound study of the motion of the residual femur within a trans-femoral socket during daily living activities other than gait.

[18] Gholizadeh, H., Osman, N. A. A., Kamyab, M., Eshraghi, A., Abas, W. A. B. W., and Azam, M. N., 2012, "Transtibial prosthetic socket pistoning: Static evaluation of Seal-In ® X5 and Dermo ® Liner using motion analysis system," Clin. Biomech., **27**, pp. 34–39.

[19] Radcliffe, C. W., and Foort, J., 1961, "The patella tendon-bearing below knee prosthesis," Univ. California, Biomech. Lab.

[20] Foort, J., 1965, "The patellar-tendon-bearing prosthesis for below-knee amputees, a review of technique and criteria.," Artif. Limbs, **9**(1), pp. 4–13.

[21] Selles, R. W., Janssens, P. J., Jongenengel, C. D., and Bussmann, J. B., 2005, "A randomized controlled trial comparing functional outcome and cost efficiency of a total surface-bearing socket versus a conventional patellar tendon-bearing socket in transtibial amputees," Arch. Phys. Med. Rehabil., **86**(January), pp. 154–161.

[22] Boutwell, E., Stine, R., Hansen, A., Tucker, K., and Gard, S., 2012, "Effect of prosthetic gel liner thickness on gait biomechanics and pressure distribution within the transtibial socket.," J. Rehabil. Res. Dev., **49**(2), pp. 227–40.

[23] Hatfield, a. G., and Morrison, J. D., 2001, "Polyurethane gel liner usage in the Oxford Prosthetic Service," Prosthet. Orthot. Int., **25**(1), pp. 41–46.

[24] Pitkin, M. R., 2010, “Biomechanics of Lower Limb Prosthetics,” (Torres 1994).

[25] Hansen, A. H., Sam, M., and Childress, D. S., 2004, “The Effective Foot Length Ratio: A Potential Tool for Characterization and Evaluation of Prosthetic Feet,” JPO J. Prosthetics Orthot., **16**(2), pp. 41–45.

[26] Fey, N. P., Klute, G. K., and Neptune, R. R., 2012, “Optimization of prosthetic foot stiffness to reduce metabolic cost and intact knee loading during below-knee amputee walking: a theoretical study.,” J. Biomech. Eng., **134**(11), p. 111005.

[27] Fey, N. P., Klute, G. K., and Neptune, R. R., 2011, “The influence of energy storage and return foot stiffness on walking mechanics and muscle activity in below-knee amputees.,” Clin. Biomech., **26**(10), pp. 1025–32.

[28] Hansen, A. H., and Childress, D. S., 2004, “Effects of shoe heel height on biologic rollover characteristics during walking.,” J. Rehabil. Res. Dev., **41**, pp. 547–554.

[29] Hansen, A. H., Childress, D. S., Miff, S. C., Gard, S. a, and Mesplay, K. P., 2004, “The human ankle during walking: implications for design of biomimetic ankle prostheses.,” J. Biomech., **37**(10), pp. 1467–74.

[30] Hill, D., and Herr, H., 2013, “Effects of a powered ankle-foot prosthesis on kinetic loading of the contralateral limb : A case series,” IEEE Int. Conf. Rehabil. Robot., p. in press.

[31] Herr, H. M., and Grabowski, A. M., 2012, “Bionic ankle-foot prosthesis normalizes walking gait for persons with leg amputation,” Proc. R. Soc. B., **279**(1728), pp. 457–64.

[32] Au, S., Berniker, M., and Herr, H., 2008, “Powered ankle-foot prosthesis to assist level-ground and stair-descent gaits.,” Neural Netw., **21**(4), pp. 654–66.

[33] Sup, F., Varol, H. A., Mitchell, J., Withrow, T. J., and Goldfarb, M., 2009, “Preliminary Evaluations of a Self-Contained Anthropomorphic Transfemoral Prosthesis.,” IEEE/ASME Trans. Mechatronics, **14**(6), pp. 667–676.

[34] Mehmet Oymagil, A., Hitt, J. K., Sugar, T., and Fleeger, J., 2007, “Control of a regenerative braking powered ankle foot orthosis,” 2007 IEEE 10th International Conference on Rehabilitation Robotics, ICORR’07, pp. 28–34.

[35] Bellman, R. D., Holgate, M. A., and Sugar, T. G., 2008, “SPARKy 3: Design of an active robotic ankle prosthesis with two actuated degrees of freedom using regenerative kinetics,” 2008 2nd IEEE RAS EMBS Int. Conf. Biomed. Robot. Biomechatronics, pp. 511–516.

[36] Hitt, J., Sugar, T., Holgate, M., and Bellman, R., 2010, “An Active Foot-Ankle Prosthesis with Biomechanical Energy Regeneration,” J. Med. Devices, **4**(011003), pp. 1–9.

[37] D'Andrea, S., Wilhelm, N., Silverman, A. K., and Grabowski, A. M., 2014, "Does Use of a Powered Ankle-foot Prosthesis Restore Whole-body Angular Momentum During Walking at Different Speeds?," Clin. Orthop. Relat. Res., **472**(10), pp. 3044–54.

[38] Alley, R., 2011, "The High-Fidelity Interface : Skeletal Stabilization through Alternating Soft Tissue Compression and Release Randall Alley , BSc , CP , LP , FAAOPceo ," pp. 3–5.

[39] Pohlig, K., 2014, "Socket The Pohlig Bionic Socket System (PBSS)."

[40] Ziegler-Graham, K., MacKenzie, E. J., Ephraim, P. L., Travison, T. G., and Brookmeyer, R., 2008, "Estimating the prevalence of limb loss in the United States: 2005 to 2050.," Arch. Phys. Med. Rehabil., **89**(3), pp. 422–9.

[41] Owings, M., and Kozak, L., Ambulatory and Inpatient Procedures in the United States, 1996.

[42] Staff, N., 2008, "Amputation Statistics by Cause Limb Loss in the United States Amputation Statistics by Cause Limb Loss in the United States," Phys. Med. Rehabil., pp. 1–3.

[43] Ziegler-Graham, K., MacKenzie, E. J., Ephraim, P. L., Travison, T. G., and Brookmeyer, R., 2008, "Estimating the prevalence of limb loss in the United States: 2005 to 2050.," Arch. Phys. Med. Rehabil., **89**(3), pp. 422–9.

[44] Waters, R. L., Perry, J., Antonelli, D., and Hislop, H., 2010, "Energy cost of walking of amputees : the influence of level of amputation The Influence of Walking of Level of Amputees : of Amputation," pp. 42–46.

[45] Waters, R. L., and Mulroy, S., 1999, "The energy expenditure of normal and pathologic gait," Gait Posture, **9**(3), pp. 207–31.

[46] Waters, R. L., Perry, J., Antonelli, D., and Hislop, H., 1976, "Energy cost of walking of amputees: the influence of level of amputation," J. Bone Jt. Surg., **58**, pp. 42–46.

[47] Hammarlund, C. S., Carlström, M., Melchior, R., and Persson, B. M., 2011, "Prevalence of back pain, its effect on functional ability and health-related quality of life in lower limb amputees secondary to trauma or tumour: a comparison across three levels of amputation," Prosthet. Orthot. Int., **35**(1), pp. 97–105.

[48] Norvell, D. C., Czerniecki, J. M., Reiber, G. E., Maynard, C., Pecoraro, J. a, and Weiss, N. S., 2005, "The prevalence of knee pain and symptomatic knee osteoarthritis among veteran traumatic amputees and nonamputees.," Arch. Phys. Med. Rehabil., **86**(3), pp. 487–493.

[49] Struyf, P. a, van Heugten, C. M., Hitters, M. W., and Smeets, R. J., 2009, "The prevalence of osteoarthritis of the intact hip and knee among traumatic leg amputees.," Arch. Phys. Med. Rehabil., **90**(3), pp. 440–6.

[50] Portnoy, S., Yizhar, Z., Shabshin, N., Itzchak, Y., Kristal, a, Dotan-Marom, Y., Siev-Ner, I., and Gefen, a, 2008, "Internal mechanical conditions in the soft tissues of a residual limb of a trans-tibial amputee.," J. Biomech., **41**(9), pp. 1897–909.

[51] Chadderton, H. C., 1978, "Prostheses, pain and sequelae of amputation, as seen by the amputee.," Prosthet. Orthot. Int., **2**, pp. 12–14.

[52] Miller, W. C., Deathe, a B., Speechley, M., and Koval, J., 2001, "The influence of falling, fear of falling, and balance confidence on prosthetic mobility and social activity among individuals with a lower extremity amputation.," Arch. Phys. Med. Rehabil., **82**(9), pp. 1238–44.

[53] Adler, A. I., Boyko, E. J., Ahroni, J. H., and Smith, D. G., 1999, "Lower-extremity amputation in diabetes. The independent effects of peripheral vascular disease, sensory neuropathy, and foot ulcers.," Diabetes Care, **22**, pp. 1029–1035.

[54] Smith, D. G., 2003, "Transtibial Amputations: Successes and Challenges," inMotion, **13**, pp. 1–6.

[55] Zajac, F. E., Neptune, R. R., and Kautz, S. A., 2003, "Biomechanics and muscle coordination of human walking: Part II: Lessons from dynamical simulations and clinical implications," Gait Posture, **17**, pp. 1–17.

[56] Neptune, R. R., Zajac, F. E., and Kautz, S. A., 2004, "Muscle force redistributes segmental power for body progression during walking," Gait Posture, **19**, pp. 194–205.

[57] Neptune, R. R., and McGowan, C. P., 2011, "Muscle contributions to whole-body sagittal plane angular momentum during walking," J. Biomech., **44**, pp. 6–12.

[58] LaPre, A. K., and Sup, F., 2013, "Redefining Prosthetic Ankle Mechanics," IEEE International Conference on Rehabilitation Robotics.

[59] LaPre, A. K., Umberger, B. R., and Sup, F., 2014, "Simulation of a Powered Ankle Prosthesis with Dynamic Joint Alignment," Proc. - IEEE Int. Conf. Engineering in Medicine and Biology Society, pp. 1618–1621.

[60] Lapre, A. K., Drive, G., and Umberger, B. R., 2016, "A Robotic Ankle – Foot Prosthesis With Active Alignment," **10**(June), pp. 1–9.

[61] LaPre, A. K., and Sup, F., 2015, "A Control Strategy for an Active Alignment Transtibial Prosthesis," ASME 2015 Dynamic Systems and Control Conference, p. V001T18A005.

[62] Nllic, 2008, "Amputation Statistics by Cause Limb Loss in the United States Amputation Statistics by Cause Limb Loss in the United States," Phys. Med. Rehabil., pp. 1–3.

[63] M, P., 1999, "Lowering the forces and pressures on amputee stump with rolling joint foot.," Biomechanics, **6(7)**, pp. 315–318.

[64] Hagberg, K., and Brånemark, R., 2001, "Consequences of non-vascular trans-femoral amputation: a survey of quality of life, prosthetic use and problems.," Prosthet. Orthot. Int., **25**(3), pp. 186–94.

[65] Ferris, A. E., Aldridge, J. M., Rábago, C. a, and Wilken, J. M., 2012, "Evaluation of a Powered Ankle-Foot Prosthetic System During Walking.," Arch. Phys. Med. Rehabil., **in press**.

[66] Gefen, A., "Internal Mechanical Conditions in the Soft Tissues of the Residual Limb in Trans- Tibial Amputees," pp. 2–3.

[67] MR, P., 1995, "Mechanical outcome of a rolling joint prosthetic foot, and its performance in dorsiflexion phase of the trans-tibial amputee gait," J. Prosthetics Orthot., **7**, pp. 114–123.

[68] Coleman, K. L., Boone, D. a., Smith, D. G., and Czerniecki, J. M., 2001, "Effect of trans-tibial prosthesis pylon flexibility on ground reaction forces during gait," Prosthet. Orthot. Int., **25**(3), pp. 195–201.

[69] Sanders, J. E., Bell, D. M., Okumura, R. M., and Dralle, a J., 1998, "Effects of alignment changes on stance phase pressures and shear stresses on transtibial amputees: measurements from 13 transducer sites.," IEEE Trans. Rehabil. Eng., **6**(1), pp. 21–31.

[70] Kapp, S., and Cummings, D., 2002, Atlas of Amputations and Limb Deficiencies: Surgical, Prosthetic, and Rehabilitation Principles; Transtibial Amputation: Prosthetic Management, American Academy of Orthopedic Surgeons, Rosemont, IL.

[71] Boone, D. a, Kobayashi, T., Chou, T. G., Arabian, A. K., Coleman, K. L., Orendurff, M. S., and Zhang, M., 2013, "Influence of malalignment on socket reaction moments during gait in amputees with transtibial prostheses.," Gait Posture, **37**(4), pp. 620–626.

[72] Seelen, H. a. M., Anemaat, S., Janssen, H. M. H., and Deckers, J. H. M., 2003, "Effects of prosthesis alignment on pressure distribution at the stump/socket interface in transtibial amputees during unsupported stance and gait," Clin. Rehabil., **17**(7), pp. 787–796.

[73] Hill, D. A., 2012, "Effects of a Powered Ankle Prosthesis on Shock Absorption and Residual Limb / Socket Interface Pressure."

[74] Silverman, A. K., and Neptune, R. R., 2012, "Muscle and prosthesis contributions to amputee walking mechanics: a modeling study.," J. Biomech., **45**(13), pp. 2271–8.

[75] Delp, S. L., Anderson, F. C., Arnold, A. S., Loan, P., Habib, A., John, C. T., Guendelman, E., and Thelen, D. G., 2007, "OpenSim: open-source software to create and analyze dynamic simulations of movement.," IEEE Trans. Biomed. Eng., **54**(11), pp. 1940–50.

[76] Anderson, F. C., and Pandy, M. G., 2001, "Dynamic optimization of human walking," J. Biomech. Eng., **123**, pp. 381–90.

[77] Yamaguchi, G. T., and Zajac, F. E., 1989, "A planar model of the knee joint to characterize the knee extensor mechanism.," J. Biomech., **22**(1), pp. 1–10.

[78] Delp, S. L., Loan, J. P., Hoy, M. G., Zajac, F. E., Topp, E. L., and Rosen, J. M., 1990, "An interactive graphics-based model of the lower extremity to study orthopaedic surgical procedures.," IEEE Trans. Biomed. Eng., **37**(8), pp. 757–67.

[79] Umberger, B. R., 2010, "Stance and swing phase costs in human walking," J. R. Soc. Interface, **7**, pp. 1329–1340.

[80] Demers, M. S., Pal, S., and Delp, S. L., 2014, "Changes in tibiofemoral forces due to variations in muscle activity during walking.," J. Orthop. Res., **32**(6), pp. 769–76.

[81] Gailey, R., Allen, K., Castles, J., Kucharik, J., and Roeder, M., 2008, "Review of secondary physical conditions associated with lower-limb amputation and long-term prosthesis use.," J. Rehabil. Res. Dev., **45**(1), pp. 15–29.

[82] Johnson, V. J., Kondziela, S., and Gottschalk, F., 1995, "Pre and post-amputation mobility of trans-tibial amputees: correlation to medical problems, age and mortality.," Prosthet. Orthot. Int., **19**(3), pp. 159–164.

[83] Au, S. K., and Herr, H. M., 2008, "Powered ankle-foot prosthesis," IEEE Robot. Autom. Mag., **15**(3), pp. 52–59.

[84] Bergelin, B. J., and Voglewede, P. a., 2012, "Design of an Active Ankle-Foot Prosthesis Utilizing a Four-Bar Mechanism," J. Mech. Des., **134**(6), p. 061004.

[85] Sun, J., and Voglewede, P. a., 2013, "Powered Transtibial Prosthetic Device Control System Design, Implementation, and Bench Testing," J. Med. Device., **8**(1), p. 011004.

[86] Jia, X., Zhang, M., and Lee, W. C. C., 2004, "Load transfer mechanics between trans-tibial prosthetic socket and residual limb--dynamic effects.," J. Biomech., **37**(9), pp. 1371–1377.

[87] Hachisuka, K., Dozono, K., Ogata, H., Ohmine, S., Shitama, H., and Shinkoda, K., 1998, "Total surface bearing below-knee prosthesis: Advantages, disadvantages, and clinical implications," Arch. Phys. Med. Rehabil., **79**(7), pp. 783–789.

[88] Henrot, P., Stines, J., Walter, F., Martinet, N., Paysant, J., and Blum, A., 2000, "Imaging of the painful lower limb stump.," Radiographics, **20**, pp. S219–S235.

[89] LaPre, A. K., and Sup, F., 2013, "Redefining prosthetic ankle mechanics: Non-anthropomorphic ankle design," Proc. - IEEE Int. Conf. on Rehabilitation Robotics, pp. 1–5.

[90] Sup, F., Bohara, A., and Goldfarb, M., 2008, "Design and Control of a Powered Transfemoral Prosthesis.," Int. J. Rob. Res., **27**(2), pp. 263–273.

[91] Hang, C. C., Åström, K. J., and Ho, W. K., 1991, "Refinements of the Ziegler–Nichols tuning formula," IEE Proc. D Control Theory Appl., **138**(2), p. 111.

[92] Caputo, J. M., and Collins, S. H., 2014, "A universal ankle-foot prosthesis emulator for human locomotion experiments.," J. Biomech. Eng., **136**(3), p. 035002.

[93] Varol, H. A., Sup, F., and Goldfarb, M., 2010, "Multiclass real-time intent recognition of a powered lower limb prosthesis.," IEEE Trans. Biomed. Eng., **57**(3), pp. 542–51.

[94] Shultz, A. H., Mitchell, J. E., Truex, D., Lawson, B. E., and Goldfarb, M., 2013, "Preliminary evaluation of a walking controller for a powered ankle prosthesis," Proc. - IEEE Int. Conf. Robot. Autom., pp. 4837–4843.

[95] Struyf, P. a., van Heugten, C. M., Hitters, M. W., and Smeets, R. J., 2009, "The Prevalence of Osteoarthritis of the Intact Hip and Knee Among Traumatic Leg Amputees," Arch. Phys. Med. Rehabil., **90**(3), pp. 440–446.

[96] Smith, D. G., and Medical, A. C. A., "Transtibial Amputations Successes and Challenges."

[97] Eilenberg, M. F., Geyer, H., and Herr, H., 2010, "Control of a powered ankle-foot prosthesis based on a neuromuscular model," IEEE Trans. Neural Syst. Rehabil. Eng., **18**(2), pp. 164–73.

[98] Ficanha, E. M., Rastgaar, M., and Kaufman, K. R., 2014, "A two-axis cable-driven ankle-foot mechanism," Robot. Biomimetics, **1**(1), pp. 1–13.

[99] Zahedi, M. S., Spence, W. D., Solomonidis, S. E., and Paul, J. P., 1986, "Alignment of lower-limb prostheses.," J. Rehabil. Res. Dev., **23**(2), pp. 2–19.

[100] Eshraghi, A., Osman, N. A. A., Gholizadeh, H., Karimi, M., and Ali, S., 2012, "Pistoning assessment in lower limb prosthetic sockets.," Prosthet. Orthot. Int., **36**, pp. 15–24.

[101] Papaioannou, G., Mitrogiannis, C., Nianios, G., and Fiedler, G., 2010, "Assessment of Internal and External Prosthesis Kinematics during Strenuous Activities Using Dynamic Roentgen Stereophotogrammetric Analysis," JPO J. Prosthetics Orthot., pp. 8–10.

[102] Eshraghi, A., Abu Osman, N. A., Karimi, M., Gholizadeh, H., Soodmand, E., and Wan Abas, W. A. B., 2014, "Gait biomechanics of individuals with transtibial amputation: effect of suspension system.," PLoS One, **9**(5), p. e96988.

[103] Lilja, M., Johansson, T., and Oberg, T., 1993, "Movement of the tibial end in a PTB prosthesis socket: a sagittal X-ray study of the PTB prosthesis.," Prosthet. Orthot. Int., **17**(1), pp. 21–6.

[104] Kadaba, M. P., Ramakrishnan, H. K., and Wootten, M. E., 1990, "Measurement of Lower-Extremity Kinematics during Level Walking," J. Orthop. Res., **8**, pp. 383–392.

[105] Apkarian, J., Naumann, S., and Cairns, B., 1989, "A three-dimensional kinematic and dynamic model of the lower limb.," J. Biomech., **22**(2), pp. 143–55.

[106] Challis, J. H., 1995, "A procedure for determining rigid body transformation parameters," J. Biomech., **28**(6), pp. 733–737.

[107] Cappello, a, La Palombara, P. F., and Leardini, a, 1996, "Optimization and smoothing techniques in movement analysis.," Int. J. Biomed. Comput., **41**(3), pp. 137–151.

[108] Veldpaus, F. E., Woltring, H. J., and Dortmans, L. J. M. G., 1988, "A least-squares algorithm for the equiform transformation from spatial marker co-ordinates," J. Biomech., **21**(1), pp. 45–54.

[109] Spoor, C. W., and Veldpaus, F. E., 1980, "Rigid body motion calculated from spatial co-ordinates of markers," J. Biomech., **13**(4), pp. 391–393.

[110] Winter, D. A., and Sienko, S. E., 1988, "Biomechanics of below-knee amputee gait," J. Biomech., **21**(5), pp. 361–367.

[111] Sanderson, D. J., and Martin, P. E., 1996, "Joint kinetics in unilateral below-knee amputee patients during running," Arch. Phys. Med. Rehabil., **77**(12), pp. 1279–1285.

[112] Sanderson, D. J., and Martin, P. E., 1997, "Lower Extremity Kinematic and Kinetic Adaptions in Unilateral Below-Knee Amputees During Walking," Gait Posture, **6**, pp. 126 – 136.

[113] Czerniecki, J. M., Gitter, A., and Munro, C., 1991, "Joint moment and muscle power output characteristics of below knee amputees during running: The influence of energy storing prosthetic feet," J. Biomech., **24**(1).

[114] Czerniecki, J. M., Gitter, A. J., and Beck, J. C., 1996, "Energy transfer mechanisms as a compensatory strategy in below knee amputee runners," J. Biomech., **29**(6), pp. 717–722.

[115] Lu, T. W., and O'Connor, J. J., 1999, "Bone position estimation from skin marker co-ordinates using global optimisation with joint constraints," J. Biomech., **32**(2), pp. 129–134.

[116] Convery, P., and Murray, K. D., 2000, "Ultrasound study of the motion of the residual femur within a trans-femoral socket during gait," Prosthet. Orthot. Int., **24**(3), pp. 226–232.

[117] Erikson, U., and Lemperg, R., 1969, "Roentgenological study of movements of the amputation stump within the prosthesis socket in below-knee amputees fitted with a PTB prosthesis," Acta Orthop Scand, **40**(4), pp. 520–529.

[118] Grevsten, S., and Erikson, U., 1975, "A roentgenological study of the stump-socket contact and skeletal displacement in the PTB-Suciton Prosthesis.," Ups. J. Med. Sci., **80**(1), pp. 49–57.

[119] Bocobo, C. R., Castellote, J. M., Mackinnon, D., and Gabrielle-bergman, A., 1998, "Videofluoroscopic evaluation of prosthetic fit and residual limbs following transtibial amputation," J. Rehabil. Res. Dev., **35**(1), pp. 6–13.

[120] Sanders, J. E., Karchin, A., Fergason, J. R., and Sorenson, E. a, 2006, "A noncontact sensor for measurement of distal residual-limb position during walking.," J. Rehabil. Res. Dev., **43**(4), pp. 509–516.

[121] Seth, A., Sherman, M., Reinbolt, J. a., and Delp, S. L., 2011, "OpenSim: a musculoskeletal modeling and simulation framework for in silico investigations and exchange," Procedia IUTAM, **2**, pp. 212–232.

[122] Kobayashi, T., Orendurff, M. S., Zhang, M., and Boone, D. a., 2015, "Socket reaction moments in transtibial prostheses during walking at clinically perceived optimal alignment," Prosthet. Orthot. Int.

[123] Kobayashi, T., Arabian, A. K., Orendurff, M. S., Rosenbaum-Chou, T. G., and Boone, D. a, 2014, "Effect of alignment changes on socket reaction moments while walking in transtibial prostheses with energy storage and return feet.," Clin. Biomech. (Bristol, Avon), **29**(1), pp. 47–56.